Progress in Oceanography 78 (2008) 257–303

Contents lists available at ScienceDirect

Progress in Oceanography

journal homepage: www.elsevier.com/locate/pocean

Freshwater transport estimates and the global overturning circulation: Shallow, deep and throughflow components

Lynne D. Talley *

Scripps Institution of Oceanography, University of California San Diego, 9500 Gilman Drive, La Jolla, CA 92093-0230, USA

ARTICLE INFO

Article history:
Received 9 June 2007
Received in revised form 16 May 2008
Accepted 23 May 2008
Available online 6 June 2008

Keywords:
Global circulation
Freshwater
Salinity
Transport
Water masses

ABSTRACT

Meridional ocean freshwater transports and convergences are calculated from absolute geostrophic velocities and Ekman transports. The freshwater transports are analyzed in terms of mass-balanced contributions from the shallow, ventilated circulation of the subtropical gyres, intermediate and deep water overturns, and Indonesian Throughflow and Bering Strait components. The following are the major conclusions:

1. Excess freshwater in high latitudes must be transported to the evaporative lower latitudes, as is well known. The calculations here show that the northern hemisphere transports most of its high latitude freshwater equatorward through North Atlantic Deep Water (NADW) formation (as in [Rahmstorf, S., 1996. On the freshwater forcing and transport of the Atlantic thermohaline circulation. Climate Dynamics 12, 799–811]), in which saline subtropical surface waters absorb the freshened Arctic and subpolar North Atlantic surface waters (0.45 ± 0.15 Sv for a 15 Sv overturn), plus a small contribution from the high latitude North Pacific through Bering Strait (0.06 ± 0.02 Sv). In the North Pacific, formation of 2.4 Sv of North Pacific Intermediate Water (NPIW) transports 0.07 ± 0.02 Sv of freshwater equatorward.

   In complete contrast, almost all of the 0.61 ± 0.13 Sv of freshwater gained in the Southern Ocean is transported equatorward in the *upper* ocean, in roughly equal magnitudes of about 0.2 Sv each in the three subtropical gyres, with a smaller contribution of <0.1 Sv from the Indonesian Throughflow loop through the Southern Ocean. The large Southern Ocean deep water formation (27 Sv) exports almost no freshwater (0.01 ± 0.03 Sv) or actually imports freshwater if deep overturns in each ocean are considered separately (−0.06 ± 0.04 Sv).

   This northern–southern hemisphere asymmetry is likely a consequence of the "Drake Passage" effect, which limits the southward transport of warm, saline surface waters into the Antarctic [Toggweiler, J.R., Samuels, B., 1995a. Effect of Drake Passage on the global thermohaline circulation. Deep-Sea Research I 42(4), 477–500]. The salinity contrast between the deep Atlantic, Pacific and Indian source waters and the denser new Antarctic waters is limited by their small temperature contrast, resulting in small freshwater transports. No such constraint applies to NADW formation, which draws on warm, saline subtropical surface waters .
2. The Atlantic/Arctic and Indian Oceans are net evaporative basins, hence import freshwater via ocean circulation. For the Atlantic/Arctic north of 32°S, freshwater import (0.28 ± 0.04 Sv) comes from the Pacific through Bering Strait (0.06 ± 0.02 Sv), from the Southern Ocean via the shallow gyre circulation (0.20 ± 0.02 Sv), and from three nearly canceling conversions to the NADW layer (0.02 ± 0.02 Sv): from saline Benguela Current surface water (−0.05 ± 0.01 Sv), fresh AAIW (0.06 ± 0.01 Sv) and fresh AABW/LCDW (0.01 ± 0.01 Sv). Thus, the NADW freshwater balance is nearly closed within the Atlantic/Arctic Ocean and the freshwater transport associated with export of NADW to the Southern Ocean is only a small component of the Atlantic freshwater budget.

   For the Indian Ocean north of 32°S, import of the required 0.37 ± 0.10 Sv of freshwater comes from the Pacific through the Indonesian Throughflow (0.23 ± 0.05 Sv) and the Southern Ocean via the shallow gyre circulation (0.18 ± 0.02 Sv), with a small export southward due to freshening of bottom waters as they upwell into deep and intermediate waters (−0.04 ± 0.03 Sv).

* Tel.: +1 858 534 6610; fax: +1 858 534 9820.
E-mail address: ltalley@ucsd.edu

0079-6611/$ - see front matter
doi:10.1016/j.pocean.2008.05.001

The Pacific north of 28°S is essentially neutral with respect to freshwater, −0.04 ± 0.09 Sv. This is the nearly balancing sum of export to the Atlantic through Bering Strait (−0.07 ± 0.02 Sv), export to the Indian through the Indonesian Throughflow (−0.17 ± 0.05 Sv), a negligible export due to freshening of upwelled bottom waters (−0.03 ± 0.03 Sv), and import of 0.23 ± 0.04 Sv from the Southern Ocean via the shallow gyre circulation.

3. Bering Strait's small freshwater transport of <0.1 Sv helps maintains the Atlantic–Pacific salinity difference. However, proportionally large variations in the small Bering Strait transport would only marginally impact NADW salinity, whose freshening relative to saline surface water is mainly due to air-sea/runoff fluxes in the subpolar North Atlantic and Arctic. In contrast, in the Pacific, because the total overturning rate is much smaller than in the Atlantic, Bering Strait freshwater export has proportionally much greater impact on North Pacific salinity balances, including NPIW salinity.

1. Introduction

The ocean's horizontal and vertical salinity structure is central to determining the location of intermediate and abyssal water formation, that is, the structure of the interbasin overturning circulation (e.g. Gordon, 1986; Schmitz, 1995). The Atlantic and Indian Oceans are the most saline and the Pacific the freshest of the non-polar oceans; the Southern Ocean and Arctic are the freshest at the surface but intermediate in salinity at mid-depth (Fig. 1a and b). These large-scale salinity differences are created by the atmospheric water vapor transport. For the mean state of the oceans, which is the subject here, atmospheric water vapor transport must be balanced exactly by oceanic freshwater transport, whose direction is thus determined externally. The magnitude of the salinity differences between large-scale regions depends on the ocean's mass transports which can depend on the salinity differences, leading to a complex system with feedbacks, as shown by Stommel (1961), whose work has spawned many increasingly sophisticated studies of the effects of freshwater forcing on circulation and overturn.

Within the ocean, freshwater transport follows the myriad pathways of the circulation and overturn. It is useful to examine the contributions of the different major pathways to the total and hence to maintenance of observed large-scale salinity differences.

This is a long paper, covering multiple aspects of the global ocean's freshwater balance. It has been structured so that the sections can be read nearly independently, so that a reader interested in, say, the Indonesian Throughflow or Bering Strait or the role of North Atlantic Deep Water formation in freshwater transports, can skip to that section, and read it with only minimal reference to other sections.

The calculations are introduced in Section 1.1. Section 1.2 is a review of the role of salinity in circulation and overturn, as partial motivation for studying freshwater transports; it is included in the spirit of this journal's ongoing role in providing review material.

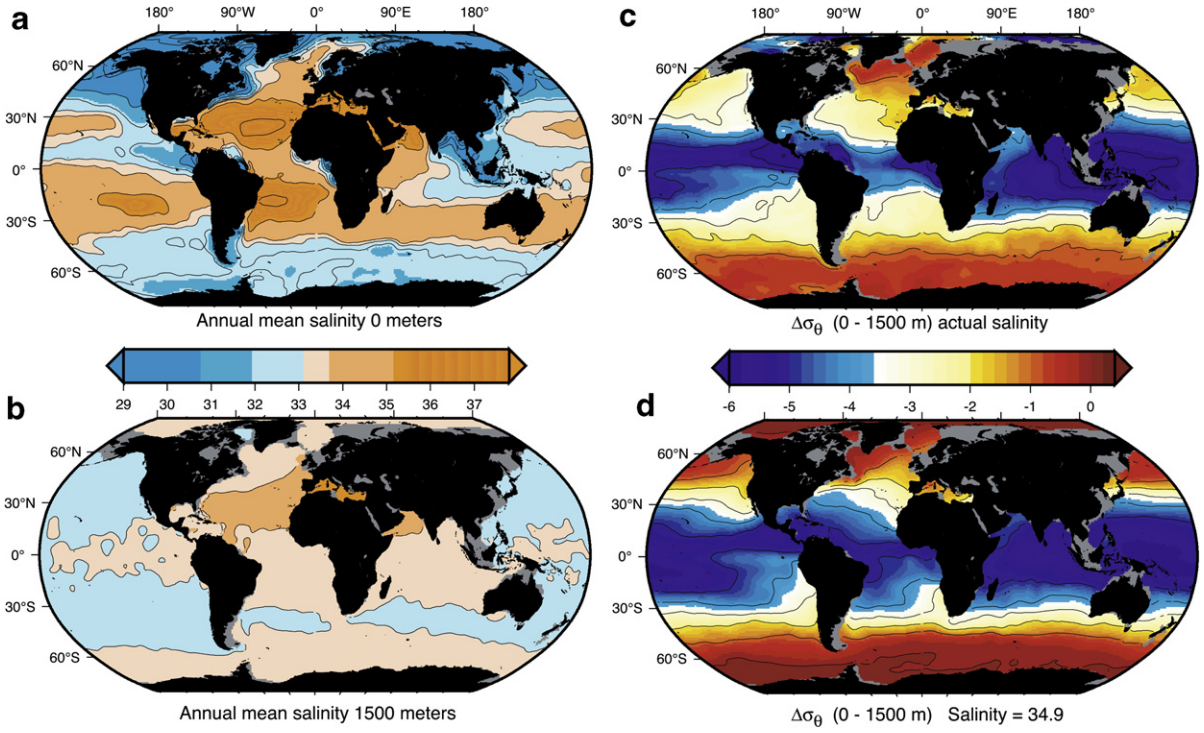

Fig. 1. (a) Surface salinity in winter (JFM for northern hemisphere, JAS for southern hemisphere), (b) annual mean salinity at 1500 m, (c) potential density (σ_θ) difference (surface winter minus 1500 m annual mean values), and (d) potential density (σ_θ) difference (surface winter minus 1500 m annual mean values) if salinity is set to a uniform value of 34.9. Based on Levitus and Boyer (1994) and Levitus et al. (1994) climatological temperature and salinity. (For interpretation of the references to colour in this figure legend, the reader is referred to the web version of this article.)

The data sets and method are described in Section 2 and Talley (2003), along with a discussion of uncertainties and error estimates. The total freshwater transports, including interbasin exchanges, are presented in Section 3. Freshwater transports for the subtropical gyres in each ocean are described in Section 4. Special aspects associated with the Indonesian Throughflow and Bering Strait are discussed in Sections 5 and 6. Freshwater transports associated with intermediate and deep water overturns, hence water mass formation, are described in Sections 7 and 8, focused on northern and southern overturns, respectively. The global overturning circulation and its freshwater transports are summarized in Section 9. Overall results are summarized in Section 10 and the Abstract. Acronyms are listed in Table 1.

1.1. Introduction to the new freshwater transport calculations

The principal purpose and novelty of these calculations compared with recent global analyses of freshwater transport (e.g. Wijffels, 2001; Ganachaud and Wunsch, 2003) are to show how the freshwater transports are divided among mass-balanced portions of the circulation, including the near-surface gyres and the overturns associated with intermediate and deep water formation. This study is similar to the decompositions for heat transport in Talley (1999, 2003). The roles of Bering Strait and the Indonesian Throughflow are also examined and compared with previous treatments (Wijffels et al., 1992; Robbins and Toole, 1997; Macdonald, 1998).

Freshwater transport calculations require an absolute geostrophic velocity data set, Ekman transports and salinity observations. As in Talley (1999, 2003) and Talley et al. (2003), absolute geostrophic velocity analyses were obtained from Reid (1994, 1997, 2003) for each of the three ocean basins. The Reid velocity analyses do not include error estimates. A Monte Carlo method is used to estimate error here.

In the heat transport analysis (Talley, 2003), it was shown that shallow overturn in the wind-driven subtropical gyres carries most of the heat in the North Pacific since it has no deep water ventilation and only weak intermediate water formation (North Pacific Intermediate Water or NPIW). On the other hand, North Atlantic heat transport is about equally divided between the shallow overturn, intermediate water formation (Labrador Sea Water or LSW) and deep water formation (North Atlantic Deep Water or NADW). In the southern hemisphere, formation of Lower Circumpolar Deep Water (LCDW) in the south and its upwelling into Indian and Pacific Deep Waters (IDW and PDW) in the tropics carries about as much heat as NADW formation. Because part of the southern hemisphere's low salinity intermediate water, Antarctic Intermediate Water (AAIW), is advected within the subducting South Pacific subtropical gyre, the impact of AAIW on heat transport could not be separated from the gyre transport.

As in the earlier heat transport presentation, total freshwater transports and their divergences, which must be calculated prior to the component calculations, are presented first (Section 3) for comparison with previous observational estimates. Large-scale freshwater transport analyses include Ganachaud and Wunsch (2003), henceforth GW03, who used a global box inverse model with hydrographic data (Ganachaud and Wunsch, 2000; Macdonald and Wunsch, 1996; Macdonald, 1998), and Sloyan and Rintoul (2001a) (henceforth SR2001) who used a box inverse for the Southern Ocean. Some of the hydrographic section data used in these published analyses, especially in the Atlantic, were more modern and had higher resolution spatial sampling than Reid's, likely yielding more accurate total divergences.

The total freshwater transports, divergences and estimated errors presented here are similar to GW03, SR2001, and the air-sea flux estimates of Wijffels et al. (1992) and Wijffels (2001) based on Baumgartner and Reichel (1975). Rendering of deep water and abyssal circulation might be more accurate in this analysis than in GW03, because the Reid (1994, 1997, 2003) geostrophic reference velocities for each station pair on each section were based not only on large-scale mass balance in layers, but also on careful comparison of the resulting circulations with tracer patterns throughout the water column. Therefore, calculation of the small freshwater transports associated with most of the deep overturn components can be considered with some confidence.

The new results concerning the relative roles of different circulation and overturning mechanisms for freshwater transport are presented in Sections 4–9.

The next subsection is a brief discussion of the relation between salinity distribution and water mass formation. Readers who are more interested in the calculation and results should proceed directly to Section 2.

1.2. Review of salinity distributions, overturn and global change

The gross differences between the different ocean basin's salinities (Fig. 1) result from the patterns of atmospheric water vapor transport (e.g. Seidov and Haupt, 2003). There is net precipitation and runoff in the fresher basins (Pacific, Arctic, Southern Ocean) and net evaporation in the saline basins (Atlantic and Indian Oceans). This means that there is atmospheric water transport from the evaporative to the precipitation regions, that is, from the Atlantic and Indian Oceans to the Pacific and from low latitudes to the polar regions (Zaucker and Broecker, 1992). In the ocean there must be equal and opposite freshwater transport, from the fresher to the saltier regions: from the Pacific to the Atlantic (through Bering Strait and possibly Drake Passage) (Aagaard and Carmack, 1989; Rintoul, 1991), and from the Pacific to the Indian Ocean through the Indonesian Throughflow (Piola and Gordon, 1984). There is also freshwater transport from the Arctic to the Atlantic, and from the Southern Ocean to the Pacific, Atlantic and Indian Oceans. These transports are associated with the overturning circulations in the upper ocean and with intermediate and deep water mass formation.

These gross salinity differences result in variations in location and vigor of intermediate and deep overturn in the different ocean basins (Fig. 2). The saline North Atlantic and its adjacent seas produce a large amount of dense water through open ocean

Table 1
Acronyms

AABW	Antarctic Bottom Water
AAIW	Antarctic Intermediate Water
BS	Bering Strait
CDW	Circumpolar Deep Water
IDW	Indian Deep Water
ITF	Indonesian Throughflow
LCDW	Lower Circumpolar Deep Water
LSW	Labrador Sea Water
MOW	Mediterranean Overflow Water
NADW	North Atlantic Deep Water
NPIW	North Pacific Intermediate Water
NSOW	Nordic Seas Overflow Water
PDW	Pacific Deep Water
SAMW	Subantarctic Mode Water
UCDW	Upper Circumpolar Deep Water
PW	PetaWatt (1×10^{15} W)
PWT	PetaWatt ("temperature transport")
Sv	Sverdrup (1×10^{6} m^3/s)
MSv	Sverdrup for freshwater balance with mass balance
FSv	Sverdrup for freshwater balance without mass balance

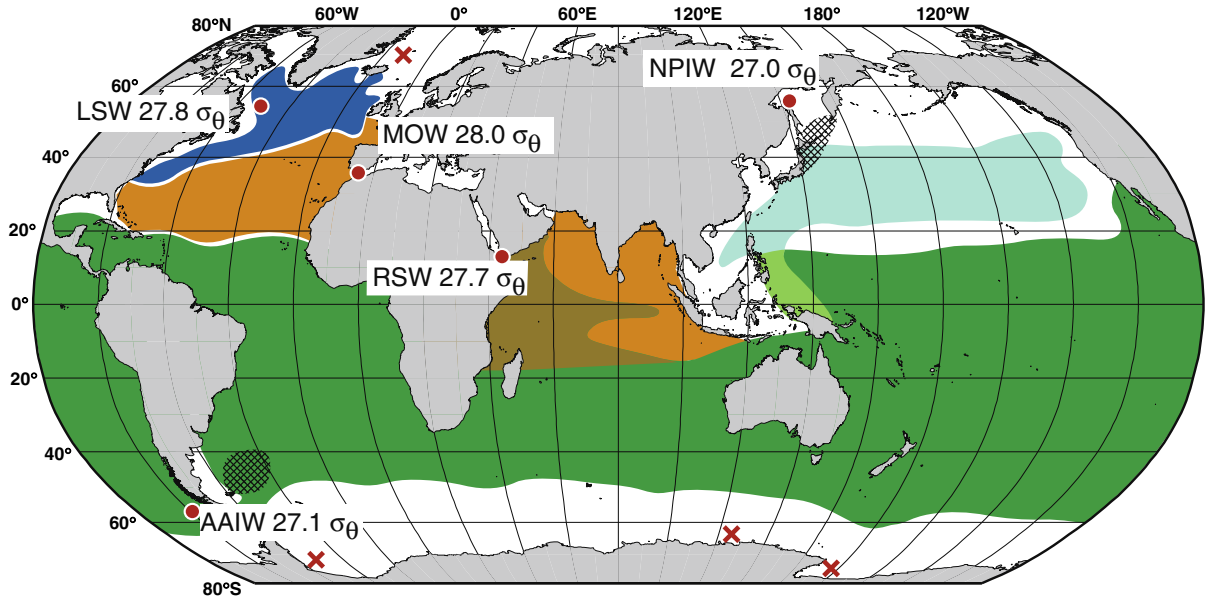

Fig. 2. Schematic of low salinity (blue, green and blue-green) and high salinity (orange) intermediate water masses, after Talley (1999). The overlap of Red Sea Water and AAIW is shown in brown; the overlap of NPIW and AAIW is shown with an intermediate shade of green. Red dots represent intermediate water sources; these are sites of open ocean convection (LSW and AAIW), or sill overflow (MOW and Red Sea Water), or shelf brine rejection (NPIW). Potential density at each source is listed. Red X's represent deep and bottom water sources. (For interpretation of the references to color in this figure legend, the reader is referred to the web version of this article.)

convection and subsequent entrainment of upper ocean waters. The saline Indian Ocean, which has no high northern latitudes, nevertheless produces dense, saline intermediate water in the salty Red Sea. The intermediate salinity Southern Ocean produces dense water through brine rejection during ice formation, which enhances the salinity of the near-surface source waters. The freshest North Pacific is unable to produce very dense water through either mechanism, and produces only a limited amount of low-density intermediate water through brine rejection.

The relative densities of the intermediate water masses at their sources (Fig. 2) are correlated with the relative salinity in their source regions, regardless of whether they are identified locally as high or low salinity water masses. The highest density intermediate waters are in the North Atlantic (Labrador Sea Water and Mediterranean Overflow Water) and the Indian Ocean (Red Sea Water); both oceans have generally high salinity (Fig. 1). The two lower density intermediate waters, Antarctic Intermediate Water and North Pacific Intermediate Water, are formed in the generally lower salinity basins.

That salinity has a role in controlling overturn is widely assumed and substantiated, through modeling studies and inference from observations. Specifics of the circulation response to a given large-scale and large-magnitude salinity change is an area of active research. Numerous studies consider the impact of a large input of freshwater at the sea surface in the northern North Atlantic. Some of these studies were motivated by the Younger Dryas glacial termination in which the North Atlantic overturn was shut down, associated with a large input of freshwater at the sea surface (e.g. Broecker et al., 1988; Saenko et al., 2007), and by modern evidence for modulation of northern North Atlantic convection associated with surface freshwater inputs (e.g. Dickson et al., 1996). As an example of the complexity of overturning response to a freshwater input, a weakening of subpolar North Atlantic overturn due to surface freshening can be shown to be reversed by lagged advection of more saline subtropical waters into the subpolar region (e.g. Vellinga and Wood, 2002); the co-existence of fresher subpolar and saltier subtropical surface waters is a signature of strengthened meridional atmospheric water vapor transport, with stronger evaporation at mid-latitudes and stronger precipitation at higher latitudes. Such a weakening followed by reestablishment of overturn is suggested by observations over the past several decades as well (Hátún et al., 2005).

The impact of salinity on locations of overturn can be illustrated pedagogically by examining the salinity dependence of the difference in climatological density between the surface and 1500 m (Fig. 1c and d). This depth range is chosen because the deepest open ocean convection extends down to about 1000–2000 m in the very limited locations where it occurs (e.g. Marshall and Schott, 1999), and only extremely rarely to the bottom. The minimum difference in density between the surface and 1500 m occurs in the northern North Atlantic, the Weddell Sea and the Ross Sea (Fig. 1c). These are the locations of the densest water formation. Within the Mediterranean and Japan Seas, deep convection in their northwestern regions is also associated with the location of the minimum density difference. If the density difference between the sea surface and 1500 m depended on temperature alone, setting salinity everywhere to 34.9 (Fig. 1d), the possible regions for dense overturn could expand greatly. The North Pacific would have almost the same potential for deep overturn as the North Atlantic. (This is obviously an overly simplified view; if density had no salinity dependence, the temperature stratification would develop differently. In fact, artificial density inversions appear in Fig. 1d in large regions of the Southern Ocean and Arctic where potential temperature increases with depth, supported by the strong halocline in these regions. And the highest density water is formed over shallow continental shelves through brine rejection or evaporation processes.)

Thus, the salinity distribution is correlated with interbasin differences in the overturning circulation. The mean salinity differences between the oceans are themselves created by differences in net evaporation/precipitation/runoff (atmospheric freshwater transport), with the equilibrium salinity distribution then including the ocean's freshwater transports (Stommel and Csanady, 1980; Broecker et al., 1990).

The relations between salinity difference, freshwater transport and volume transport are illustrated in Fig. 3, showing simple examples of freshwater transport due to nearly horizontal ex-

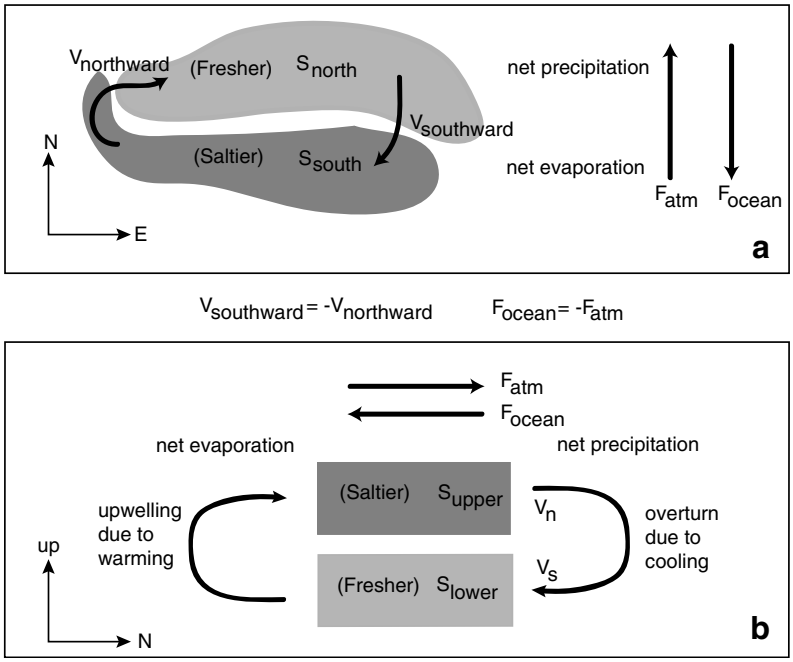

Fig. 3. Two-box illustrations of freshwater transport. (a) Volume exchange in the horizontal between regions of higher and lower salinity. In the subtropical gyres there is a small change in density, hence shallow overturn, associated with this exchange, but such a density change is not necessary for freshwater transport. (b) Volume exchange in the vertical associated with buoyancy gain and loss. In both panels, the atmospheric freshwater transport from the evaporation to the precipitation region is set, and the oceanic freshwater transport must be equal and opposite, pointing from the precipitation region to the evaporation region. Volume transports that connect the two boxes must balance.

change and due to overturn, hence water mass formation. This schematic can be useful as a reference point for the detailed calculations in the sections that follow. A grossly simplified equation for oceanic freshwater transport between two boxes designated as, say, "north" and "south", of salinity S_{south} and S_{north} is:

$$F_{\text{ocean}} = V_{\text{southward}}(1 - S_{\text{north}}/S_{\text{o}}) + V_{\text{northward}}(1 - S_{\text{south}}/S_{\text{o}}) = V(S_{\text{south}} - S_{\text{north}})/S_{\text{o}} \quad (1a)$$

where F_{ocean} is the total freshwater transport set by the atmosphere; the equal and opposite exchange volume transports are $V = V_{\text{northward}} = -V_{\text{southward}}$; S_{o} is an arbitrary reference salinity. (See Section 2.2 for complete derivations for which this is a major simplification.) Thus,

$$(S_{\text{south}} - S_{\text{north}}) = F_{\text{ocean}} S_{\text{o}}/V \quad (1b)$$

In the simplest view, the salinity difference is determined by the freshwater transport F_{ocean} that is imposed by the atmosphere and by the exchange volume transports that are set by the forcing for the ocean circulation. Feedbacks between salinity difference and V, with a set freshwater transport F_{ocean}, were explored by Stommel (1961). More complex feedbacks that also affect the atmospheric freshwater transport through changes in ocean surface temperature distribution resulting from changes in salinity distribution, and that hence change the required balancing F_{ocean}, are mainly addressed in climate models.

In the upper layers of each ocean basin there are saltier and fresher regions associated with local regions of net evaporation and precipitation/runoff (e.g. Fig. 3a). Ocean freshwater transport is required within each basin to maintain these local mean salinity differences. Hence there must be freshwater transport away from the tropical and high latitude precipitation regions and towards the subtropical evaporation regions. This basin-scale freshwater transport is carried by the shallow overturning circulation of the gyres within the basins and is examined herein for each subtropical gyre.

Ocean freshwater transport does not feed back directly on the atmosphere since surface salinity does not directly affect evaporation or precipitation. This differs from heat transport, which can directly affect surface temperature. However, ocean freshwater transport is important for ocean stratification, particularly in high latitudes where temperatures are uniformly low and freshened surface waters determine the mixed layer depth (e.g. Fig. 1d). Therefore, salinity is implicated in more convoluted climate feedbacks, since salinity stratification can affect overturn and hence surface temperature, which in turn can affect the wind, precipitation and evaporation and sea ice (e.g. Dickson et al., 1996; Weaver et al., 1999; Keeling and Stephens, 2001; Vellinga and Wood, 2002; Hátún et al., 2005; Peterson et al., 2006; Saenko et al., 2007).

Large-scale salinity changes are useful for detecting global change in atmospheric water vapor transport (IPCC, 2007). If the atmosphere warms overall, water vapor content should increase, which necessitates an increase in both precipitation and evaporation. However, changes in precipitation, runoff and evaporation are difficult to detect directly (IPCC, 2007). Salinity changes are a time integral of the forcing changes, and therefore inherently less noisy. Salinity changes observed globally from 1955 to 1998 (Boyer et al., 2005) suggest a freshwater redistribution within the oceans associated with greater precipitation (evaporation) in regions of net precipitation (evaporation). The Pacific is becoming slightly fresher while the Atlantic and Indian Oceans are becoming slightly saltier. In the Pacific and Indian Oceans there has been a freshening of higher latitude intermediate waters and increase in salinity in the subtropical evaporation regions (Wong et al., 1999, 2001). In the Atlantic Ocean, salinity has increased in the subtropical high salinity regions and had been decreasing for several decades at higher latitudes (Dickson et al., 2003; Curry et al., 2003; Curry and Mauritzen, 2005); the subpolar freshening has recently reversed (ICES, 2006), likely due to the northward transport of more

saline waters from the subtropics mentioned above (Hátún et al., 2005). Thus, study of the basic aspects of freshwater transport is useful for understanding regional stratification and ocean overturn.

2. Data sets, methods and uncertainties

Wijffels et al. (1992) and Wijffels (2001) provide a thorough discussion of freshwater transport calculations as well as a review of prior estimates based on hydrography and air-sea fluxes ($E - P - R$). Hydrographic, wind and air-sea freshwater flux (evaporation, precipitation and runoff) data sets are described in Section 2.1, methods including choices of Bering Strait and Indonesian Throughflow properties are described in Section 2.2, and uncertainties and error estimates are discussed in Section 2.3.

2.1. Data sets

Direct estimates of lateral freshwater transport through a vertical cross-sectional area require velocity, temperature and salinity observations. The freshwater transports and divergences are calculated here using the Reid (1994, 1997, 2003) absolute geostrophic velocity analyses for coast-to-coast hydrographic sections and accompanying temperature and salinity data. Section locations are apparent in Fig. 5a and Table 2 below. Ekman transports are calculated using National Center for Environmental Predictions (NCEP) annual mean reanalysis winds for 1979–2005 (Kalnay et al., 1996) with Levitus et al. (1994) climatological near-surface salinities. These replace the Ekman calculations using the older Hellerman and Rosenstein (1983) wind stress climatology in Talley (1999, 2003); therefore, heat transports have been updated throughout the tables here, but are not discussed except in conjunction with freshwater transports in Section 9. Reported weakness of the NCEP winds (Large, personal communication, 2007) may be the cause of an apparently unphysical result for North Pacific Intermediate Water overturn here (Section 7.3), but otherwise did not appear to create contradictions of generally accepted ideas of water mass transformations. The 1994 climatological salinity data set has been superceded by regularly updated World Ocean Atlas products from the National Oceanographic Data Center, available online at http://www.nodc.noaa.gov/OC5/indprod.html; the 1994 product is completely adequate for the present task, which was begun a number of years ago when it was the readily available product.

Reid (personal communication) provided the geostrophic reference velocities at the ocean bottom used in Reid (1994, 1997, 2003), for every station pair on the sections (19 zonal sections with 1738 station pairs, hence bottom reference velocities). An additional five zonal sections from those analyses were examined in Talley (2003) and were not included here because of large discrepancies attributable to especially poor sampling or combinations of non-synoptic data sets. The geostrophic reference velocities were selected by Reid to balance mass on each of the sections and to yield a circulation consonant with tracer distributions at every level in the water column, with the total mass balance subject to specified assumptions about Bering Strait and Indonesian Throughflow transports. Ekman transport was not included in the Reid mass balances. Assumptions here about the strait and (non-zero) Ekman transports differ from Reid's, requiring section-wide adjustments in the bottom reference velocities, as described below.

The section-based freshwater transports and divergences are compared with air-sea fluxes of freshwater. The 1979–2005 NCEP reanalysis is used for evaporation and precipitation (http://www.cgd.ucar.edu/cas/catalog/newbudgets, 2007; Kalnay et al., 1996). Runoff estimates are from Dai and Trenberth (2002), henceforth DT02 (http://www.cgd.ucar.edu/cas/catalog/dai/index.html, 2007).

This analysis is concerned with the mean circulation and transports and not with fluctuations, which are usually at a level of less than 5–10% of the mean signal. The hydrographic data set, spanning 1957–1996, is combined with wind, air-sea flux and surface salinity climatologies that span somewhat different decades. Within the accuracy of these calculations, as reflected in the quantitative uncertainty estimates given throughout the tables and text, this is defensible.

2.2. Methods

Mass, salt and freshwater transports through a vertical section are given by

$$\begin{aligned} M &= \rho v \, dA \\ S &= \rho s v \, dA \\ F &= M - S = \rho v (1 - s) dA \end{aligned} \qquad (2a, b, c)$$

Here ρ, v and s are density (kg m^{-3}), velocity normal to the vertical area (m/s) and salinity as reported in full mks units (kg/kg), that is, the usual salinity multiplied by 0.001 kg/g. There is no net salt transport ($S = 0$) when (2) is integrated over a vertical section, for which $dA = da\,dz$ where a is the along-section coordinate and z is depth, and where the section (or section plus a strait flow) is closed so that mass must be nearly conserved. Mass and freshwater transport are balanced by precipitation/evaporation/runoff ($P - E + R$) in the area enclosed by the section(s). Following Wijffels et al. (1992), this is expressed as

$$\begin{aligned} \delta &= E - P - R = \oint\!\!\oint \rho v \, dA \\ 0 &= \oint\!\!\oint \rho v s \, dA \\ \delta &= E - P - R = \oint\!\!\oint \rho v \left(1 - \frac{s}{s_o}\right) dA \end{aligned} \qquad (3a, b, c)$$

where v is velocity, positive relative to the inward normal to the closed contour. (That is, if there is net transport of freshwater into the closed region, then there must be net evaporation in the region.) The arbitrary constant s_o is chosen to be 34.9, which is close to the mean salinity of 34.83 for all sections used (see below). The integral on the RHS of (3c) is called the *freshwater transport*, and is in units of kg/s. Transports are listed here throughout as Sverdrups (Sv) since this is a more convenient unit of transport. Instead of volume transport though, the definition used here is mass transport: 1 Sv = 1×10^9 kg/s. Mass must be balanced for (3c) to be unique; otherwise it depends on the reference salinity. More exactly, mass is nearly balanced, as the small deviation from exact balance is the actual freshwater gain or loss, e.g. (3a).

The units of freshwater and mass transport are the same. To distinguish between freshwater and mass transport (except in the abstract), two practical units are introduced: (1) "FSv", or Sverdrups of "freshwater", for non-mass-balanced components of the freshwater transport that depend on the reference salinity and that are listed only to show the specifics of each mass-balanced calculation, and (2) "MSv", or Sverdrups of mass-balanced freshwater when the components are summed so as to balance overall mass. [Similarly, Hall and Bryden (1982) and Talley (2003) used the usual heat transport units of PetaWatts (PW) when mass was balanced, and PetaWatts of temperature transport ("PWT") when mass was not balanced.] Use of "MSv" instead of "Sv" helps to distinguish between the small residual freshwater transports and the much larger mass transports of different components of the circulation.

The integral (3c) was computed for each quasi-zonal hydrographic section. For all but one zonal section considered here, mass is not balanced in the total transports because of Bering Strait and/

Table 2
Total meridional freshwater transports (1 Sv = 1 × 10^9 kg/s) and transport components, for NCEP reanalysis winds, Bering Strait and ITF transports of 1 and 10 Sv are assumed

Section	Dates	Ship, number of stations used	Geostrophic transport (Sv)	Mean and standard deviation of salinity (depth-weighted)	(1) Geostrophic FW transport (FSv)	Ekman transport (Sv)	Mean Ekman layer salinity	(2) Ekman FW transport (FSv)	Total transport (Sv)	(3) Relative FW transport (FSv) (1) + (2)	(4) Section FW transport associated with Bering Strait and *ITF* (*italics*) (Tables 6 and 7) (FSv)	Total FW transport (MSv) (Bering Strait and ITF removed) (3) + (4)
Atlantic 59°N	March–April 1962	Erika Dan, 55	0.26 ± 20.29	34.987 ± 0.167	−0.588 ± 0.235	−1.27 ± 0.12	34.759 ± 0.540	0.000 ± 0.004	−1.00	−0.588 ± 0.235	−0.003	−0.591
Atlantic 53°N	January–February 1962	Erika Dan, 44	1.15 ± 11.26	34.955 ± 0.136	−0.380 ± 0.119	−2.16 ± 0.16	34.782 ± 0.643	−0.003 ± 0.007	−1.00	−0.383 ± 0.119	−0.002	−0.385
Atlantic 45°N	April 1957	Discovery, 40	1.42 ± 9.98	35.041 ± 0.143	−0.411 ± 0.126	−2.40 ± 0.21	34.981 ± 0.797	0.024 ± 0.013	−1.00	−0.387 ± 0.126	−0.004	−0.391
Atlantic 36°N	June–July 1981	Atlantis II, 101	1.27 ± 7.88	35.219 ± 0.159	−0.493 ± 0.064	−2.27 ± 0.23	36.116 ± 0.551	0.088 ± 0.010	−1.00	−0.405 ± 0.066	−0.010	−0.415
Atlantic 24°N	August–September 1981	Atlantis II, 112	−5.83 ± 12.57	35.163 ± 0.130	−0.061 ± 0.139	4.82 ± 0.10	36.811 ± 0.368	−0.288 ± 0.009	−1.00	−0.349 ± 0.139	−0.008	−0.357
Atlantic 16°S	April 1957	Crawford, 33	6.77 ± 32.03	34.898 ± 0.039	−0.672 ± 0.047	−7.77 ± 0.28	36.614 ± 0.447	0.419 ± 0.025	−1.00	−0.253 ± 0.052	0.000	−0.253
Atlantic 24°S	October 1958, November 1972	Crawford, Melville, 46	2.27 ± 14.57	34.870 ± 0.047	−0.031 ± 0.030	−3.27 ± 0.08	36.272 ± 0.520	0.126 ± 0.009	−1.00	0.095 ± 0.030	0.001	0.096
Atlantic 32°S	April–May 1959, November 1972	Atlantis, Melville, 41	−2.15 ± 13.58	34.797 ± 0.066	0.241 ± 0.035	1.15 ± 0.23	35.865 ± 0.426	−0.026 ± 0.008	−1.00	0.215 ± 0.036	0.003	0.212
Pacific 47°N	August–September 1985	T. Thompson, 115	5.31 ± 3.50	34.475 ± 0.082	0.207 ± 0.029	−4.31 ± 0.23	32.951 ± 0.383	−0.256 ± 0.015	1.00	−0.049 ± 0.032	0.012	−0.061
Pacific 35°N	Several	Several, 72	5.09 ± 8.38	34.532 ± 0.057	−0.019 ± 0.042	−4.09 ± 0.62	34.224 ± 0.483	−0.058 ± 0.020	1.00	−0.077 ± 0.046	0.011	−0.088
Pacific 24°N	March–June 1985	T. Thompson, 215	−7.61 ± 10.03	34.585 ± 0.050	−0.094 ± 0.044	8.62 ± 0.28	34.832 ± 0.501	−0.033 ± 0.012	1.00	−0.127 ± 0.046	0.009	−0.138
Pacific 10°N	February–May 1989	Moana Wave, 211	−28.60 ± 24.78	34.632 ± 0.022	−0.266 ± 0.060	29.61 ± 1.36	34.139 ± 0.275	0.543 ± 0.040	1.01	0.277 ± 0.072	0.008	0.269
Pacific 28°S	June–July 1967	El Tanin, 100	14.20 ± 15.02	34.670 ± 0.082	0.081 ± 0.075	−3.21 ± 0.57	35.473 ± 0.327	0.055 ± 0.013	11.00	0.136 ± 0.077	−0.006, *−0.057* (Table 5)	0.199
Pacific 43°S	March–May 1967	El Tanin, 78	3.33 ± 9.58	34.578 ± 0.081	0.109 ± 0.044	7.66 ± 0.22	34.508 ± 0.518	0.132 ± 0.024	11.00	0.241 ± 0.050	0.009, *−0.01*	0.232
Indian 8°N: Arabian Sea[a]	August–September 1995	Knorr, 57	5.10 ± 17.46 (2.79 ± 17.40)	34.951 ± 0.066	0.460 ± 0.056 (0.464 ± 0.056)	−5.10 (−2.79 ± 0.93)	35.438 ± 0.432	0.084 (0.045 ± 0.023)	0.01 (0.00)	0.544 ± 0.060 (0.509 ± 0.060)	0.0	0.544 (0.509)
Indian 8°N: Bay of Bengal[a]	September–October 1995	Knorr, 38	3.81 ± 12.64 (1.12 ± 12.61)	34.822 ± 0.093	0.129 ± 0.164 (0.124 ± 0.164)	−3.80 (−1.11 ± 0.62)	33.169 ± 0.537	−0.179 (−0.050 ± 0.034)	−0.01 (0.01)	−0.050 ± 0.167 (0.074 ± 0.167)	0.0	−0.050 (0.074)
Indian 8°S[a]	December–January 1995/1996	Knorr, 160	22.39 ± 36.55 (6.26 ± 36.64)	34.755 ± 0.057	−0.185 ± 0.158 (−0.254 ± 0.158)	−32.39 (−16.26 ± 1.13)	34.683 ± 0.409	−0.293 (−0.129 ± 0.027)	−10.0 (−10.0)	−0.478 ± 0.161 (−0.383 ± 0.161)	*−0.06*, *−0.06*	−0.418 (−0.323)
Indian 20°S	April–June 1995	Knorr, 131	2.52 ± 14.23	34.775 ± 0.031	−0.062 ± 0.038	−12.52 ± 0.25	34.960 ± 0.098	0.011 ± 0.004	−10.0	−0.051 ± 0.039	*0.08*	0.031
Indian 32°S	November–December 1987	Discoverer, 108	−10.82 ± 18.99	34.756 ± 0.066	0.272 ± 0.084	0.82 ± 0.30	35.637 ± 0.150	−0.015 ± 0.007	−10.0	0.257 ± 0.085	*0.12*	0.377
Bering Strait		Roach et al. (1995)		~32.5					0.86	0.06 ± 0.02		
Indonesian Throughflow		Gordon et al. (1999) and Vranes et al. (2002)		~34.5					9.3 (~10)	0.11 ± 0.05		

Freshwater transports are relative to a mean salinity of 34.9. Units "FSv" indicate that mass is not balanced and thus values depend on the reference salinity. Units "MSv" indicate that mass is balanced, so values are independent of reference salinity.

[a] 8°N uses September Ekman transport and 8°S uses December Ekman transport (Fig. 4a). Analysis using annual Ekman transport is in parentheses.

or the ITF. Thus, freshwater "transport" through these sections depends on the reference salinity in (3c). However, the net mass transport into the regions *between* sections is balanced since each section is assumed to have exactly the prescribed Bering Strait and/or ITF transport. Therefore, the freshwater transport divergences between the sections are meaningful, and independent of the reference salinity. This assumption was tested and found to be accurate by computing all freshwater transports with three widely differing reference salinities (34.4, 34.9, 35.3), which of course yielded very different freshwater transport components (FSv), but identical mass-balanced freshwater transports (MSv).

All sections in the Atlantic (Pacific) include southward (northward) transport due to Bering Strait (BS) throughflow from the Pacific to the Arctic/Atlantic. Roach et al. (1995) estimated 0.86 Sv flow through Bering Strait. Reid (1994, 1997) net transports through the zonal sections due to Bering Strait range from 1.35 to 2 Sv. Here, BS transport is set to 1 Sv on all affected sections and BS mean salinity is assigned to be 32.5 (Aagaard and Carmack, 1989; Wijffels et al., 1992), although the actual salinity has considerable seasonal and interannual variability (Roach et al., 1995). The freshwater transport component through Bering Strait relative to 34.9 is thus 0.07 FSv. Aagaard and Carmack (1989) reported 0.8 Sv and salinity 32.5, yielding a freshwater component of 0.06 FSv; Woodgate and Aagaard (2005) reported an additional 0.08 Sv at salinity 30, which yields a additional freshwater component relative to 34.9 of 0.01 FSv, for a total of 0.07 FSv. To obtain the freshwater transport divergence associated with BS in the region north of a given Pacific or Atlantic section, this component should be combined with the freshwater transport component due to the 1 Sv of transport through the given section (Section 6; Table 7 below).

The South Pacific sections also include northward throughput to feed the Indonesian Throughflow (ITF) to the Indian Ocean. The Indian Ocean sections south of the equator include southward transport from the ITF. The ITF transport through Makassar Strait in the Indonesian passages from the Pacific to the Indian is approximately 9.3 Sv, with considerable variability (Gordon et al., 1999; Vranes et al., 2002). The total ITF is likely larger due to flow through Lifamatola Strait (e.g. Van Bennekom et al., 1988), but long-term direct observations are only now being made (Gordon, A., Sprintall, J., personal communication). Here, as in Talley (2003) and Talley et al. (2003), it is assumed that the ITF transport is 10 Sv, similar to the 10–11 Sv in Macdonald's (1998) global inverse solution, SR2001's Southern Ocean inverse solution, and Stammer et al.'s (2003) global state estimation; property budgets in the Indonesian Seas suggest 12 Sv (Talley and Sprintall, 2005). An ITF salinity of 34.5 is assumed, following Toole and Warren (1993).

Reid (1997) assumed a smaller northward transport through the South Pacific of 4 Sv to feed both the ITF and Bering Strait; Reid (2003) assumed a southward transport through the Indian Ocean of 5 Sv. These are too small to be consistent with the above-mentioned observations, and so these transports, which are embedded in the original reference velocities obtained from Reid and used herein, are adjusted upwards, as described next.

Reid's (1994, 1997, 2003) solutions balance mass on the zonal sections, including his choices of Bering Strait and ITF transports, but without Ekman transport. Here different choices of Bering Strait and ITF transports are applied, and Ekman transport is included. This is done with a uniform adjustment to geostrophic velocities on each section, as in Talley (2003) and Talley et al. (2003). These uniform adjustments do not generally corrupt the overturning circulation or its vertical distribution where Ekman transport is small, but uncertainty is larger on the tropical sections where Ekman transport is large (Talley et al., 2003).

In practice, the calculation (3c) for each section is

$$\delta = \int_{\text{ekman}} \rho v_{\text{ek}}(1 - s_{\text{ek}}(a)/s_{\text{o}})\mathrm{d}a + \int\int_{\text{section}} \rho v_{\text{geos}}(1 - s_{\text{prof}}(a,z)/s_{\text{o}})\mathrm{d}a\,\mathrm{d}z \tag{4}$$

The Ekman transport v_{ek} perpendicular to the hydrographic section is calculated from the NCEP average wind stress interpolated along the hydrographic section. The climatological salinity at 30 m (Levitus et al., 1994) is assigned to the Ekman transport as in Talley (2003). The geostrophic velocities v_{geos} were calculated every 10 dbar for each hydrographic station pair, using Reid's (1994, 1997, 2003) reference velocities for each station pair. These velocities were then further adjusted with the same uniform correction to match the Ekman transport and the assumption about ITF and Bering Strait throughput. Salinity s_{prof} was assigned to each velocity from the CTD profiles or bottle data interpolated to 10 dbar intervals using an Akima cubic spline.

Eq. (4) is sometimes simplified for bulk or box models as

$$\delta = \sum \rho V_i(1 - S_i/s_{\text{o}}) \tag{5}$$

in which the total transports and mean salinities from a large area (e.g. a complete section or complete surface) are combined and then several such large sections (i) are summed, rather than integrating more finely over the closed section. While this decomposition is often useful for interpretation and in fact is used here for the ITF and BS, it is seen below that the correct sign for freshwater transports often *cannot* be attained from (5), especially within the upper ocean gyre circulations where vertical shear and salinity gradients are large. Details of velocity and salinity distributions can matter. This is not a statement about the time-dependent "eddy component" of the transport (Wijffels, 2001), only that mean flow shears and large-scale salinity variations within "bulk" components must be resolved. This spatial variability of the mean circulation is sometimes referred to as standing eddies.

The magnitude of the time-dependent, eddy component cannot be estimated from this present analysis. Meijers et al. (2007) found that eddy components are negligible in gyre interiors, which characterizes most of the sections used here and especially the mid-subtropics sections in Sections 4–9. A study of eddy heat transport in the North Pacific, near the latitude of the 24°N section used here, found that mass and heat transport are dominated by the large-scale circulation, with eddies contributing about 10% (Roemmich and Gilson, 2001).

Three or four separate freshwater calculations are presented for each quasi-zonal hydrographic section (see locations in Fig. 5a): (1) total freshwater transports and divergences (see Section 3; Figs. 5 and 6 and Tables 2–4), (2) mass-balanced transports associated with the ventilated layer of the subtropical gyre (warm, poleward western boundary currents and the equatorward return of cooler, denser water within the subducted subtropical layers) (see Section 4; Fig. 7 and Table 5), (3) transport associated with ITF throughput on affected sections in the South Pacific and Indian Oceans and with Bering Strait throughput in the Atlantic and Pacific (see Sections 5 and 6; Figs. 7 and 11 and Tables 6–8), and (4) mass-balanced, zonally integrated overturn between isopycnal layers (see Section 7; Figs. 12–14 and Tables 9–16).

Separation of components (2) and (3) was described in Talley (2003). In brief, the maximum subduction density for each subtropical gyre was determined from the maximum winter surface density along the zero wind stress curl curve (densities listed in Table 5 and shown in Fig. 7). Transports were computed from the surface down to this maximum subduction density, including the Ekman, western boundary current and interior transports. Mass was balanced using only as much of the surface layer western boundary current transport as was necessary to balance the Ekman

Table 3
Freshwater transport divergence (1 Sv = 1 × 10^6 m^3/s), from Table 2 (Fig. 4), NCEP (1979–2005) annual mean surface fluxes integrated over the enclosed surface area, runoff into each area (Dai and Trenberth, 2002), and the sum of NCEP and runoff

Region	FW transport divergence based on Table 2, column 3 (MSv)	NCEP air-sea flux (annual mean 1979–2005) (Sv)	Runoff (Dai and Trenberth, 2002) (Sv)	Sum of NCEP flux and runoff (Sv)	Ocean surface area (10^{13} m^2)
Arctic and Atlantic north of 59°N	0.52 ± 0.24	0.15	0.16	0.31	1.79
Atlantic 53–59°N	−0.21 ± 0.26	0.03	0.04	0.07	0.20
Atlantic 45–53°N	0.00 ± 0.17	0.03	0.05	0.08	0.25
Atlantic 36–45°N	0.02 ± 0.14	−0.03	0.01	−0.02	0.65
Atlantic 24–36°N+Med.	−0.05 ± 0.15	−0.23	0.03	−0.20	1.17
(Mediterranean)	(−0.2) (Ochoa and Bray, 1991)	(−0.06)	–	(−0.06)	0.35
Atlantic 16°S–24°N	−0.10 ± 0.15	−0.56	0.43	−0.13	3.01
Atlantic 24–16°S	−0.35 ± 0.06	−0.16	0.01	−0.15	0.52
Atlantic 32–24°S	−0.12 ± 0.05	−0.08	0.01	−0.07	0.40
Pacific 47°N to Bering Strait	0.11 ± 0.03	0.18	0.08	0.26	0.82
Pacific 35–47°N	0.04 ± 0.05	0.14	0.03	0.17	1.05
Pacific 24–35°N	0.04 ± 0.06	−0.27	0.04	−0.23	1.46
Pacific 10–24°N	−0.40 ± 0.07	−0.32	0.05	−0.27	2.46
Pacific 28°S–10°N with ITF	0.26 ± 0.09	0.10	0.07	0.17	6.77
Pacific 43–28°S	−0.11 ± 0.09	−0.11	0.01	−0.10	1.92
Arabian Sea north of 8°N	−0.54 ± 0.06 (−0.50 ± 0.06)	−0.15	–	−0.15	0.43
Bay of Bengal north of 8°N	0.05 ± 0.16 (−0.07 ± 0.16)	0.02	0.08	0.1	0.23
Indian 8°S–8°N with ITF	0.85 ± 0.23 (0.84 ± 0.23)	0.16	0.02	0.18	1.89
Indian 20–8°S	−0.43 ± 0.16 (−0.34 ± 0.16)	−0.11	0.03	−0.08	0.92
Indian 32–20°S	−0.31 ± 0.09	−0.39	0.01	−0.38	0.98
Antarctic	0.72 ± 0.10	0.71	0.06	0.77	9.07
(Antarctic: Atlantic sector 32°S)[a]	0.21 ± 0.04	0.18	0.03	0.21	–
(Antarctic: Pacific sector 43°S)[a]	0.23 ± 0.04	0.38	0.00	0.38	–
(Antarctic: Indian sector 32°S)[a]	0.26 ± 0.08	0.15	0.03	0.18	–
Sum all positive values in bands (precipitation and runoff)	2.61	1.52	1.22	2.74	–
Sum all negative values in bands (evaporation)	−2.62	−2.41	–	−2.41	–
Total sum	−0.01	−0.90	1.22	0.32[b]	33.30

Bering Strait freshwater transport component is 0.07 FSv. Positive is net precipitation or runoff; negative is net evaporation.
[a] These sum to the Antarctic total. Within each line the sum is mass-balanced freshwater transport (MSv) plus ITF/Bering Strait freshwater transport (FSv) (Table 2). When summed over all three oceans, the ITF/Bering Strait transports are also mass-balanced.
[b] NCEP-alone imbalance for ocean plus land is 0.03 Sv.

Table 4
Comparison of total freshwater divergences (MSv) with Ganachaud and Wunsch (2003)

Region	Latitude range	GW03 (MSv)	This estimate (MSv)	NCEP/DT02 (Sv)
Arctic/North Atlantic/North Pacific	>45–47°N	0.4	0.42 ± 0.13	0.72
Atlantic	24–45°N	0 ± 0.15	−0.03 ± 0.19	−0.22
	19°S–24°N (GW03) 16°S–24°N	−0.1 ± 0.2	−0.10 ± 0.15	−0.13
	30–19°S (GW03) 32–16°S	−0.36 ± 0.2	−0.46 ± 0.06	−0.22
Indian	>8°S	0.1 ± 0.25	0.36 ± 0.16	0.13
	20–8°S	−0.33 ± 0.2	−0.43 ± 0.16	−0.08
	32–20°S	−0.35 ± 0.3	−0.31 ± 0.10	−0.38
Pacific	24–47°N	0.14 ± 0.26	0.08 ± 0.06	−0.06
	30°S–24°N	−0.2 ± 0.3	−0.14 ± 0.09	−0.10
Antarctic	<30°S	0.8 ± 0.9	0.61 ± 0.13	0.67

Positive is net precipitation and runoff; negative is net evaporation (Fig. 4b).

and interior transports, in all but the South Atlantic. In the South Atlantic, the extra mass transport in the surface layer resides in the eastern boundary current (Benguela Current) and so the partition for mass balance was somewhat different (Section 4.2). To calculate intermediate and deep water overturns, the shallow mass-balanced transports (and ITF transports if applicable) were removed, and then it was assumed that transformation occurs to the neighboring isopycnal layers rather than to more remote layers.

The total freshwater transport component associated with 10 Sv of ITF transport at salinity 34.5 is 0.11 FSv from the Pacific to the Indian, relative to the reference salinity of 34.9. This was incorporated in the divergences between the Pacific 10°N and 28°S sections, and between the Indian 8°N and 8°S sections. The 10 Sv of the ITF is assumed to be in the upper layer of the Agulhas in the Indian Ocean (32°S and 20°S sections) (Bryden and Beal, 2001), and not in the Leeuwin Current (as substantiated by Domingues et al., 2007), and in the upper (subducting) layer flowing northward in the interior South Pacific (Wijffels et al., 2001), choices substantiated by the layer transport profiles in Sections 5 and 7.

2.3. Uncertainties and error estimates

Many different types of calculations and estimates are involved in this global freshwater balance, each with its own sources of uncertainty and own error estimate. Sources of uncertainty are listed here and described in detail through the text. A Monte Carlo approach to error estimation for the Ekman and geostrophic components of the freshwater transports is described here and used for error estimates listed in the tables throughout.

Mass transports must be almost exactly balanced for the freshwater transport calculations; mass transport results are reported

Table 5
Shallow overturning volume, heat and freshwater transports using NCEP winds

Section	Maximum subducted density	(1) Ekman volume, FW, temperature transports (Sv, FSv and PWT) and mean salinity	(2) Shallow interior geostrophic volume, FW, temperature transports (Sv, FSv and PWT) and mean salinity	(3) Assumed ITF/BS portion of upper layer geostrophic transport (see text)	(4) Total shallow WBC volume, FW, temperature transports (Sv, FSv and PWT) and mean salinity	Density for WBC volume transport balancing Ekman and interior	(5) WBC volume, FW, temperature transports (Sv, FSv and PWT) and mean salinity for water lighter than dividing density	Mass-balanced shallow overturning gyre: circulating volume transport (Sv), FW transport (MSv) and heat transport (PW)
Atlantic 24°N	$27.3\sigma_\theta$	4.82 ± 0.10 Sv −0.288 ± 0.009 FSv 0.46 PWT 36.81 psu	−18.58 ± 1.95 Sv 1.025 ± 0.0932 FSv −1.54 PWT 36.184 psu	–	29.06 Sv −1.096 ± 0.370 FSv 2.44 PWT 36.085 psu	$25.9\sigma_\theta$	13.77 ± 2.47 Sv −0.572 ± 0.159 FSv 1.46 PWT 36.326 psu	(1) + (2) + (5) 18.6 ± 3.15 Sv 0.165 ± 0.185 MSv 0.38 PW
Atlantic 24°N alternate: Gulf Stream heat & FW proportional to total shallow Gulf Stream properties	$27.3\sigma_\theta$	4.82 ± 0.10 Sv −0.288 ± 0.009 FSv 0.46 PWT 36.81 psu	−18.58 ± 1.95 Sv 1.025 ± 0.0932 FSv −1.54 PWT 36.184 psu	–	29.06 Sv −1.096 ± 0.370 FSv 2.44 PWT 36.085 psu	No dividing density: proportional transports in Gulf Stream	13.77 ± 2.47 Sv −0.519 ± 0.158 FSv 1.15 PWT 36.085 psu	(1) + (2) + (5) 18.6 Sv 0.218 ± 0.185 MSv 0.08 PW
Atlantic 32°S	$26.2\sigma_\theta$ (local outcrop density)	1.15 ± 0.23 Sv −0.026 ± 0.008 FSv 0.09 PWT 35.865 psu	9.24 ± 0.48 Sv −0.129 ± 0.018 FSv 0.61 PWT 35.704 psu	–	−6.16 ± 0.46 Sv 0.286 ± 0.027 FSv −0.53 PWT 36.471 psu	Benguela 4.23 ± 0.24 Sv −0.057 ± 0.004 FSv 0.28 PWT 35.344 psu	Interior (2) without Benguela 5.01 ± 0.48 Sv −0.072 ± 0.018 FSv 0.33 PWT 35.747 psu	(1) + (4) + (5) 6.2 ± 0.6 Sv 0.188 ± 0.024 MSv −0.10 PW
Atlantic 32°S	$26.4\sigma_\theta$ (local outcrop density)	1.15 ± 0.23 Sv −0.026 ± 0.008 FSv 0.09 PWT 35.865 psu	9.71 ± 0.68 Sv −0.129 ± 0.022 FSv 0.63 PWT 35.635 psu	–	−7.57 ± 0.59 Sv 0.317 ± 0.030 FSv −0.62 PWT 36.273 psu	Benguela 3.29 ± 0.33 Sv −0.041 ± 0.005 FSv 0.21 PWT 35.320 psu	Interior (2) without Benguela 6.42 Sv −0.088 ± 0.030 FSv 0.42 PWT 35.747 psu	(1) + (4) + (5) 7.6 ± 0.9 Sv 0.203 ± 0.030 MSv −0.11 PW
Pacific 24°N	$26.2\sigma_\theta$	8.62 ± 0.28 Sv −0.033 ± 0.012 FSv 0.82 PWT 34.832 psu	−31.42 ± 1.64 Sv −0.214 ± 0.024 FSv −2.21 PWT 34.601 psu	–	23.40 Sv 0.169 FSv 1.97 PWT 34.727 psu	$26.12\sigma_\theta$	22.80 ± 0.61 Sv 0.161 ± 0.009 FSv 1.94 PWT 34.612 psu	(1) + (2) + (5) 31.4 ± 1.8 Sv −0.086 ± 0.028 MSv 0.55 PW
Pacific 24°N alternate: Hellerman and Rosenstein (1983) winds	$26.2\sigma_\theta$	11.34 Sv −0.048 FSv 1.08 PWT 34.832 psu	−31.65 Sv −0.214 ± 0.024 FSv −2.23 PWT 34.601 psu	–	23.40 Sv 0.169 FSv 1.97 PWT 34.727 psu	$26.12\sigma_\theta$	20.31 Sv 0.146 FSv 1.71 PWT 34.612 psu	(1) + (2) + (5) 31.7 Sv −0.116 MSv 0.56 PW
Pacific 28°S	$27.1\sigma_\theta$	−3.21 ± 0.57 Sv 0.055 ± 0.013 FSv −0.28 PWT 35.473 psu	33.33 ± 5.73 Sv −0.190 ± 0.035 FSv 1.93 PWT 34.962 psu west of 110°W	11.00 Sv −0.063 ± 0.015 FSv 0.64 PWT In interior 34.962 psu	−23.99 Sv 0.261 ± 0.032 FSv −1.53 PWT 35.135 psu	$26.80\sigma_\theta$	−19.12 ± 0.67 Sv 0.302 ± 0.012 FSv −1.36 PWT 35.406 psu	(1) + (2) − (3) + (5) 22.3 ± 5.8 Sv 0.230 ± 0.037 MSv −0.35 PW
Pacific 28°S ITF and BS loops within Pacific	–	–	–	10.00 Sv −0.057 ± 0.015 FSv 0.58 PWT 34.847 psu 1.00 Sv −0.006 ± 0.003 FSv 0.06 PWT 34.847 psu	–	–	ITF outflow −10.00 Sv −0.11 ± 0.05 FSv −0.50 PWT 34.5 psu – BS outflow −1.00 Sv −0.07 ± 0.02 FSv 0.00 PWT 32.5 psu	(3) + (5) 10 Sv −0.16 ± 0.052 MSv 0.08 PW Due to ITF 1 Sv −0.08 ± 0.02 MSv 0.06 PW Due to BS
Indian 32°S	$26.9\sigma_\theta$	0.82 ± 0.30 Sv −0.015 ± 0.007 FSv 0.06 PW 35.637 psu	37.70 ± 3.37 Sv −0.262 ± 0.015 FSv 1.93 PWT 35.159 psu	−10.00 Sv 0.116 ± 0.002 FSv −0.60 PWT In Agulhas 35.301 psu	−49.5 Sv 0.571 ± 0.009 FSv −2.96 PWT 35.301 psu	$26.88\sigma_\theta$	−48.52 ± 3.32 Sv 0.575 ± 0.009 FSv −2.92 PWT 35.309 psu	(1) + (2) − (3) + (5) 37.7 ± 5.5 Sv 0.182 ± 0.019 MSv −0.33 PW
Indian 32°S ITF loop within Indian	–	0	0	−10.00 Sv 0.116 ± 0.002 FSv −0.60 PWT In Agulhas 35.301 psu	–	–	ITF inflow 10.00 Sv 0.11 ± 0.05 FSv 0.50 PWT 34.5 psu	(3) + (5) 10 Sv 0.23 ± 0.05 MSv −0.10 PWT

Units FSv and PWT indicate freshwater and temperature transports for non-mass-balanced components. Units PW and MSv indicate units for mass-balanced components, and are independent of reference temperature or salinity for the component calculations. Reference salinity for freshwater transports is 34.9. Reference temperature for temperature transports is 0 °C.

Table 6
Sensitivity of Indian 32°S and Pacific 28°S freshwater transports to different values of ITF transport, after Table 2

Section	Total volume transport (ITF + Bering Strait) (Sv)	Geostrophic volume transport (Sv)	Raw freshwater transport components				Total	Mass-balanced freshwater transport components				
			(1) Geostrophic FW transport (FSv)	(2) Ekman FW transport (FSv) (Table 2)	(3) FW transport through ITF (FSv)	(4) FW transport through Bering Strait (Pacific only) (FSv)	(5) Total FW divergence north of section (MSv); (1) + (2) + (3) + (4) or, equally, (6) + (8) + (9) + (10)	(6) Shallow overturning gyre FW transport (MSv)	(7) ITF FW transport components through zonal section (FSv)	(8) ITF contribution to FW transport divergence north of section (MSv); (3) + (7)	(9) Bering Strait contribution to FW transport divergence north of section (MSv)	(10) Deep overturning FW transport (MSv)
Uncertainty (FSv)			±0.08	±0.01	±0.05	±0.02	±0.09					
Pacific 28°S	9.0	12.20	0.07	0.05	−0.09	−0.06	−0.03	0.21	−0.04	−0.13	−0.07	−0.04
Indian 32°S	−8.0	−8.82	0.28	−0.01	0.09	–	0.36	0.18	0.09	0.18	–	0.0
Pacific 28°S	11.0	14.20	0.08	0.05	−0.11	−0.06	−0.04	0.23	−0.05	−0.16	−0.07	−0.04
Indian 32°S	−10.0	−10.82	0.27	−0.01	0.11	–	0.37	0.18	0.12	0.23	–	−0.04
Pacific 28°S	13.0	16.20	0.09	0.05	−0.14	−0.06	−0.06	0.25	−0.06	−0.20	−0.07	−0.04
Indian 32°S	−12.0	−12.82	0.26	−0.01	0.14	–	0.39	0.17	0.12	0.26	–	−0.04
Pacific 28°S	15.0	18.20	0.11	0.05	−0.16	−0.06	−0.06	0.26	−0.07	−0.23	−0.07	−0.02
Indian 32°S	−14.0	−14.82	0.26	−0.01	0.16	–	0.41	0.17	0.11	0.27	–	−0.03

Table 7
Bering Strait contribution to freshwater transport, calculated relative to salinity 34.9

Section	Transport (Sv) due to Bering Strait	Salinity			Freshwater transport (FSv) due to BS			Section FW transport (FSv) (Table 2)	Total FW transport (MSv) after removal of BS at mean salinity
		Mean salinity	Minimum salinity	Maximum salinity	At mean salinity	At minimum salinity	At maximum salinity		
Bering Strait[a]	1	32.5	31.7	33.1	0.07	0.09	0.05	0.07	–
Atlantic 59°N	−1	34.987	33.034	35.390	0.003	−0.053	0.014	−0.59	−0.59
Atlantic 53°N	−1	34.955	33.114	35.521	0.002	−0.051	0.018	−0.38	−0.38
Atlantic 45°N	−1	35.041	33.065	35.918	0.004	−0.053	0.029	−0.38	−0.38
Atlantic 36°N	−1	35.219	33.321	36.680	0.010	−0.045	0.051	−0.40	−0.41
Atlantic 24°N	−1	35.163	34.845	37.655	0.008	−0.002	0.079	−0.33	−0.34
Atlantic 16°S	−1	34.898	33.795	37.341	−0.000	−0.032	0.070	−0.25	−0.25
Atlantic 24°S	−1	34.870	34.325	36.913	−0.001	−0.016	0.058	0.09	0.09
Atlantic 32°S	−1	34.797	34.242	36.913	−0.003	−0.019	0.058	0.21	0.21
Pacific 47°N	1	34.475	32.177	34.690	0.012	0.078	0.006	−0.04	−0.05
Pacific 35°N	1	34.532	32.728	34.893	0.011	0.062	0.002	−0.07	−0.08
Pacific 24°N	1	34.574	33.382	35.460	0.009	0.043	−0.016	−0.12	−0.13
Pacific 10°N	1	34.632	33.685	35.152	0.008	0.034	−0.007	0.28	0.27
Pacific 28°S	1	34.670	34.165	35.914	0.007	0.021	−0.029	0.13	0.12[b]
Pacific 43°S	1	34.578	33.404	35.520	0.009	0.043	−0.018	0.24	0.23[b]

[a] Minimum and maximum mean salinities from 20 mooring records 1991–1994 (Roach et al., 1995), excluding the small, fresher transport of the Alaska Coastal Current (Woodgate and Aagaard, 2005).
[b] In FSv since 10 Sv of ITF has not been removed. ITF of 10 Sv contributes −0.06 FSv at 28°S and 0.15 FSv at 43°S.

Table 8
Sensitivity of NADW and NPIW freshwater balances north of 45–47°N to Bering Strait (BS) transport

	M_{BS} (Sv)	S_{BS}	M_{upper} (Sv)	S_{upper}	$M_{NPIW,NADW}$ (Sv)	$S_{NPIW,NADW}$	M_{ASF}
North Atlantic NADW							
Base state	1	32.5	18	36	**19.44**	35	**0.44**
No BS, set inflow, set ΔS	0	32.5	18	36	**18.51**	35	**0.51**
No BS, set inflow, set air-sea flux	0	32.5	18	36	**18.44**	**35.14**	0.44
Set BS, set inflow, set air-sea flux	0.5	32.5	18	36	**18.94**	**35.07**	0.44
No BS, set ΔS, set air-sea flux	0	32.5	**15.44**	36	**15.88**	35	0.44
No air-sea flux, set overturn, set ΔS	**7.2**	32.5	18	36	**25.2**	35	0
North Pacific NPIW							
Base state	1	32.5	3.5	34.7	**2.61**	34.1	**0.11**
No BS, set inflow, set ΔS	0	32.5	2.5	34.7	**2.54**	34.1	**0.04**
No BS, set inflow, set air-sea flux	0	32.5	2.5	34.7	**2.61**	**33.24**	0.11
Set BS, set inflow, set air-sea flux	0.5	32.5	3.0	34.7	**2.61**	**33.66**	0.11
No BS, set ΔS, set air-sea flux	0	32.5	**6.25**	34.7	**6.36**	34.1	0.11
No air-sea flux, set overturn, set ΔS	**−0.9**	32.5	2.5	34.7	**3.4**	34.1	0

Bold: calculated values. Plain text: assigned values.

Table 9
North Atlantic (24°N) zonally averaged overturns

Layer	Freshwater transport (MSv) Heat transport (PW) (mass-balanced)	Layer volume transport (Sv), freshwater transport (FSv) relative to salinity 34.9, emperature transport (PWT), mean salinity of layer (psu)	Volume and total freshwater (MSv) and heat (PW) transports from conversion to LSW/NADW north of section
Total freshwater and heat transports (Table 2)	−0.357 ± 0.139 MSv 1.22 PW 35.163 psu	–	–
Shallow overturning layer (Table 5)	18.58 Sv closed circulation 0.165 ± 0.185 MSv 0.38 PW	–	–
Net intermediate–deep overturning heat transport	−0.522 MSv 0.84 PW	–	−0.522 ± 0.014 MSv 0.84 PW
Surface to 27.3σ_θ minus shallow overturn (thermocline)	–	15.29 Sv −0.524 ± 0.015 FSv 0.98 PWT 36.183 psu	6.83 Sv −0.234 ± 0.009 MSv 0.34 PW To LSW 8.47 Sv −0.290 ± 0.009 MSv 0.46 PW To NADW
27.3–27.74σ_θ (AAIW/UCDW/MOW)	–	2.53 ± 1.56 Sv −0.026 ± 0.006 FSv 0.09 PWT 35.129 psu	2.53 Sv −0.026 ± 0.006 MSv 0.09 PW To NADW
27.74σ_θ–36.96σ_2 (LSW)	–	−6.83 ± 1.93 Sv 0.007 ± 0.006 FSv −0.097 PWT 35.066 psu	–
36.96σ_2–45.91σ_4 (NSOW/NADW)		−18.96 ± 7.38 Sv 0.011 ± 0.007 FSv −0.175 PWT 34.929 psu	–
Bering Strait throughput in NADW layer	–	−1.00 Sv 34.929 psu	Remove from NADW layer balance
45.91σ_4 to bottom (AABW)	–	6.96 ± 1.08 Sv 0.009 ± 0.001 FSv 0.04 PWT 34.856 psu	6.96 Sv 0.013 ± 0.003 MSv −0.02 PW To NADW

herein to one to two decimal places even though uncertainties are larger because mass balance carried through the calculations requires the higher precision. (Actual computations were carried out at higher precision.) Freshwater transport components significant for salinity redistribution range from tenths to thousandths of Sverdrups, with comparably varying uncertainties. They are listed throughout the tables to thousandths for overall consistency, since the smallest significant values, obtained for deep transports, are of this order based on the Monte Carlo error estimates.

Uncertainties due to assumptions about the ITF transport and geographic location of this transport through the Pacific 28°S and Indian 32°S sections are discussed in Section 5.2. The resulting freshwater transport uncertainty for the ITF loops in the Pacific and Indian Oceans is ±0.05 MSv or less compared with a magnitude of about 0.2 MSv.

Uncertainties due to assumptions about BS transport and salinity, and due to assumptions of geographic location of the 1 Sv throughput on each zonal section, are discussed in Section

Table 10
South Atlantic (32°S) zonally averaged overturns

Layer	Freshwater transport (MSv), heat transport (PW)	Layer volume transport (Sv), freshwater transport (FSv) relative to salinity 34.9, temperature transport (PWT), mean salinity	Volume and total freshwater (MSv) and heat (PW) transports from conversion to NADW north of section
Total mass, freshwater and heat transports (Table 2)	−1.0 Sv 0.215 ± 0.036 FSv 0.25 PWT 34.797 psu	–	–
Shallow overturning to 26.4σ_θ (Table 5)	7.57 Sv closed circulation 0.203 ± 0.055 MSv −0.11 PW	–	–
Bering Strait throughput in NADW layer	−1.00 Sv 0.002 ± 0.001 FSv −0.01 PWT	–	–
Net intermediate–deep overturning	0.010 MSv 0.37 PW	–	0.012 ± 0.017MSv 0.37 PW
Surface to 26.4σ_θ minus shallow overturn (thermocline)	–	3.29 Sv −0.041 ± 0.010 FSv 0.21 PWT 35.680 (full layer) 35.320 (Benguela only)	3.29 Sv −0.047 ± 0.011 MSv 0.17 PW Benguela Current to NADW
26.4–26.9σ_θ (lower thermocline)	–	4.30 ± 1.28 Sv 0.003 ± 0.005 FSv 0.20 PWT 35.086 psu	−0.004 ± 0.007 MSv 0.15 PW To NADW
26.9–27.4σ_θ (AAIW)	–	5.18 ± 2.39 Sv 0.066 ± 0.007 FSv 0.13 PWT 34.400 psu	0.057 ± 0.009 MSv 0.07 PW To NADW
27.4σ_θ–45.86σ_4 (NADW and UCDW)	–	−17.63 ± 8.13 Sv −0.030 ± 0.019 FSv −0.20 PWT 34.770 psu	
Bering Strait throughput	–	−1.00 Sv −0.002 ± 0.001 FSv −0.01 PWT 34.770 psu	Assumed to flow through in NADW layer
45.86σ_4 to bottom (LCDW/AABW)	–	3.85 ± 1.80 Sv 0.014 ± 0.003 FSv 0.02 PWT 34.819 psu	0.008 ± 0.005 MSv −0.03 PW To NADW

6. The result is ±0.02 MSv compared with a magnitude of 0.06 MSv.

Uncertainties for freshwater transport associated with the shallow overturning circulation that depend on specific choices of which portions of the western boundary currents to use to balance the interior thermocline circulation are discussed for each zonal subtropical hydrographic section in Section 4. The results are generally ±0.05 MSv.

Uncertainty for the Ekman component of volume and freshwater transports was estimated using Monte Carlo simulation, assuming a normal distribution of error in Ekman transport and salinity. The assigned Ekman transport error was taken to be the standard deviation of the climatological monthly means about the annual mean transport calculated at the location of each station pair from the NCEP reanalysis winds. The mean standard deviation was then calculated from all of the stations for a given section and used in the Monte Carlo simulation. The Levitus salinity field was already an annual mean, so its assigned error was estimated as the standard deviation for each section from the geographic mean for that section. This is likely an overestimate for many sections that have a large geographic range in salinity. The Monte Carlo simulation then produced a mean and standard deviation for mass and freshwater transport, based on 100,000 iterations. The errors thus produced are listed in the tables. The mean standard deviation in Ekman transport is ±0.4 Sv, or 10% of the Ekman transport (which can be derived from the assigned transport error without the Monte Carlo simulation). Within the Indian Ocean the standard deviations are much larger percentages, 30–60%, because of the large annual monsoon cycle in the winds. The mean standard deviation for the Ekman component of freshwater transport is ±0.02 FSv, or 25% (20% if the Indian Ocean is excluded). To check sensitivity to choice of salinity error in the Monte Carlo simulation, the assigned salinity standard deviations, which average 0.43 calculated relative to the geographic mean along the given section, were reduced to 0.01. The mean standard deviation for Ekman freshwater transport from the Monte Carlo estimate was then ±0.01 FSv, or 16%. So a reasonable estimate of overall Ekman freshwater transport error is ±0.01 to 0.02 FSv.

For the geostrophic component of the transports, which are the major contribution to error, absolute geostrophic reference velocities for station pairs were provided by Reid (1994, 1997, 2003), based on overall mass transport constraints and adjustment of each station pair velocity to yield a physically reasonable circulation based on property distributions. These Reid reference velocities do not have explicit error estimates, unlike the output of inverse models (e.g. Macdonald, 1998; GW03; SR2001). In our

Table 11
North Pacific (24°N) zonally averaged overturns

Layer	Freshwater transport (MSv), heat transport (PW) (mass-balanced)	Layer volume transport (Sv), freshwater transport (FSv) relative to 34.9 psu, temperature transport (PWT), mean salinity	Volume, heat and FW transport from mass-balanced conversion to NPIW/PDW
Total freshwater and heat transports with BS removed (Table 2)	−0.138 ± 0.046 MSv 0.59 PW	–	–
Shallow overturning layer (Table 5)	31.42 Sv closed circulation −0.086 ± 0.028 MSv 0.55 PW	–	–
Net intermediate–deep overturning transports including BS	−0.052 MSv 0.04 PW	–	−0.052 ± 0.019 MSv 0.04 PW
Surface to 26.2σ_θ minus shallow overturn (thermocline)	–	0.59 Sv 0.007 ± 0.016 FSv 0.03 PWT 34.725 psu	0.59 Sv −0.017 ± 0.016 MSv 0.02 PW To NPIW
26.2–26.9σ_θ (NPIW)	–	−2.41 ± 0.61 Sv −0.098 ± 0.005 FSv −0.05 PWT 34.142 psu	–
26.9–27.6σ_θ (NPIW/AAIW/UCDW)	–	4.80 ± 2.23 Sv 0.060 ± 0.010 FSv 0.08 PWT 34.450 psu	1.00 Sv 0.009 ± 0.020 FSv 0.02 PW to Bering Strait (thus total divergence of −0.05 MSv) 1.82 Sv −0.051 ± 0.005 MSv −0.01 PW To NPIW (upward) 0.38 Sv 0.004 ± 0.007 MSv 0.004 PW To PDW1 1.60 Sv 0.010 ± 0.004 MSv 0.02 PW To PDW3
27.6σ_θ–36.96σ_2 (PDW1)	–	−0.38 ± 2.13 Sv −0.001 ± 0.007 FSv −0.002 PWT 34.620 psu	–
36.96σ_2–45.84σ_4 (PDW2)	–	1.19 ± 1.73 Sv 0.008 ± 0.006 FSv 0.007 PWT 34.663 psu	1.19 Sv 0.000 ± 0.007 MSv 0.001 PW To PDW3
45.84–45.88σ_4 (PDW3)	–	−5.56 ± 2.28 Sv −0.035 ± 0.009 FSv −0.03 PWT 34.680 psu	–
45.88σ_4 to bottom (LCDW)	–	2.77 ± 1.24 Sv 0.017 ± 0.006 FSv 0.01 PWT 34.690 psu	2.77 Sv 0.000 ± 0.007 MSv −0.002 PW To PDW3

previous publications using the Reid analyses (Talley, 1999, 2003; Talley et al., 2003), we therefore did not include error estimates. A thorough exploration of geostrophic reference velocity error requires implementation of a full box inverse model that would allow adjustment of individual reference velocities subject to overall mass transport constraints. This has not been undertaken; however, a Monte Carlo estimate of uncertainty has been applied, including a simplified version of the mass transport constraint.

The Monte Carlo estimate requires an input geostrophic reference velocity error and salinity error for each station pair and assumes a normal distribution of error. Since the uncertainty is calculated only for the given synoptic sections, and is not an estimate of the representativeness of the given sections, by far the largest uncertainty comes from the reference velocity error, and not from error in the observed geostrophic shear, so only one (reference) velocity error is applied for each station pair. The estimated standard deviation σ_{fw} in the geostrophic component of each section's freshwater transport is

$$\sigma_{\mathrm{fw}} = \sqrt{\sum_{i=1,m}\sum_{j=1,k} L_{ij}L_{ij}/km}$$
$$L_{ij} = \varepsilon_{Mj}M_i'\left(1 - \frac{S_i + \varepsilon_{sj}S_i'}{S_{\mathrm{o}}}\right) - M_i\frac{\varepsilon_{ij}S_i'}{S_{\mathrm{o}}} \qquad (5\mathrm{a,b})$$

where m is the number (index i) of station pairs for the section, k is the number (index j) of Monte Carlo iterations (k = 100,000 here), M_i' is the estimated station mass transport error for a given estimate of reference velocity error and station pair area, M_i is station pair mass transport, S_i' is the estimated salinity error, S_i is the mean salinity for the station pair, S_{o} is the mean salinity for all of the

Table 12
South Pacific (28°S) zonally averaged overturns

Layer	Volume (Sv), freshwater (FSv or MSv) and heat (PWT or PW) transports	Volume, freshwater relative to 34.9 and temperature transports (Sv, FSv, PWT), and mean salinity	Volume overturn, freshwater and heat transports (Sv, MSv, PW) from conversion to PDW, AAIW and thermocline
Total transports including mass-balanced ITF and BS (divergences for full Pacific) (Table 2)	−0.044 ± 0.094 MSv −0.43 PW 34.670 psu	–	–
Total transports without balancing mass in ITF and BS (Table 2)	11 Sv 0.136 ± 0.077 FSv 0.01 PWT		
Shallow overturning gyre (Table 5)	22.3 Sv closed circulation 0.230 ± 0.037 MSv −0.35 PW	–	–
ITF (including archipelago as part of section) (Table 5)	10 Sv closed circulation in upper layer −0.167 ± 0.052 MSv 0.08 PW	–	–
Bering Strait (including strait as part of section) (Table 5)	1 Sv closed circulation −0.066 ± 0.02 MSv 0.06 PWT	–	
Net intermediate and deep overturning	−0.031 MSv −0.22 PW	–	−0.031 ± 0.029 MSv −0.22 PW
Surface to 27.1σ_θ minus shallow overturn and ITF/BS (thermocline)	–	−4.87 Sv −0.037 ± 0.028 FSv −0.16 PWT 34.904 psu	
27.1–27.6σ_θ (AAIW or PDW1)	–	−2.77 Sv −0.021 ± 0.013 FSv −0.06 PWT 34.473 psu	–
27.6σ_θ–36.96σ_2 (PDW2)	–	−5.24 Sv −0.039 ± 0.013 FSv −0.04 PWT 34.644 psu	–
36.96σ_2–45.84σ_4 (PDW3)	–	−0.94 Sv −0.006 ± 0.007 FSv −0.01 PWT 34.686 psu	–
45.84–45.88σ_4 (LCDW1)	–	3.41 Sv 0.021 ± 0.004 FSv 0.02 PWT 34.709 psu	3.41 Sv −0.007 ± 0.019 MSv −0.10 PW To thermocline
45.88–45.92σ_4 (LCDW2)	–	1.60 Sv 0.008 ± 0.003 FSv 0.01 PWT 34.717 psu	1.46 Sv −0.004 ± 0.009 MSv −0.04 PW To thermocline 0.15 Sv −0.000 ± 0.001 MSv −0.00 PW To AAIW/PDW1
45.92σ_4 to bottom (LCDW3)	–	8.81 Sv 0.046 ± 0.008 FSv 0.03 PWT 34.720 psu	2.63 Sv −0.006 ± 0.013 MSv −0.04 PW To AAIW/PDW1 −5.24 Sv −0.012 ± 0.014 MSv −0.05 PW To PDW2 −0.94 Sv −0.000 ± 0.007 MSv −0.00 PW To PDW3

freshwater calculations (34.9 herein), and ε_{Mj}, ε_{sj} and ε_{Ij} are normally distributed random numbers with zero mean. The first term in (5b) is the dominant term, and is the reference velocity uncertainty times the salinity expression, including its uncertainty. The second term in (5b) is the salinity uncertainty times the total mass transport of the station pair. The second term was derived from the full vertical integral over the water column of the calculated velocity times a salinity error at each depth; this was integrated by parts and it was assumed that the vertical derivative of the salinity error was also a product of the assigned salinity error times normally distributed random numbers with zero mean. The mean difference over all sections in freshwater transport uncertainty between calculations with and without this last term was 0.007 FSv, so it is a small correction.

Table 13
Indian (32°S and ITF crossing) zonally averaged overturns

Layer	Volume transport (Sv), freshwater transport (FSv, MSv) and heat transport (PWT, PW)	Volume transport (Sv), component freshwater transports relative to 34.9 psu (FSv) and component temperature transports (PWT), layer mean salinity (psu)	Freshwater transport (MSv) and heat transport (PW) from upwelling north of the section
Total transports including mass-balanced ITF (divergences for full Indian) (Table 2)	0 Sv 0.367 ± 0.099 MSv −0.83 PW 34.756 psu	–	–
Total transports without balancing mass in ITF (Table 2)	−10 Sv 0.257 ± 0.085 FSv −1.33 PWT		
Shallow overturning gyre (Table 5)	37.7 Sv closed circulation 0.182 ± 0.019 MSv −0.33 PW	–	–
ITF (Table 5)	10 Sv closed circulation 0.226 ± 0.052 MSv −0.10 PW 34.5 psu	–	–
Net intermediate and deep overturning	−0.041 MSv −0.40 PW	–	−0.041 ± 0.025 MSv −0.40 PW
Surface to 26.9σ_θ minus shallow overturn and ITF (thermocline)	–	−0.71 Sv 0.003 ± 0.000 FSv −0.04 PWT 35.172 psu	–
26.9–27.1σ_θ (SAMW/upper AAIW)	–	−2.62 ± 0.87 Sv 0.001 ± 0.003 FSv −0.10 PWT 34.552 psu	–
27.1–27.3σ_θ (AAIW)	–	−4.64 ± 1.07 Sv −0.034 ± 0.004 FSv −0.12 PWT 34.417 psu	–
27.3σ_θ–36.65σ_2 (IDW and lower AAIW)	–	−6.66 ± 1.63 Sv −0.062 ± 0.005 FSv −0.12 PWT 34.476 psu	–
36.65–36.89σ_2 (IDW)	–	−1.89 ± 2.76 Sv −0.015 ± 0.008 FSv −0.03 PWT 34.631 psu	–
36.89σ_2–45.88σ_4 (NADW & CDW1)	–	6.83 ± 5.23 Sv 0.020 ± 0.011 FSv 0.06 PWT 34.736 psu	0.71 Sv 0.003 ± 0.020 MSv −0.03 PW upwell to surface layer 2.62 Sv 0.009 ± 0.005 MSv −0.07 PW upwell to SAMW 3.50 Sv −0.015 ± 0.006 MSv −0.06 PW upwell to AAIW
45.88–46.0σ_4 (CDW2)	–	9.86 ± 4.73 Sv 0.051 ± 0.014 FSv 0.04 PWT 34.721 psu	1.14 Sv −0.002 ± 0.002 MSv −0.03 PW upwell to AAIW 6.66 Sv −0.027 ± 0.010 MSv −0.09 PW upwell to IDW/lower AAIW 1.89 Sv −0.005 ± 0.008 MSv −0.02 PW upwell to IDW/lower AAIW 0.16 Sv 0.000 ± 0.017 MSv 0.00 PW downwell to CDW3
46.0σ_4 to bottom (CDW3)	–	−0.16 ± 3.00 Sv 0.000 ± 0.017 FSv −0.002 PWT 34.697 psu	

Table 14
Southern Ocean zonally averaged overturns (32°S in the Atlantic and Indian; 28°S in the Pacific)

Layer	Atlantic: volume transport (Sv), freshwater transport (FSv), temperature transport (PWT), mean salinity	Indian: volume transport (Sv), freshwater transport (FSv), temperature transport (PWT), mean salinity	Pacific: volume transport (Sv), freshwater transport (FSv), temperature transport (PWT), mean salinity	Total (A + I + P): volume transport (Sv), freshwater transport (FSv), heat transport (PW)	Layer overturn (Sv), freshwater transport (MSv) and heat transport (PW)	Total volume transport from Sloyan and Rintoul (2001a), their Table 5 with their layer numbers
Total	−1.00 Sv 0.215 ± 0.036 FSv 0.25 PWT	−10.00 Sv 0.257 ± 0.085 FSv −1.23 PWT	11.00 Sv 0.136 ± 0.077 FSv 0.07 PWT	0.00 Sv 0.608 ± 0.120 MSv −0.91 PW	–	−0.77 Sv
1. Ekman layer	1.15 ± 0.23 Sv −0.026 ± 0.008 FSv 0.09 PWT 35.865 psu	0.82 ± 0.30 Sv −0.015 ± 0.007 FSv 0.06 PWT 35.637 psu	−3.21 ± 0.57 Sv 0.055 ± 0.013 FSv −0.28 PWT 35.473 psu	−1.23 ± 0.68 Sv 0.014 ± 0.017 FSv −0.13 PWT	Upper ocean 9.24 ± 2.83 Sv, 0.538 ± 0.026 MSv, −0.62 PW downwelling south of 30°S to lower thermocline (SAMW & AAIW)	
2. Surface to 26.1σ_θ	1.77 ± 0.54 Sv 0.159 ± 0.003 FSv 0.01 PWT 35.802 psu	−11.71 ± 0.63 Sv 0.264 ± 0.006 FSv −0.98 PWT 35.726 psu	3.83 ± 1.10 Sv 0.015 ± 0.013 FSv 0.21 PWT 35.398 psu	−6.11 ± 1.38 Sv 0.437 ± 0.016 FSv −0.76 PWT		4.19 Sv Layers 1–9
3. 26.1–26.4σ_θ	0.12 ± 0.56 Sv 0.040 ± 0.004 FSv 0.00 PWT 35.499 psu	−3.32 ± 0.47 Sv 0.051 ± 0.003 FSv −0.21 PWT 35.504 psu	1.30 ± 0.35 Sv −0.006 ± 0.004 FSv 0.07 PWT 35.107 psu	−1.90 ± 0.81 Sv 0.084 ± 0.006 FSv −0.13 PWT		−0.22 Sv Layer 10
4. 26.4–26.9σ_θ	4.55 ± 1.07 Sv −0.008 ± 0.004 FSv 0.20 PWT 35.086 psu	3.47 ± 2.87 Sv −0.005 ± 0.012 FSv 0.16 PWT 35.000 psu	1.69 ± 1.03 Sv 0.017 ± 0.007 FSv 0.07 PWT 34.737 psu	9.71 ± 3.24 Sv 0.004 ± 0.014 FSv 0.43 PWT	Lower thermocline (SAMW & AAIW)	4.96 Sv Layer 11
5. 26.9–27.1σ_θ	2.47 ± 0.67 Sv 0.024 ± 0.002 FSv 0.08 PWT 34.529 psu	−2.61 ± 0.86 Sv 0.001 ± 0.003 FSv −0.10 PWT 34.552 psu	2.52 ± 1.22 Sv 0.046 ± 0.004 FSv 0.06 PWT 34.399 psu	2.37 ± 1.64 Sv 0.072 ± 0.005 FSv 0.04 PWT		−0.65 Sv Layers 12–13
6. 27.1–27.4σ_θ	2.71 ± 1.82 Sv 0.042 ± 0.007 FSv 0.05 PWT 34.332 psu	−7.46 ± 1.75 Sv −0.060 ± 0.006 FSv −0.18 PWT 34.426 psu	−1.11 ± 1.61 Sv −0.006 ± 0.006 FSv −0.03 PWT 34.391 psu	−5.86 ± 2.99 Sv −0.025 ± 0.011 FSv −0.16 PWT	Deep waters 2.84 ± 2.09 Sv, 0.060 ± 0.007 MSv, 0.16 PW upwelling south of 30°S to lower thermocline; 26.98 ± 10.83 Sv,	−7.17 Sv Layers 14–15
7. 27.4σ_θ–36.8σ_2	−2.45 ± 1.74 Sv −0.022 ± 0.005 FSv −0.03 PWT 34.536 psu	−5.60 ± 2.35 Sv −0.048 ± 0.007 FSv −0.09 PWT 34.559 psu	−1.96 ± 2.13 Sv −0.017 ± 0.007 FSv −0.03 PWT 34.539 psu	−10.02 ± 3.62 Sv −0.087 ± 0.011 FSv −0.14 PWT	0.009 ± 0.030 MSv, −0.27 PW downwelling south of 30°S to bottom waters	−16.05 Sv Layer 16
8. 36.8σ_2–45.80σ_4	−10.16 ± 4.81 Sv −0.002 ± 0.008 FSv −0.12 PWT 34.826 psu	4.76 ± 4.06 Sv 0.015 ± 0.009 FSv 0.05 PWT 34.714 psu	−5.71 ± 5.50 Sv −0.042 ± 0.014 FSv −0.05 PWT 34.654 psu	−11.11 ± 8.36 Sv −0.030 ± 0.019 FSv −0.12 PWT		−22.30 Sv Layer 17
9. 45.80–45.86σ_4	−5.03 ± 2.10 Sv −0.006 ± 0.002 FSv −0.04 PWT 34.874 psu	1.51 ± 1.90 Sv 0.003 ± 0.005 FSv 0.01 PWT 34.741 psu	0.68 ± 1.70 Sv 0.005 ± 0.006 FSv 0.00 PWT 34.689 psu	−2.84 ± 3.30 Sv 0.002 ± 0.008 FSv −0.03 PWT		−2.36 Sv Layer 18
10. 45.86–45.92σ_4	0.86 ± 0.87 Sv 0.002 ± 0.001 FSv 0.01 PWT 34.837 psu	4.95 ± 2.23 Sv 0.023 ± 0.006 FSv 0.03 PWT 34.731 psu	4.15 ± 1.10 Sv 0.024 ± 0.005 FSv 0.02 PWT 34.710 psu	9.96 ± 2.64 Sv 0.048 ± 0.008 FSv 0.05 PWT	Bottom waters	23.53 Sv Layer 19
11. 45.92–46.0σ_4	2.33 ± 0.93 Sv 0.009 ± 0.003 FSv 0.01 PWT 34.766 psu	5.36 ± 3.30 Sv 0.030 ± 0.011 FSv 0.02 PWT 34.716 psu	8.81 ± 1.87 Sv 0.046 ± 0.008 FSv 0.03 PWT 34.716 psu	16.49 ± 3.90 Sv 0.085 ± 0.014 FSv 0.05 PWT		23.91 Sv Layer 20
12. 46.0σ_4 to bottom	0.67 ± 0.15 Sv 0.003 ± 0.000 FSv 0.00 PWT 34.728 psu	−0.16 ± 1.10 Sv 0.000 ± 0.006 FSv −0.00 PWT 34.697 psu	0.00 Sv NA NA NA	0.51 ± 1.11 Sv 0.004 ± 0.006 FSv 0.00 PWT		1.11 Sv Layer 21

"Upwelling" and "downwelling" refer to vertical transport in the southern ocean, south of 30°S, and are balanced by the opposite north of 30°S. Individual freshwater transports (FSv) are reported relative to a mean salinity of 34.9 psu. Total freshwater and heat transports (MSv, PW) in right column are mass-balanced.

The mass transport error estimate M_i' assigned to each station pair is based on Robbins and Toole's (1997) choice of velocity shear over the bottom 500 m of the pair to represent velocity error. For stations shallower than 500 m, a range of choices was tested, from no error to the total difference in velocity from bottom to top. Because most station pairs on the sections were deeper than 500 m, the choice had little effect on the calculated error. I also chose to use the average error over all of the station pairs rather than the individual station pair error. The Monte Carlo error in mass transport itself, based on 100,000 iterations, is large; for 24°N in the Pacific for instance, the result for transport is −7.61 ± 11.44 Sv. This is essentially the error that would be obtained by propagation of error for each station pair. Comparable large transport errors are obtained for all sections.

For freshwater transport, the mass transports must balance. Using 24°N again as an example, a mean mass transport error of ±11.44 is far from the required 1 Sv balance, with similarly very large values on the other sections (Table 2). If the full Robbins and Toole (1997) bootstrap method were applied, an inverse model would be run for each Monte Carlo simulation, imposing the correct mass transport constraint which for this section is based on Ekman and Bering Strait

Table 15
Summary of freshwater transport components (FSv) and mass-balanced sums (MSv) across 30°S, oriented to overturnings north of 30°S (Tables 10, 12 and 13)

	Atlantic	Indian	Pacific	Total
Shallow overturning	0.203 ± 0.055 MSv	0.182 ± 0.019 MSv	0.230 ± 0.037 MSv	0.615 ± 0.069 MSv
ITF	–	0.116 ± 0.002 FSv (−10 Sv)	−0.057 ± 0.015 FSv (+10 Sv)	0.059 ± 0.015 MSv
Bering Strait	0.002 ± 0.001 FSv (−1 Sv)	–	−0.006 ± 0.003 FSv (+1 Sv)	−0.004 ± 0.003 MSv
Intermediate/deep overturning	0.010 ± 0.017 MSv	−0.041 ± 0.025 MSv	−0.031 ± 0.029 MSv	−0.062 ± 0.046 MSv
Total	0.215 ± 0.036 FSv (−1 Sv)	0.257 ± 0.085 FSv (−10 Sv)	0.136 ± 0.077 FSv (+11 Sv)	0.608 ± 0.120 MSv

Net volume transports (Sv) are listed for non-mass-balanced freshwater transports in parentheses, associated with ITF (10 Sv) and Bering Strait throughput (1 Sv). Uncertaintites in last row ("Total") are from Table 2.

Table 16
Summary of intermediate and deep overturning freshwater transports (MSv) across 30°S, oriented to overturnings south of 30°S (Table 14 and Fig. 12b)

Southern Ocean intermediate/deep overturning	Atlantic	Indian	Pacific	Total
Shallow to LCDW	–	0.73 Sv down −0.001 ± 0.002 MSv −0.03 PW Layers 1:4 to 8:12 with 0.182 MSv shallow overturn and 0.116 FSv ITF throughput removed	4.87 Sv down −0.014 ± 0.014 MSv −0.14 PW Layers 1:5 to 9:12 with 0.230 MSv shallow overturn, −0.057 FSv ITF and −0.006 FSv BS removed	5.6 Sv down −0.015 ± 0.014 MSv −0.17 PW
"AAIW"/SAMW to LCDW	–	10.08 Sv down −0.016 ± 0.015 MSv −0.10 PW Layers 5:6 to 8:12	1.11 Sv down 0.000 ± 0.006 MSv −0.16 PW Layers 6 to 9:12	11.19 Sv down −0.016 ± 0.016 MSv −0.26 PW
NADW to shallow[a]	7.59 Sv up −0.051 ± 0.018 MSv 0.33 PW Layers 7:9 to1:4 with 0.203 MSv shallow overturn removed	–	–	7.59 Sv up −0.051 ± 0.018 MSv 0.33 PW
NADW to AAIW/shallow	5.18 Sv up 0.055 ± 0.009 MSv 0.02 PW Layers 7:9 to 5:6 with 0.002 FSv BS throughput removed	–	–	5.18 Sv up 0.055 ± 0.009 MSv 0.02 PW
NADW/IDW/PDW to LCDW	3.85 Sv down 0.008 ± 0.005 MSv −0.03 PW Layers 7:9 to 10:12	5.60 Sv down −0.024 ± 0.010 MSv −0.11 PW Layers 7 to 8:12	7.67 Sv down −0.017 ± 0.022 MSv −0.05 PW Layers 7:8 to 9:12	17.12 Sv down −0.033 ± 0.025 MSv −0.19 PW
Ocean total	0.012 ± 0.017 MSv 0.32 PW	−0.041 ± 0.025 MSv −0.24 PW	−0.031 ± 0.029 MSv 0.000 MSv −0.35 PW	−0.060 ± 0.042 MSv −0.27 PW

Shallow overturn, ITF and BS are removed (see Table 15). "Up" or "down" are upwelling or sinking south of 30°S. Layer numbers from Table 14.
[a] The 7.6 Sv that leaves the Atlantic in the NADW layer and that returns to the Atlantic in the "Agulhas leakage" may take at least this following route: (1) 3.9 + 0.7 Sv sinking to LCDW in the Southern Ocean, and then upwelling to the surface (ITF) in the Pacific and Indian Oceans, respectively; (2) 2.5 Sv up to AAIW in the Southern Ocean and then on up to surface in the Pacific; and (3) 0.5 Sv up to the surface in the Southern Ocean and then joining the ITF flow in the Pacific (Fig. 12).

transport. In the absence of an inverse model, a uniform velocity correction is applied here to each Monte Carlo simulation to provide mass balance, which is the same principal as in the basic calculation, to match the measured Ekman transport and assigned Bering Strait and ITF transports. The geostrophic freshwater transport errors listed in Table 2 thus have enforced mass balance after application of random velocity error for each station pair based on the deep velocity shear. As an example, the geostrophic freshwater transport uncertainty for the Pacific 24°N section is ±0.04 FSv with the mass balance constraint, and ±0.11 FSv without it.

Salinity error for the geostrophic component of freshwater transport is assigned as 0.01 throughout. This is a conservative estimate of measurement error, especially for WOCE sections, which have much smaller absolute error (<0.003). Using the Pacific 24°N example, the geostrophic freshwater transport uncertainty is ±0.04, ±0.06, ±0.13 and ±0.26 FSv with 0.001, 0.02, 0.05 and 0.01 salinity errors, respectively.

The mean geostrophic freshwater transport uncertainty over all of the sections, as listed in the column labeled (1) in Table 2, is ±0.08 FSv. Without the enforced mass balance constraint, the mean uncertainty increases to ±0.11 FSv. With a low salinity error of 0.001, the mean uncertainty remains ±0.08 FSv. With salinity error of 0.02, 0.05 and 0.1, the mean uncertainty is ±0.09, ±0.14 and ± 0.23 FSv, respectively.

The freshwater transport uncertainties vary greatly from section to section, from a low of ±0.02 for Pacific 47°N to a high of ±0.23 for Atlantic 59°N; high values between ±0.1 and ±0.2 are found on most North Atlantic sections and the Indian 8°S and 8°N (Bay of Bengal) sections. High values are not simply associated with either high mass transport error or with high geographic salinity standard deviation (Fig. 4 and fourth and fifth columns of Table 2), but are much more closely associated with their product (Fig. 4d). The correlations over all of the 19 sections between freshwater transport uncertainty and mass transport uncertainty, salinity standard deviation, and their product are 0.3, 0.6 and 0.9, respectively.

The net freshwater transport error for each section, based on the geostrophic and Ekman uncertainties, is given in the column la-

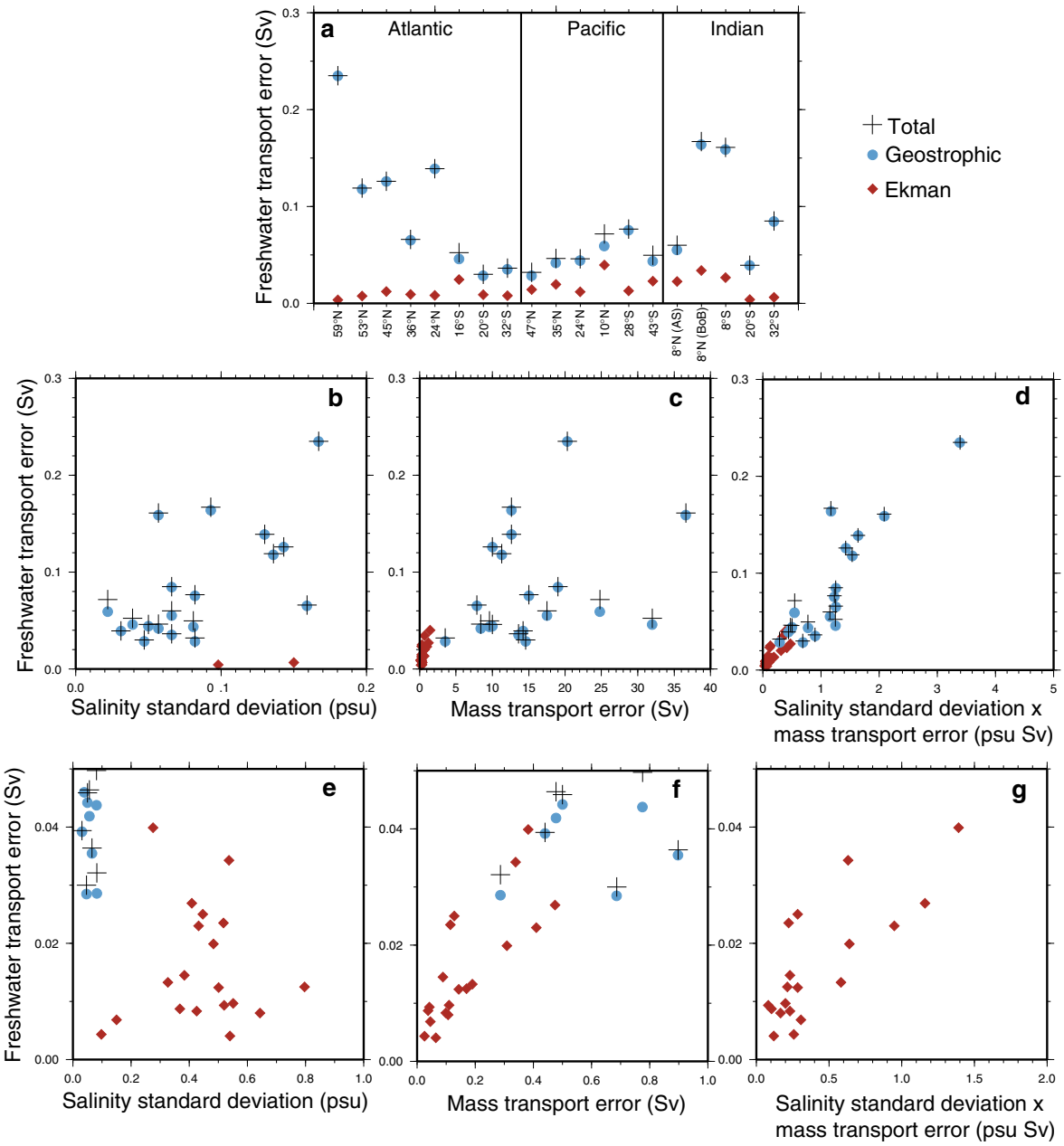

Fig. 4. Freshwater transport uncertainties (crosses) based on Monte Carlo estimates for the geostrophic (blue circles) and Ekman components (red diamonds). (a) Uncertainties as a function of (a) hydrographic section, (b, e) standard deviation of salinity along the section, (c, f) uncertainty in mass transport (Sv), and (d, g) product of salinity standard deviation and mass transport uncertainty. (For interpretation of the references to color in this figure legend, the reader is referred to the web version of this article.)

beled (3) in Table 2. The Ekman contributions are small, and so these net values are only slightly higher than the geostrophic freshwater transport uncertainties (Fig. 4a).

Uncertainties in freshwater transport divergences (Section 3; Tables 3 and 4 below) are based on these section uncertainties and on the error estimates of ±0.02 and ±0.05 FSv for BS and the ITF.

Uncertainties in freshwater transports associated with different mass-balancing components of the circulation (Sections 4–9, Tables 5 and 9–16 below) are computed using the same Monte Carlo strategy for each section outlined above, but separating out the specific mass-balancing circulation component. For the shallow gyre transports, the geostrophic interior, western boundary current and Ekman uncertainties were computed separately and combined through straightforward propagation of error (see Table 5); in each case the total top-to-bottom mass transport for each Monte Carlo iteration was balanced. For example, for the Pacific 24°N section, the Ekman, geostrophic interior ($\sigma_\theta < 26.2$ kg/m^3), and balancing Kuroshio ($\sigma_\theta < 26.12$ kg/m^3) portions had freshwater transport uncertainties of ±0.012, ±0.024 and ±0.009 FSv, for a combined uncertainty of ±0.028 MSv.

For intermediate and deep overturns (Section 7; Tables 9–13), freshwater transport uncertainties were calculated for the mass-balanced overturning components within the same Monte Carlo iteration. For the Pacific 24°N example (Table 11), the uncertainty is largest for the topmost layer overturn, and less than 0.01 FSv for the remaining deeper overturns; this is the primary reason for retaining three decimal places in listing freshwater transports and uncertainties throughout the paper and tables, since many of the deep overturn uncertainties are less than 0.005 FSv.

Whenever circulation components had to be combined, that is, could not be easily calculated together in a single Monte Carlo iteration, simple propagation of error was used to estimate the uncertainty of the combined mass-balanced components. In general, this resulted in a larger estimate of uncertainty than if the calculation could be done in a single step.

3. Total freshwater transports and divergences

Total freshwater divergences are presented first for comparison with air-sea fluxes and previously published freshwater transport estimates, especially the global estimates of Ganachaud and Wunsch (2003). This is the starting point for the shallow and deep overturning decompositions of the ensuing sections, which are the novel calculations for this study.

Section freshwater transports and the components for calculation through each section are given in units of freshwater transport (FSv) relative to the arbitrary reference salinity of 34.9 (Figs. 5 and 6 and Table 2). If the mass transports due to the ITF and Bering Strait are removed from each section, the remaining mass transport on each section is 0 Sv and the freshwater transport an absolute number (MSv). This absolute freshwater transport is estimated in the last column of Table 2, after assigning the ITF and BS transports through each section as described in Sections 5 and 6. Sections in the Atlantic at 32°N, 8°N, 8°S, 11°S and 40°S that are included in Reid (1994) and Talley (2003) are not included because of large errors attributable to either undersampling, combined non-synoptic cruises or large low latitude variability (Talley, 2003).

Freshwater divergences between all sections are shown in Figs. 5a and 6b and c and listed in Table 3. The freshwater divergences for much larger regions are used in Fig. 5b and Table 4 to highlight the large-scale basin-to-basin differences in freshwater balances and for comparison with GW03. These are compared with air-sea fluxes and runoff within each region (Fig. 6d and Tables 3 and 4, using NCEP 1979–2005 reanalysis and DT02). The runoff values in DT02 are internally consistent with the NCEP evaporation/precipitation.

The total gain of freshwater by the ocean must equal the total loss of freshwater, due to precipitation/runoff and evaporation, respectively. Dividing the ocean into the smallest regions available from the full set of zonal hydrographic sections used here, the freshwater transport divergence is 2.7 MSv for all discrete net precipitation/runoff regions and −2.7 MSv for all discrete net evaporation regions (rounded from ±2.66 in Table 3). These balance to the required 0.0 MSv. The corresponding NCEP values for the same discrete regions are 1.52 Sv of precipitation and −2.41 Sv of evaporation; adding the net DT02 runoff of 1.22 Sv yields a global sum of 0.32 Sv. NCEP by itself balances freshwater for the globe including both land and ocean, with a net 0.03 Sv (not listed in Table 3). DT02 is used in Table 3 for runoff, resulting in an imbalance of 0. 32 Sv; as they note in their paper, DT02 is "wetter" than NCEP. (The total amount of precipitation/runoff and total amount of evaporation are much larger than these since each discrete region has both evaporation and precipitation. Thus, this calculation is not an estimate of the total amount of water cycling between the atmosphere and ocean/land.)

With the larger discrete regions of Fig. 5b and Table 4, the sums for all of the net precipitation/runoff regions and, separately, all the net evaporation regions are ±1.5 MSv (rounded from ±1.47 MSv). The NCEP estimates for the same larger discrete regions are ±1.6 MSv (rounded from ±1.62 MSv) (Table 4).

The largest regions of net precipitation/runoff in this hydrographic estimate are the Southern Ocean and combined Arctic/subpolar North Atlantic (henceforth "Arctic"). In the Southern Ocean, the direct estimate yields 0.72 ± 0.10 MSv of freshwater gain from the atmosphere using 43°S as the Pacific boundary (Fig. 5a and Table 3), or 0.61 ± 0.13 MSv using 28°S as the Pacific boundary (Fig. 5b and Table 4). The "Arctic" freshwater gain from the atmosphere is 0.52 ± 0.23 MSv north of 60°N (Atlantic) and Bering Strait (Pacific), or 0.42 ± 0.13 MSv north of 45–47°N in both oceans. GW03 obtained 0.7 and 0.4 MSv for the Southern Ocean south of 30°S and "Arctic" north of 47°N, so this calculation is comparable (Table 4). SR2001 obtained a comparable 0.5 MSv for the Southern Ocean south of 30°S.

Air-sea fluxes and runoff from NCEP/DT02 yield 0.8 MSv for the Southern Ocean with 43°S as the Pacific boundary and 0.6 MSv with 28°S as the Pacific boundary, with air/sea flux dominating runoff (Tables 3 and 4). This is also comparable to the direct estimate here.

The air-sea flux and runoff for the Arctic north of 59°N/Bering Strait is 0.31 from NCEP/DT02, comparable to this direct estimate. If these estimates are extended southward to 45°N in the Atlantic (not Pacific), thus including most of the surface freshwater input that reduces the NADW salinity relative to the saline surface inflow, the section-based and NCEP/DT02 estimates are 0.31 ± 0.13 and 0.5 MSv, respectively, which are comparable if the error in the NCEP estimate is similar.

North of 30°S, the Atlantic/Arctic and Indian Oceans are net evaporative and the Pacific is neutral or has weak net precipitation: −0.28 ± 0.04, −0.38 ± 0.10 and 0.04 ± 0.10 MSv, respectively (Fig. 5b and Tables 2 and 4), incorporating uncertainties from the bounding sections, BS and the ITF. For comparison with GW03, between "30°S" and "45°N" the Atlantic, Indian and Pacific are net evaporative or neutral/weak evaporation here: −0.59 ± 0.14, −0.38 ± 0.10 and −0.06 ± 0.09 MSv, respectively. For the same regions, GW03 obtain −0.5, −0.6 and −0.1 MSv, comparable to these values given the GW03 uncertainty estimates of ±0.2 to 0.3.

The Atlantic/Arctic total of −0.28 ± 0.04 MSv (net evaporation) north of 32°S is the sum of relative freshwater transport of 0.21 FSv across 32°S and inward relative freshwater transport of 0.07 FSv through Bering Strait.

The Indian total of −0.38 ± 0.10 MSv (evaporation north of 32°S) is the sum of 0.26 FSv across 32°S and 0.11 FSv inward from the Indonesian Throughflow. Robbins and Toole's (1997) Indian Ocean freshwater transport across 32°S is −0.31 MSv, comparable to this estimate and to the NCEP estimate of −0.33 MSv (Table 4), whereas Bryden and Beal (2001) obtained a larger −0.54 MSv. The large net evaporation calculated here in the Arabian Sea and large net precipitation in the tropical Indian Ocean (Table 3 and Fig. 5a) likely result from inadequate sampling of the monsoon with the single hydrographic section (Tables 3 and 4 and Fig. 5a). More moderate values were obtained by GW03 (Table 4), although the values here fall marginally within GW03's error bars.

The Pacific total of 0.04 ± 0.10 MSv (net precipitation) is the sum of 0.13 FSv into the Pacific across 28°S, −0.11 FSv westward through the ITF, and −0.07 FSv northward through Bering Strait. For the entire Pacific north of 32°S, Wijffels et al. (2001) found a net gain of 0.1 ± 0.1 MSv of freshwater, which encompasses the estimate here.

The Southern Ocean sectors could be included in the separate Atlantic, Indian and Pacific sectors, although zonal transports between them were not calculated. If the total Southern Ocean freshwater flux of 0.60 ± 0.13 MSv south of 30°S (Tables 3 and 4) is divided between the sectors at 20°E, 147°E and 70°W according to their relative widths, net precipitation is added to each ocean's total: Atlantic 0.14 MSv, Indian 0.20 MSv, Pacific 0.26 MSv (Fig. 5b). (For comparison, the NCEP fluxes for the same Southern Ocean regions are 0.2, 0.2 and 0.3 MSv, totaling 0.6 MSv, so the Indian sector of the Southern Ocean might have relatively less precipitation per unit area than the Atlantic.) The totals for the Atlantic/Arctic and Indian sectors remain evaporative even with the addition of the Southern Ocean sectors (−0.13 and −0.18 MSv, respectively), while the Pacific sector is freshened (0.30 MSv) (bottom row in Fig. 5b).

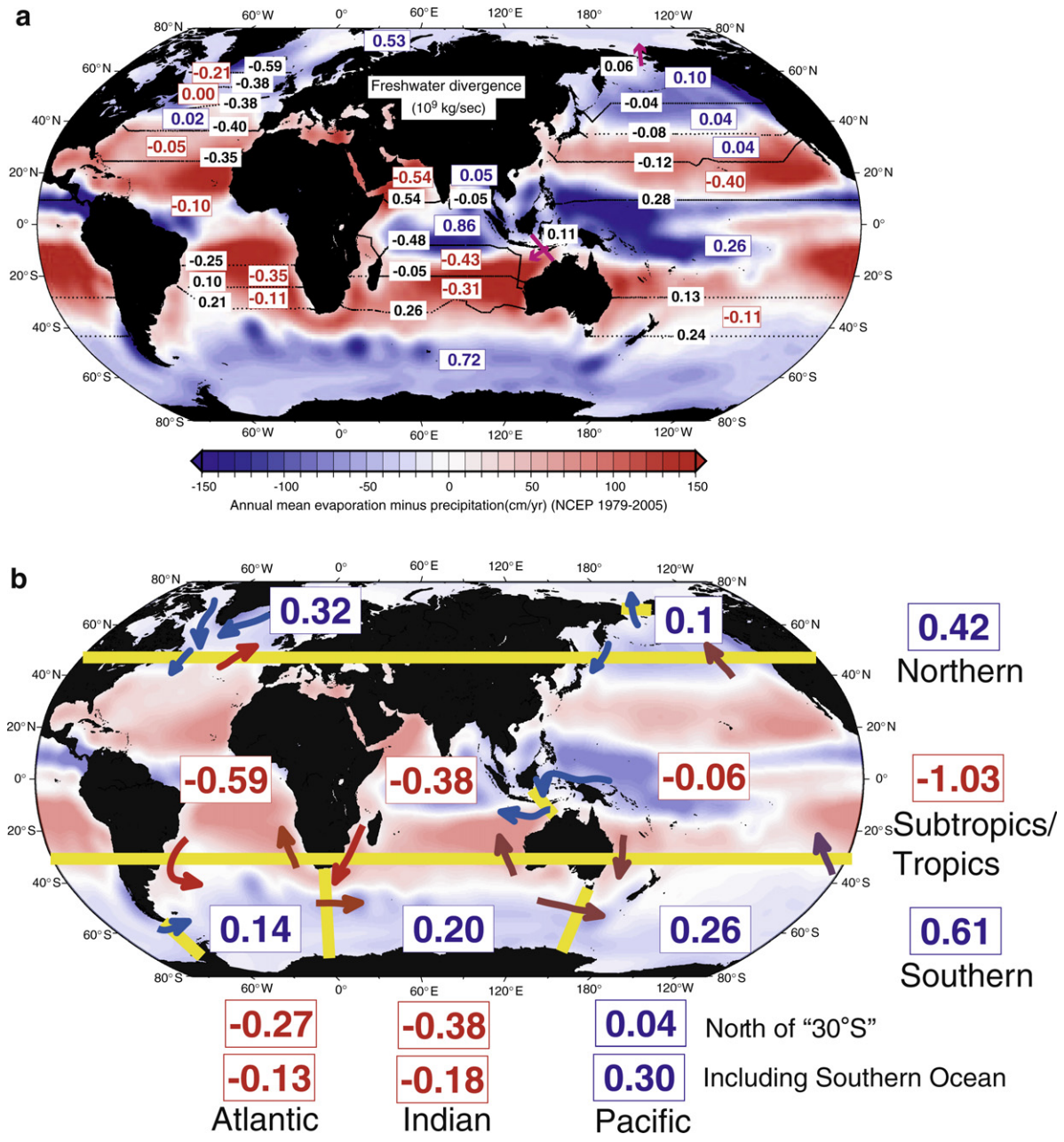

Fig. 5. Divergences of freshwater transport (MSv) based on synoptic hydrographic section velocities and salinities. Geostrophic velocities are adapted from Reid (1994, 1997, 2003) and Ekman transports are from NCEP, assuming 10 and 1 Sv for the Indonesian and Bering Strait throughflows, respectively. Positive numbers (blue) require net precipitation/runoff and negative numbers (red) indicate net evaporation (Tables 3 and 4). The underlying map is the NCEP annual mean (1979–2005) surface evaporation minus precipitation (cm/year) from the atmosphere to the ocean (http://www.cgd.ucar.edu/cas/catalog/newbudgets, 2007). (a) Divergences (MSv) for each zonal section pair (Tables 2 and 3). Also given is freshwater transport (FSv) relative to salinity 34.9 for each zonal section (black numbers); most values depend on the reference salinity because there is net mass transport through most sections. Uncertainties are given in Tables 2 and 3. (b) Divergences (MSv) for larger regions, summed by latitude band shown at right and summed by ocean basin across the bottom (first row is north of "30°S"; second row includes Southern Ocean divergence divided proportionally by area) (based on Table 4). Arrows are a schematic of fresher through saltier transports that maintain the divergences. Blue: fresher water transport. Red: saltier water export. Brown through purple: progressively fresher water. Uncertainties are given in Table 4. (For interpretation of the references to color in this figure legend, the reader is referred to the web version of this article.)

These basin-wide divergences require freshwater transport through the ocean. The largest redistributions of freshwater are quasi-meridional, between the subtropics/tropics and the Southern Ocean and "Arctic" (Fig. 5b). As noted above and described below (Sections 6 and 7.1), the salty/fresh exchange in the northern North Atlantic moves saline upper ocean water into the "Arctic" to balance the surface flux of freshwater there, and moves fresh water southward out of the "Arctic", primarily in the North Atlantic Deep Water. Redistribution between the low latitudes and the Southern Ocean is the same order of magnitude as the "Arctic"–Atlantic exchange, but takes place almost wholly within the upper ocean (Sections 4, 5 and 8).

Redistribution of freshwater from the Pacific to the Atlantic and Indian is also required. The Pacific north of 30°S is neutral in freshwater; freshwater loss through Bering Strait and the ITF is essentially balanced by inflow of freshwater from the south (Sections 4–6). More saline water flows back from the Atlantic and Indian to the Pacific; this must occur through the Southern Ocean, arguably through the deep water transports (Sections 8 and 9).

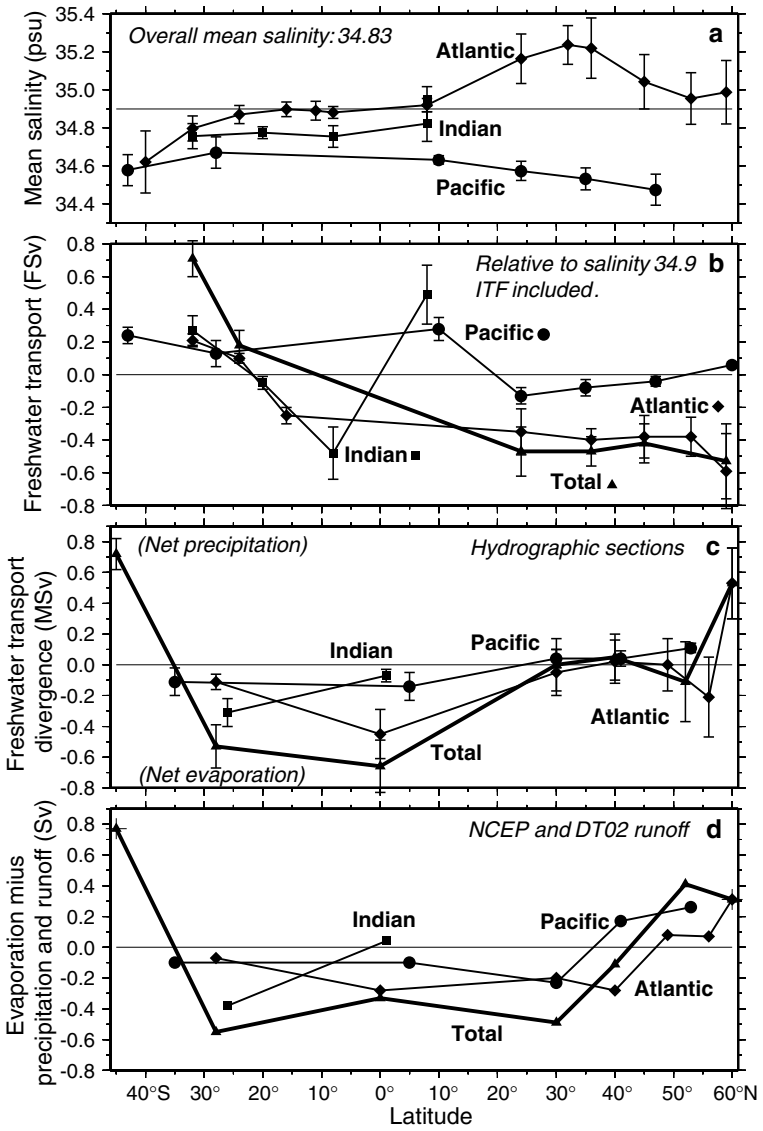

Fig. 6. (a) Mean and standard deviation of salinity for each zonal section in the analysis. (b) Freshwater transport (FSv), with a reference salinity of 34.9, for each ocean and summed for the globe where available in all oceans. (c) Divergence of freshwater transport (MSv), which is independent of reference salinity. (d) Net evaporation minus precipitation/runoff (cm/year) for each of the latitude bands of (c), based on evaporation and precipitation from NCEP reanalysis (1979–2005) and runoff from Dai and Trenberth (2002).

Errors in freshwater transports and divergences are proportionally large. GW03 estimate errors on the order of 0.2–0.3 MSv in each ocean region defined by the "30°S" and "45°N" sections (e.g. Table 4), which is roughly equivalent to the total divergence in each region. The mean error for the same regions in this estimate is ±0.12 MSv. The standard deviation of the difference between GW03 and the transport divergence estimates here is just 0.1 MSv, which suggests that these two independent calculations of freshwater transport are equally valid, lending additional credibility to the present estimate particularly in moving forward to individual circulation components in the following sections. (The mean difference is 0.0 MSv since the total divergence for both estimates is 0.0 MSv.)

The mean difference between the regional transport divergences here and the NCEP/DT02 estimates for regions with positive divergences (net evaporation), (hydrographic minus NCEP/DT02) is 0.2 MSv, and for negative differences (net precipitation/runoff) it is −0.1 MSv; the hydrographic section-based regional estimates are larger in magnitude than the NCEP/DT02 regional estimates. Also indicative of large error, the standard deviation for all regional transport divergences compared with NCEP/DT02 is 0.3 MSv (Table 3), which can be reduced to 0.2 MSv if tropical regions are excluded, given larger error there due to large Ekman transports and monsoons. This level of error is consistent with the GW03 error estimate. The large monsoonal variation in the tropical Indian Ocean circulation (e.g. Schott and McCreary, 2001; Schott et al., 2002; Beal and Chereskin, 2003) is not captured in the Reid (2003) single section estimates, leading to large freshwater divergences between tropical sections and large differences from NCEP/DT02 annual averages.

Although these total freshwater transport errors are large, there is still important information in even the small freshwater transports, since their signs and order of magnitude are robust indications of the differences in salinity between the mass-balancing components of the circulation that carry the freshwater.

4. Subtropical shallow overturning transports

Subduction in the subtropical gyres from the sea surface down through the thermocline carries heat poleward from the tropics

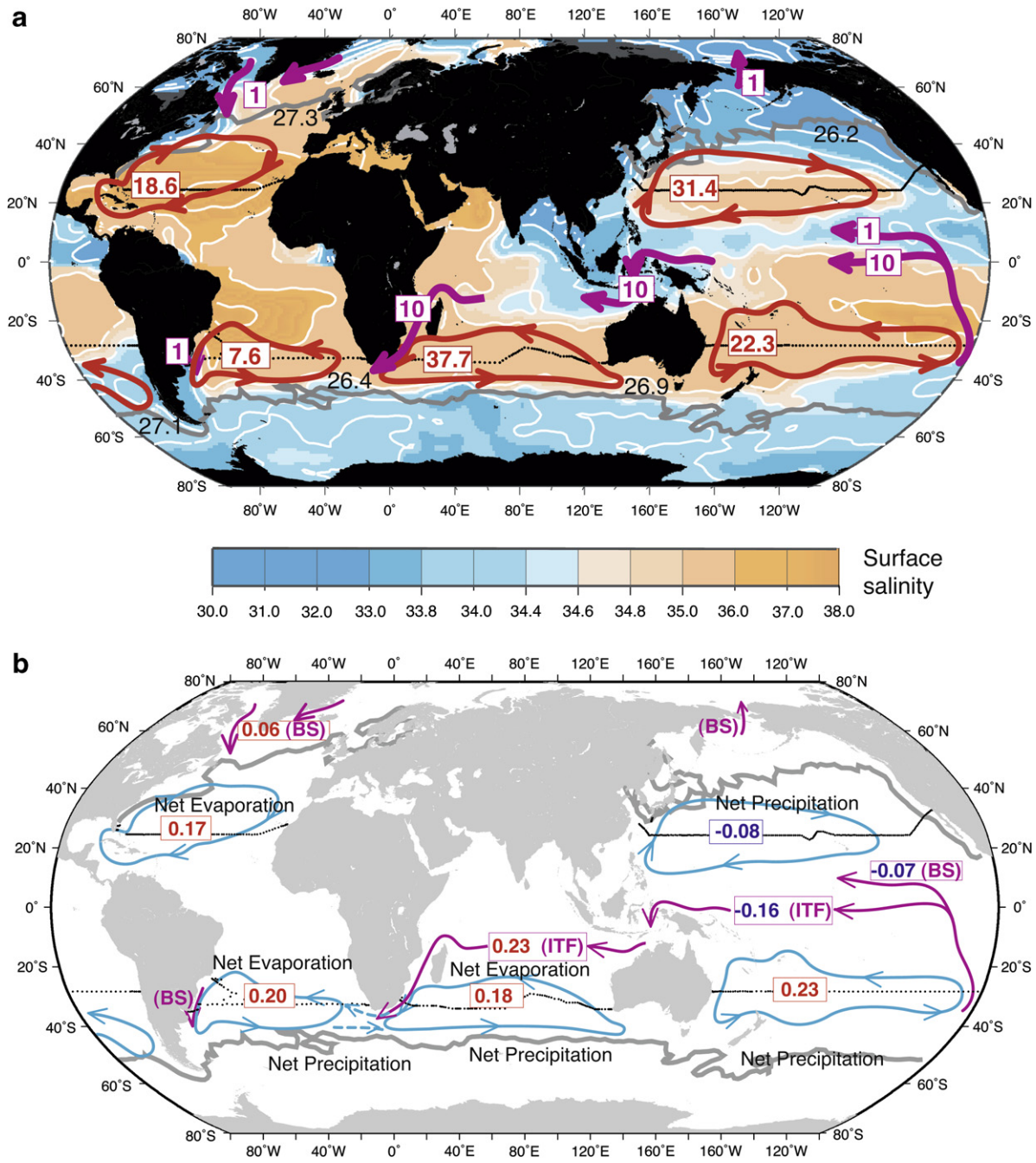

Fig. 7. Transports for the subtropical gyres, Indonesian Throughflow (ITF) and Bering Strait (BS). See Table 5 for the calculations and uncertainties. Representative surface streamlines for each subtropical gyre are based on Reid's (1994, 1997, 2003) surface steric height (Hanawa and Talley, 2001; Talley, 2003). (a) Mass transport (Sv). Red: mass-balanced gyre transports to bottom of pycnocline. Purple: transports associated with the ITF and BS. Black numbers: maximum subtropical winter surface density (kg/m^3) for each gyre, based on zero wind stress curl from Hellerman and Rosenstein (1983) (gray) and winter surface density (not shown). The underlying contoured map is the annual mean surface salinity (Levitus et al., 1994). (b) Freshwater transports (MSv) for each mass-balanced subtropical gyre (red and blue), for the mass-balanced ITF throughput in the Pacific and Indian Oceans (purple), and for the BS throughput in the Pacific and Atlantic Oceans (purple). Red and blue numbers are northward and southward freshwater transport, respectively. For the ITF and BS, red (blue) numbers indicate associated net evaporation (precipitation/runoff) within the basin. (For interpretation of the references to color in this figure legend, the reader is referred to the web version of this article.)

across 24°N and 30°S (Talley, 2003). This results from warm poleward western boundary currents and cooled equatorward interior flow, since the major ocean heat loss regions in the subtropics are poleward of these zonal sections.

Freshwater is also transported by the subducting, shallow overturning circulation in the subtropical gyres (Fig. 7 and Table 5). The principal result shown here is that the three southern hemisphere subtropical gyres transport freshwater equatorward by advecting high latitude fresher water equatorward in the interior of the gyres and saltier water poleward in the western boundary currents (Fig. 7b, South Atlantic schematic shown). For the northern hemisphere, on the other hand, the direction of the freshwater transport is ambiguous since the 24°N sections are located close to the evaporation centers. In the North Atlantic, the maximum evaporation is north of the section, so the interior circulation carries salty water equatorward while the Gulf Stream carries somewhat fresher tropical surface water northward, resulting in northward freshwater transport.

The shallow gyre freshwater transport calculations follow the same procedure as the heat transport calculations in Talley

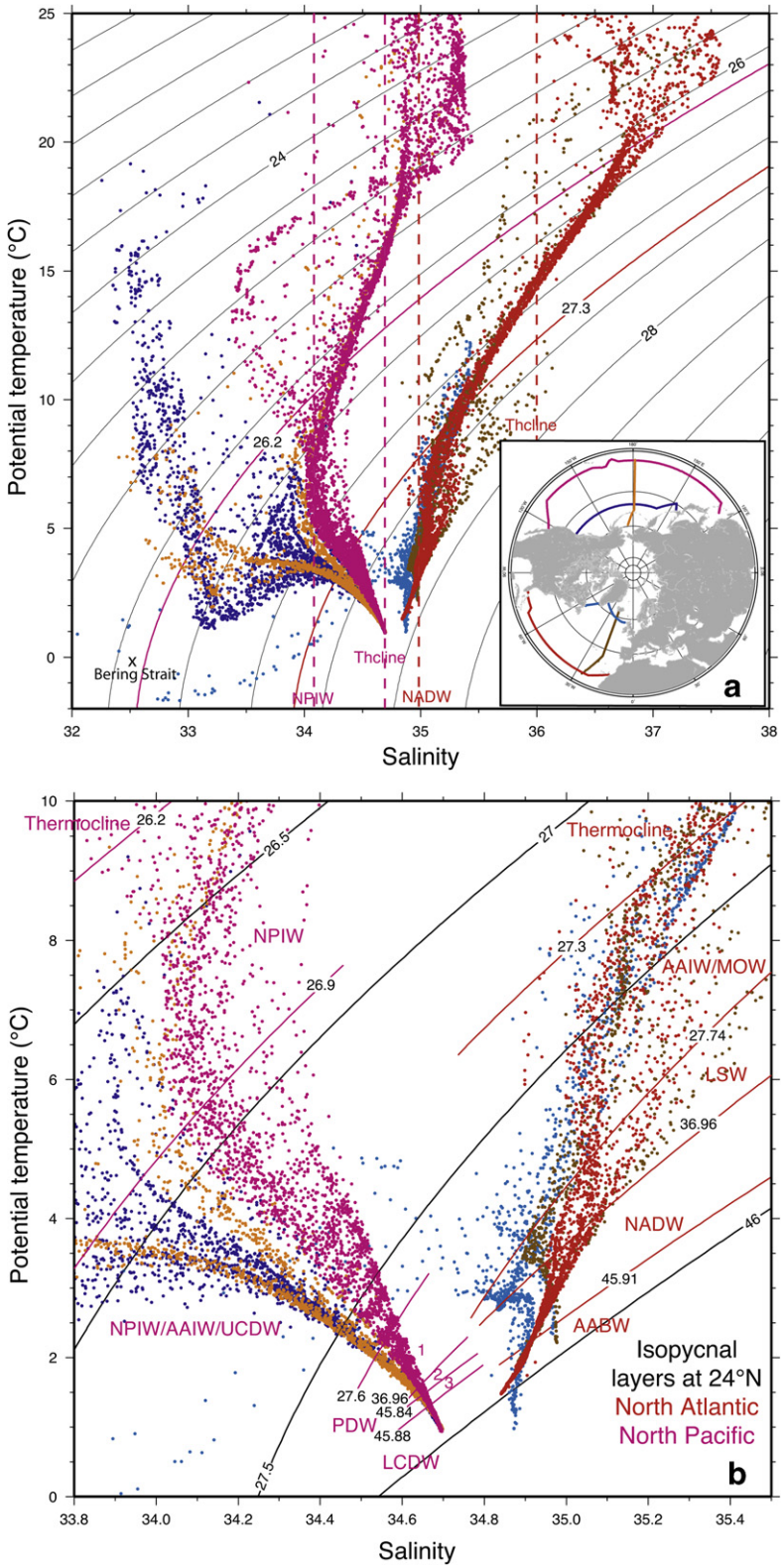

Fig. 8. North Atlantic and North Pacific potential temperature (°C) – salinity relations at 24°N, for zonal sections at the northernmost locations bracketing the Arctic, and for meridional sections through the northern subtropics and subpolar regions. Inset map shows location of stations and color key. All data are from WOCE. (a) Full temperature and salinity range. Heavy black contours: bottom of thermocline defined in Section 4. Dashed vertical lines: approximate salinity of labeled layers for the Bering Strait discussion (Section 6 below). Black ×: approximate property for Bering Strait throughflow. (b) Deep temperature and salinity range. Sparse black contours: potential density σ_θ and σ_4. Red and magenta contours and labels: isopycnal layers for the North Atlantic and North Pacific analyses in Section 7 (Tables 9 and 11). (For interpretation of the references to color in this figure legend, the reader is referred to the web version of this article.)

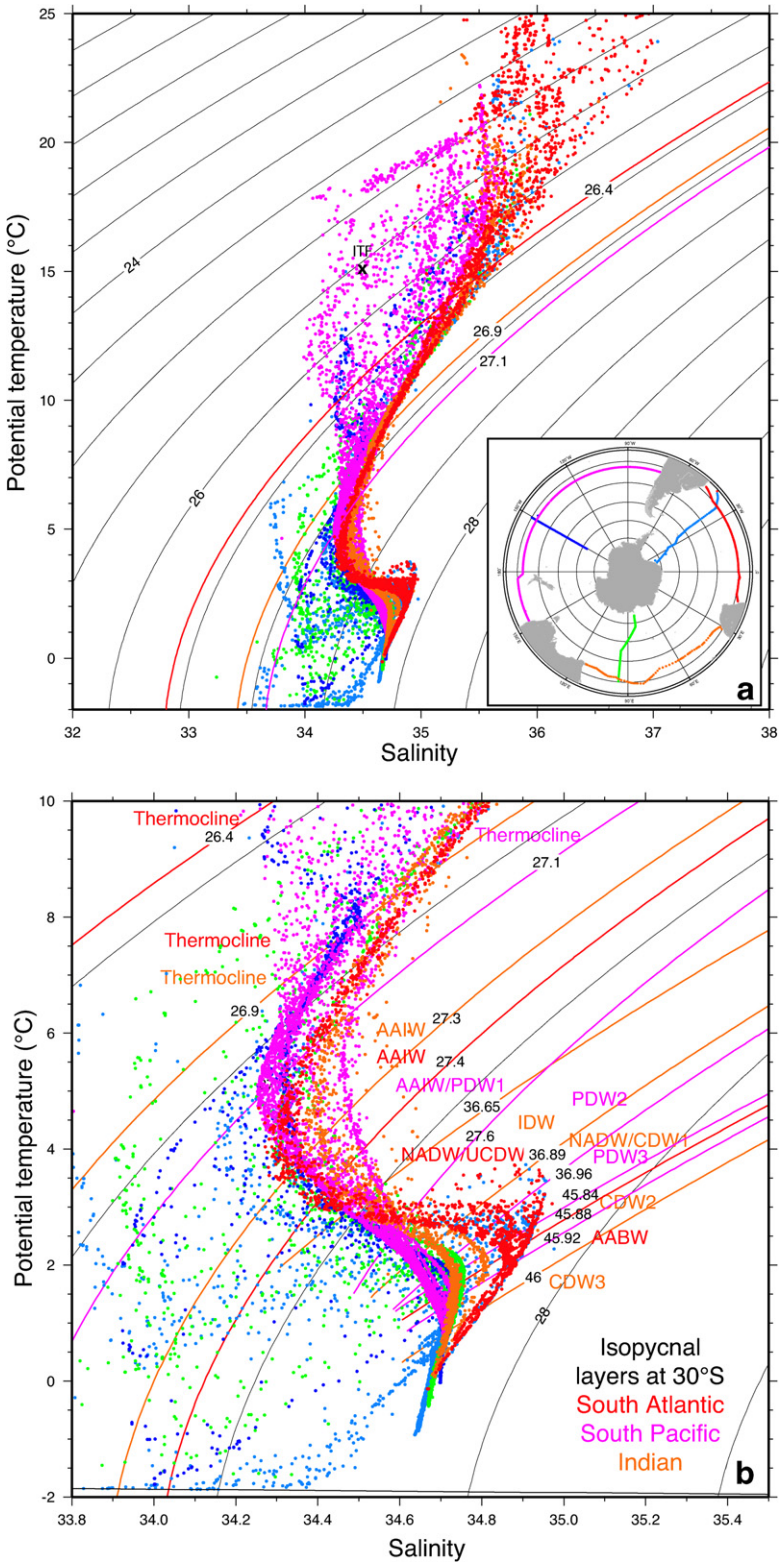

Fig. 9. South Atlantic, South Pacific and Indian potential temperature (°C) – salinity relations at 30°S and for meridional sections southward from this latitude. Inset map shows location of stations and color key. All data are from WOCE. (a) Full temperature and salinity range. Color contours: bottom of thermocline defined in Section 4. Black ×: approximate property for Indonesian Throughflow. (b) Deep temperature and salinity range. Sparse black contours: potential density σ_θ and σ_4. Red, magenta and orange contours and labels: isopycnal layers for the South Atlantic, South Pacific and Indian analyses in Section 7 (Tables 10, 12 and 13). (For interpretation of the references to color in this figure legend, the reader is referred to the web version of this article.)

(2003) (see Section 2). The bottom of the subtropical ventilated thermocline is identified as the maximum outcropping density in the winter at the zero wind stress curl location: 27.3σ_θ (North Atlantic), 26.2σ_θ (North Pacific), 26.9σ_θ (Indian) and 27.1σ_θ (South Pacific). The South Atlantic choice is arbitrary between about 26.2σ_θ and 26.9σ_θ; heat and freshwater transports are insensitive to this choice (Talley, 2003). Talley (2003) used 26.2σ_θ for the South Atlantic, but 26.4σ_θ is also chosen here to match the full

Southern Ocean calculation in Section 8. The newly calculated mass and heat transport values differ somewhat from Talley (2003) since NCEP winds were used here for Ekman transports. The updated winds also result in slightly different interior balances because net geostrophic transports are adjusted to balance Ekman transport.

The potential temperature–salinity relations for each of these subtropical sections in Figs. 8 and 9 include the isopycnals chosen for the base of the thermocline. All of the calculated shallow overturn freshwater transport on each section is within the property envelope at lower densities. For all sections except the South Atlantic's, the bounding isopycnal choice is well within or at the bottom of the tight potential temperature–salinity relation of the thermocline ("Central Water"); the South Atlantic's thermocline potential temperature–salinity is very similar to the Indian Ocean's, reflecting the continuity of the two gyres, and the arbitrariness of a choice of bounding isopycnal for the South Atlantic. This has little effect on the shallow freshwater transport calculated for the South Atlantic, as described below.

4.1. North Atlantic at 24°N

The 24°N section is located on the south side of the main subtropical evaporation cell. Its subducting upper layer circulation carries high salinity southward away from the evaporation region. Net shallow freshwater transport is thus northward. The high salinity water subducts south of this section and forms the shallow salinity maximum layer, which is also called Subtropical Underwater (Worthington, 1976; Hanawa and Talley, 2001; O'Connor et al., 2005). In detail, in the layer above $27.3\sigma_\theta$ the Gulf Stream carries 29.0 Sv northward, the subtropical gyre carries 18.6 Sv southward, and the Ekman transport is 4.8 Sv northward (Table 5). Mass balance allocates 13.8 Sv of the 29.0 Sv in the Gulf Stream to the shallow overturn. If the 13.8 Sv is the least dense water in the Gulf Stream ($\sigma_\theta < 25.9$ kg/m^3), the freshwater transport for the shallow overturn is 0.17 ± 0.19 MSv, which is northward but with large uncertainty.

This northward direction for freshwater transport, albeit with large error, seems paradoxical given that the mean salinities of the Gulf Stream and interior Ekman transport are higher (36.33 and 36.81, respectively) than the mean salinity of the interior geostrophic layer (36.18) (Table 5). However, the southward interior flow is vertically sheared and much stronger at the sea surface where salinity is higher than in the northward Gulf Stream (bulge of highest salinity points in the potential temperature–salinity relation in Fig. 8a). The northward freshwater transport is thus largely due to the nearly horizontal circulation at densities lower than 26.0 kg/m^3. This is an example of why (5) is not an accurate simplification of (4) (Section 2.2).

As noted in Talley (2003), about half of the Gulf Stream above the maximum subduction density continues northward into the intermediate and deep water overturn. This results in a large uncertainty in the heat transport calculation for the subducting circulation, since it is not clear which part of the shallow Gulf Stream should be connected into the subducting circulation. The sensitivity to this choice is lower for freshwater transport than for heat transport, since the freshwater transport is dominated here by the very saline southward near-surface interior flow. If, instead of choosing the least dense part of the Gulf Stream for the 13.8 Sv required for mass balance, the mass transport is distributed evenly over the shallow Gulf Stream, the freshwater transport remains northward at 0.22 ± 0.19 MSv (Table 5, 24°N alternate). The mean salinity of the shallow Gulf Stream (36.09) is lower than the mean salinity of the least dense part of the shallow Gulf Stream (36.33), leading to this estimate being slightly greater than the original 0.17 MSv.

4.2. South Atlantic at 32°S

The main evaporation cell and highest surface salinities for the South Atlantic lie north of this section, leading to northward freshwater transport in the closed subtropical gyre. For the calculation, it is difficult to define a local maximum subduction density since the South Atlantic and Indian subtropical gyres are connected. Therefore, several arbitrary choices were tested, as in Talley (2003), yielding similar net results for the subtropical gyre's freshwater transport. Two of these choices, 26.2 and $26.4\sigma_\theta$, are shown in Table 5. The higher subduction density was chosen for discussion, and matches one of the layers in the Southern Ocean analysis (Section 8).

The freshwater transport associated with the subducting gyre is northward at 0.19 ± 0.02 MSv (Fig. 7b and Table 5). This results from a salty southward Brazil Current and fresher northward interior and Ekman flows, and is insensitive to the choice of local outcrop density. In detail, in the subducting layer above $26.4\sigma_\theta$, the Brazil Current carries 7.6 Sv southward, the subtropical gyre carries 9.7 Sv northward, and the Ekman transport is 1.2 Sv northward. The Brazil Current is therefore too weak to balance the 10.9 Sv of northward Ekman and interior flow. Mass balance is achieved by excluding the easternmost part of the northward interior flow from the closed shallow gyre overturn, which thus has a strength of 7.6 Sv. That is, the upper layer of the Benguela Current is excluded (3.3 Sv for $26.4\sigma_\theta$); this water is a flows northward with deeper Benguela Current water to the North Atlantic, returning southward across this section as North Atlantic Deep Water (Section 7.2).

This 0.19 MSv is equivalent in magnitude to the freshwater transport of the other two southern hemisphere subtropical gyres (Sections 4.4 and 4.5; Table 5). The mass transport circulating in the Brazil Current gyre is three to five times weaker but the salinity contrast between the western boundary current and interior flow (35.75 and 35.64, respectively) is larger than in the other two oceans, leading to equivalent freshwater transports. In the potential temperature–salinity diagram (Fig. 9a), the Brazil Current has the saltiest water along 30°S (also evident in the vertical sections of Figs. 12 and 18 below).

4.3. North Pacific at 24°N

This North Pacific section lies close to the subtropical salinity maximum. The net freshwater transport for the shallow overturn is southward: -0.09 ± 0.03 MSv. In detail, in the subducting layer above $26.2\sigma_\theta$, the Kuroshio carries 23.4 Sv northward, the subtropical gyre carries 31.4 Sv southward, and the Ekman transport is 8.6 Sv northward. These transports nearly balance, leaving only 0.6 Sv of the Kuroshio to continue northward into the subpolar gyre, reduced from the 3.3 Sv in Talley (2003) because of the lower NCEP Ekman transport.

With Hellerman and Rosenstein (1983) winds, Talley (2003) calculated 11.3 Sv of Ekman transport and a throughput of 3.3 Sv from the shallow Kuroshio to NPIW formation and Bering Strait. The associated shallow overturning freshwater transport is -0.11 MSv, so effectively the same as with NCEP winds despite the significant difference in Ekman transport. As in the North Atlantic 24°N section, the mean salinities and total volume transports of the three components (Kuroshio, Ekman and southward interior) are not good predictors of the freshwater transport direction. If summed using the simplification (5), the freshwater transport obtained would be small and northward.

The southward freshwater transport of the shallow gyre arises from the higher salinity of the northward Ekman transport compared with the southward interior transport (34.83 and 34.60, respectively); the Kuroshio above the dividing density has approximately the same salinity as the interior (Table 5). The sign of

freshwater transport here is sensitive to the exact latitude of the zonal section. Estimates from subtropical sections lying farther from the evaporation maximum would be more useful.

The impact of the passage of 1 Sv of water through 24°N and out through Bering Strait is calculated from the 0.06 ± 0.02 FSv freshwater component at Bering Strait and 0.01 FSv of the total −0.12 ± 0.05 FSv crossing 24°N (Table 7; Section 6 below). The net divergence of freshwater transport (precipitation) between 24°N and Bering Strait is 0.18 ± 0.05 MSv (Fig. 5a), of which 0.07 MSv can be associated with this 1 Sv.

4.4. South Pacific at 28°S

The 28°S section lies in the center of the high salinity of the subtropical gyre and south of the center of the evaporation region (Figs. 5 and 7a). The freshwater transport of the mass-balanced subducting gyre is northward: 0.23 ± 0.04 MSv, due to northward interior flow of fresh water and southward flow of saltier water in the Ekman layer and East Australian Current (EAC) (34.96, 35.47 and 35.41, respectively, Table 5). In detail, the northward interior shallow geostrophic transport above 27.1σ_θ is 33.3 Sv, the southward Ekman transport is −3.2 Sv, and the EAC transport is −24.0 Sv (Table 5 and Fig. 10b and d). It is assumed that 11 Sv flows through the section to the ITF and Bering Strait (BS). (See Section 5 for a discussion of sensitivity to this assumption.) Assignment of the location for the ITF/BS transport at 28°S is arbitrary. If it occurs in the surface layer interior flow, −19.1 Sv of the EAC is needed to balance the remaining flows (Table 5). This can be accommodated at EAC densities less than 26.8σ_θ. The remaining −4.9 Sv of the EAC would then continue southward and eventually re-enter the South Pacific as deep water, supporting the Pacific–Indian "supergyre" concept (Speich et al., 2002; Ridgway and Dunn, 2007).

On the other hand, if all of the shallow EAC transport is used to balance the interior and Ekman flows, there is a net northward flow in the shallow interior of 6.2 Sv, which could be assigned to the ITF and Bering Strait flows, requiring an additional 3.8 Sv from a deeper layer (not listed in Table 5). None of the EAC would then enter the Antarctic Circumpolar Current. The freshwater transport for the mass-balanced subducting gyre is then 0.16 ± 0.04 MSv, which is only slightly smaller despite the very different assumptions about ITF and Bering Strait transport through the South Pacific section.

Thus, the freshwater transport for the shallow subducting gyre is about 0.2 MSv northward towards the higher evaporation region, independent of how the ITF/BS throughputs are assigned to the section.

The freshwater transport divergence associated with the ITF crossing 28°S is −0.16 ± 0.05 MSv, assuming a closed mass balance of 10 Sv northward across 28°S balanced by 10 Sv of fresher water flowing westward at salinity 34.5 through the Indonesian Passages (Fig. 7b; Section 5).

The freshwater transport divergence associated with the 1 Sv of Bering Strait throughput is a total of 0.08 ± 0.02 MSv of net precipitation/runoff for the ocean north of 28°S, obtained from the 0.07 FSv outflow component through Bering Strait itself and 0.01 FSv crossing the 28°S section.

Thus, the shallow gyre and ITF/BS freshwater transports in the South Pacific have opposite impacts of about the same magnitude, with the shallow gyre importing freshwater and the ITF/BS exporting freshwater. When considered with the small freshwater transport for the deeper overturning components (Section 7.4), this near balance reflects the nearly zero net precipitation/evaporation in the Pacific north of the 28°S section.

4.5. Indian at 32°S

This Indian Ocean section is south of the main evaporation center. It is nearly coincident with the maximum surface salinity

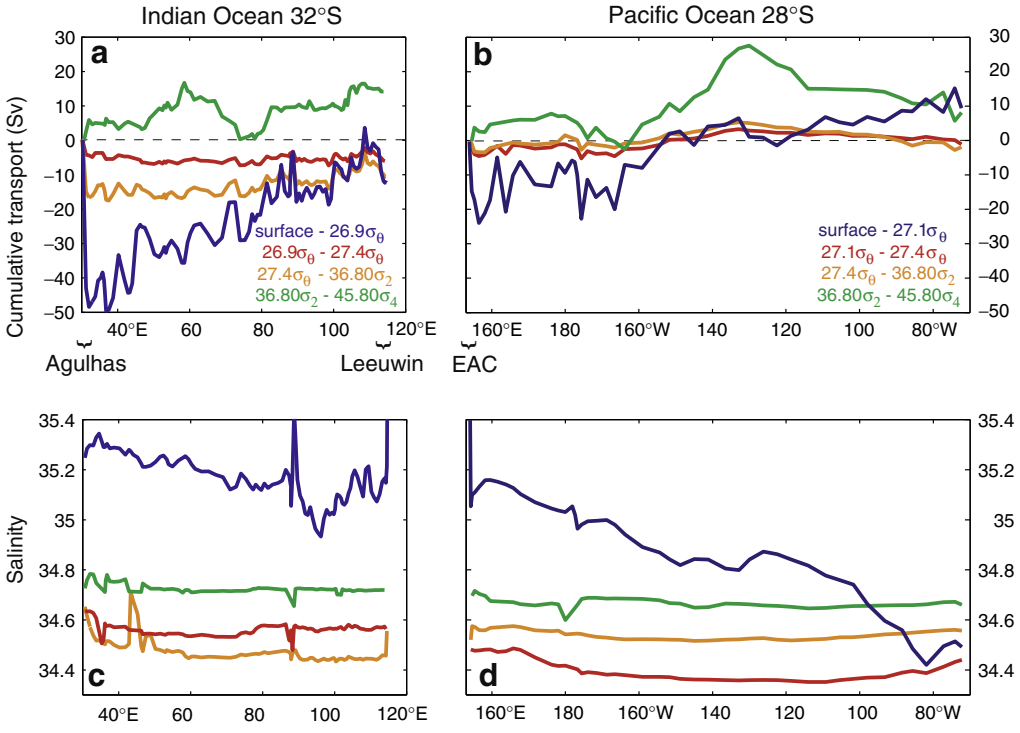

Fig. 10. Cumulative transport (Sv) in the top 3 or 4 isopycnal layers for (a) the Indian Ocean section at 32°S and (b) the Pacific Ocean section at 28°S. Layer-mean salinities are shown in (c) and (d). Figs. 13, 14 and 18 below show the isopycnal depths and complete salinity distribution.

(Fig. 7a). The freshwater transport in the mass-balanced shallow gyre is northward, 0.18 ± 0.02 MSv. This is accomplished by southward flow of saline water in the Agulhas and northward flow of fresher interior water (Fig. 10c), with a negligible Ekman mass transport contribution (mean salinities of 35.31, 35.16 and 35.64, respectively, Table 5). In detail, the interior geostrophic transport above $26.9\sigma_\theta$ is 37.7 Sv northward and Ekman transport is 0.8 Sv northward (Figs. 7a and 10 and Table 5). The assumed ITF transport is 10.0 Sv. Following Talley (2003), this ITF transport is assumed to be balanced by southward transport across 32°S within the upper part of the Agulhas, whose total transport above $26.9\sigma_\theta$ is −49.5 Sv. Thus, all but −1.0 Sv of the shallow Agulhas is required to balance the interior, Ekman and ITF flows.

The freshwater transport crossing 32°S associated with the ITF is 0.23 ± 0.05 MSv, with inflow of 10 Sv from the Pacific through the Indonesian passages and outflow of 10 Sv to the south in the upper layer of the Agulhas (Section 5; Fig. 7b).

Thus, the shallow subducting gyre and the ITF contributions to freshwater transport in the Indian Ocean are of the same magnitude and sign, both about 0.2 MSv, and both associated with net evaporation north of 32°S.

4.6. Summary

Because the subtropical zonal sections lie close to the surface salinity maxima of the subtropical gyres, the sign of the freshwater transport on each section is dominated by the location of the sections relative to the centers of subtropical evaporation and high salinity (Fig. 7). The poleward shallow overturning heat transports (Talley, 2003) were much simpler, since the subtropical sections lie cleanly between the tropical heating and high latitude cooling regions. In the three southern hemisphere oceans, where the sections are all located somewhat south of the evaporation centers, the transport is northward towards the southern hemisphere's high evaporation regions. In the North Atlantic on the other hand, freshwater transport is northward towards the highest evaporation region. In the North Pacific, there is enough precipitation at higher latitudes compared with the North Atlantic that the freshwater transport sign is southward.

The order of magnitude of the shallow overturning freshwater transport for each gyre is 0.1–0.2 MSv. This is the same order of magnitude as the surface freshwater divergences between pairs of sections due to air-sea forcing (Tables 3 and 4).

5. Indonesian throughflow and freshwater transport

5.1. Freshwater transport divergences

Part of the freshwater transport divergence in the Pacific and Indian Oceans is associated with the ITF waters exiting the Pacific and entering the Indian Ocean (Piola and Gordon, 1984), at an assumed salinity of 34.5 and volume transport of 10 Sv (based on Gordon et al., 1999). (See Sections 2 and 3.) This redistribution of freshwater, which is a robust result, is important in maintaining the lower salinity of the Pacific compared with the Indian Ocean. It is associated with atmospheric freshwater transport out of the Indian and into the Pacific Ocean (although not necessarily as part of the same atmospheric circulation pattern). In this calculation, there is also a small export of freshwater from the Southern Ocean via the combined Pacific–Indian ITF path since the Agulhas outflow salinity is higher than the Pacific inflow salinity, associated with the 10 Sv transit through the Southern Ocean that balances the ITF.

In the Indian Ocean, the net freshwater transport divergence associated with the passage of ITF water through the basin is 0.23 ± 0.05 MSv into the tropical Indian Ocean (Fig. 7b and Table 5). This is the sum of 0.11 ± 0.05 FSv at the ITF and 0.12 ± 0.002 FSv in the upper layer of the Agulhas at 32°S (Table 2, column labeled 4). That is, the inflowing ITF is fresher (10 Sv at 34.5) than the southward outflow of more saline water in the Agulhas (10 Sv at 35.3, Table 13 below). The other possible outflow, in the Leeuwin Current, is also saline (see Section 5.2 for discussion of why it is assumed that the outflow is in the Agulhas). The ITF loop requires net evaporation in the Indian Ocean that is in addition to the net evaporation calculated for the shallow overturning gyre freshwater budget (Section 4.5).

In the Pacific, the flow of 10 Sv across 28°S to feed the ITF has a freshwater transport divergence of −0.16 ± 0.05 MSv north of 28°S (Fig. 7b), requiring net freshening north of 28°S. That is, the inflow of 10 Sv across 28°S from the Southern Ocean is saltier (34.96) than the fresher outflow through the Indonesian passages (34.5). This freshwater transport estimate is the sum of −0.11 ± 0.05 FSv due to the 10 Sv exiting through the ITF, and −0.05 ± 0.02 FSv due to the 10 Sv entering from the south across 28°S, calculated as a proportion of the total freshwater transport component in this layer (Table 2, column labeled 4).

A different picture of the freshwater budget for the ITF flow through the Pacific is obtained using the 43°S section instead of 28°S. The freshwater transport divergence for the 43°S and ITF sections is 0.05 MSv, summed from 0.16 FSv crossing 43°S and −0.11 FSv exiting through the ITF. That is, the mean salinity of the broad northward flow in the upper layer above $27.1\sigma_\theta$ at 43°S is 34.37, which is *fresher* than the ITF outflow, so the total budget requires net evaporation north of 43°S rather than net precipitation. Given the result of net freshening north of 28°S in the previous paragraph, the net evaporation occurs between 43°S and 28°S.

Looking at the Pacific and Indian Oceans together, the Agulhas outflow is saltier than the northward flow into the Pacific across either 43°S or 28°S. Thus, there is net northward freshwater transport out of the Southern Ocean associated with the complete ITF loop, of 0.07 MSv using 28°S and 0.09 MSv using 43°S. Thus, part of the required northward export of freshwater from the Southern Ocean is carried by the ITF loop, with an order of magnitude that is comparable to the export due to each of the three southern hemisphere subtropical gyres (Section 4; Fig. 7b).

5.2. Uncertainties

The ITF throughput is associated with net evaporation in the Indian and net precipitation in the Pacific (north of 28°S, but net evaporation if 43°S is considered the boundary), based on the salinities of the inflow from the Pacific, outflow to the Indian and the ITF itself. Uncertainties in the magnitude and in the sum of the opposing Indian and 28°S Pacific contributions are examined here (Table 6). The magnitudes of 0.23 ± 0.05 MSv and −0.16 ± 0.05 MSv (Indian and Pacific) given above are sensitive to the assumed ITF volume transport and assigned location of flow across 32°S and 28°S, as well as to the more general sensitivities to reference velocity and Ekman transport. Here sensitivity to the assumed ITF transport and location are discussed as they are specific to the ITF budget.

5.2.1. ITF volume transport

The 10 Sv mean ITF assigned here is an estimate for an incompletely observed and highly variable flow. The mean might be as large as 15 Sv (Schott, personal communication). The global inverse and state estimates listed in Section 2 support a choice of 10–12 Sv (Macdonald, 1998; SR2001; Stammer et al., 2003). Budgets within the Indonesian Seas suggest a net 12 Sv, with 9 Sv through the shallow Makassar Strait and 3 Sv through the deeper Lifamatola Strait, which could be distributed in the Indian Ocean's westward South Equatorial Current as 9 Sv above 500 m and 3 Sv down to about 1200 m (about $27.3\sigma_\theta$) (Talley and Sprintall, 2005). Lower

values have been derived or assigned in previous treatments (e.g. 6.7 Sv in Toole and Warren, 1993; 5.3 Sv in Robbins and Toole, 1997; 5 Sv in Reid, 2003).

In Table 6, a range of ITF transports from 8 to 14 Sv is examined, with relative freshwater transport of 0.09–0.16 FSv within the throughflow ("3" in Table 6). Increasing the volume transport increases the net precipitation and net evaporation associated with the ITF loops, with a maximum range of uncertainty of 0.1 MSv. The ranges for an 8–14 Sv ITF are −0.13 to −0.23 MSv net precipitation for the Pacific and 0.18–0.27 MSv net evaporation for the Indian ("8" in Table 6). The sum of the Pacific and Indian ITF loops is 0.05, 0.07, 0.06 and 0.04 MSv net evaporation (precipitation) north (south) of the sections for 8–14 Sv ITF volume transport, hence smaller uncertainty than for the separate Pacific and Indian divergences.

Total freshwater divergence for the Pacific and Indian ("5" in Table 6), which includes all freshwater transport components in addition to the ITF loops, increases in magnitude with increasing ITF, with an uncertainty range of 0.05 MSv. The Pacific is diagnosed as more precipitative (−0.03 to −0.06 MSv) and the Indian as more evaporative (0.36–0.41 MSv) with increasing ITF transport, that is, as more water moves through the system. However, this increase does not equal the increase in the ITF loops' freshwater transport themselves.

Increasing the ITF transport has a negligible effect on the Indian shallow overturning transport. However, increasing the ITF transport has a side effect of increasing the northward shallow overturning freshwater transport in the Pacific, from 0.21 to 0.26 MSv. This partially offsets the increase in ITF loop precipitation for the Pacific. The shallow gyre freshwater transport increases, even though the volume transport around the shallow gyre decreases (from 21 to 16 Sv) as the ITF transport is increased from 8 to 14 Sv. This is because the southward gyre return flow in the EAC is assigned to the lowest density and hence saltiest EAC water; a weaker EAC volume transport captures the saltiest water, thus increasing the northward freshwater transport associated with the shallow gyre.

Deep overturning freshwater transport ("10" in Table 6) in the Indian is impacted by changing ITF transport assumptions; with the weakest 8 Sv ITF, the upper layer of the Agulhas has extra volume transport that must be made up from deep upwelling into the saline surface layer, which results in a net 0.0 MSv. At the larger ITF transports, deep upwelling only goes up into the fresher intermediate layers, and the net freshwater transport is −0.04 MSv (at 10 and 12 Sv ITF).

To summarize, a reasonable range in ITF transport (8–14 Sv) yields an uncertainty of ±0.05 MSv for the ITF loop's component of the freshwater transport in the Indian and Pacific, an uncertainty of ±0.02 MSv to the sum for the Indian and Pacific, an uncertainty of ±0.02 MSv for the shallow overturning gyres that are impacted, and an uncertainty of at most ±0.02 MSv for the deep/intermediate overturning.

5.2.2. Geographic assignment of ITF throughput

The geographic assignment of the 10 Sv for the ITF through the Pacific 28°S and Indian 32°S sections is now examined, assisted by Fig. 10. First it is argued that the assignment of ITF throughput to the top layer in the Agulhas and to the top layer in the interior Pacific is sensible, and then sensitivity to these choices is examined roughly.

The ITF volume was assigned to the Agulhas in the top layer (surface to 26.9σ_θ, 0–800 m) for the following reasons. First, the lack of a large volume of transformation of surface waters into deep waters within the Indian Ocean suggests that the ITF transport should be assigned to the upper ocean since these surface waters cannot be drawn downward in great volume. Secondly, the Agulhas transport in this layer (Fig. 10a) easily accommodates this 10 Sv along with the 38.5 Sv needed to return the shallow gyre circulation. If the ITF transport were distributed more evenly over the ocean depth, possibly unphysical increases in upwelling from deep layers to the surface layer would be required to feed the large upper ocean Agulhas transport, as evidenced in even reducing to the 8 Sv ITF in the Agulhas (Section 5.2; Table 6). Thirdly, even if part of the ITF volume is in the upper layer of the Leeuwin Current, the salinity there is even higher than in the Agulhas and so the ITF loop freshwater transport would be even greater. And, recently, Domingues et al. (2007) indicate that the Leeuwin Current source is not the ITF but rather eastward flows in the subtropical gyre. Fourthly, the inshore portion of the upper ocean Agulhas has been shown to carry low latitude Indian Ocean waters, which could easily include the ITF waters (Beal et al., 2006).

A maximum, but unphysical, uncertainty in net Indian evaporation due to the ITF can be estimated by assigning the 10 Sv to the entire 32°S section, which has a freshwater transport component of 0.26 FSv (Table 2) instead of the 0.12 FSv for just the Agulhas surface layer (Table 5); the total ITF loop evaporation in the Indian Ocean would be 0.37 MSv instead of 0.23 MSv. When the 10 Sv is assigned to the full water column of just the Agulhas, with a total southward transport of −66.8 Sv and freshwater transport component of 0.38 FSv, the ITF freshwater component is 0.06 FSv and the associated evaporation is reduced to 0.17 MSv. These would seem to be physically unpalatable choices because they require a large downward flux of ITF water from the upper ocean to the deep layers somewhere north of 32°S, and a compensating increased upwelling of deep waters to the surface layers to feed the large, near-surface Agulhas transport.

A more physically plausible choice for exploring uncertainty is to assign the ITF transport to the top two layers in the Agulhas in proportion to the total Agulhas transport in these two layers (−49.5 and −14.6 Sv in the layers surface to 26.9σ_θ and 26.9–27.3σ_θ). The freshwater transport component for the 10 Sv of ITF transport is then 0.07 FSv, yielding a total ITF loop evaporation of 0.18 MSv. If the ITF transport were all assigned to the surface layer in the Leeuwin Current, which is not a reasonable assumption based on observations and models (Domingues et al., 2007), which has a southward transport of −11.5 Sv and mean salinity of 35.22 in this analysis, the freshwater transport component would be 0.13 FSv and the total ITF loop for the Indian would be 0.24 MSv, very similar to the estimate assuming all transport is in the surface layer of the Agulhas.

In the Pacific, the 10 Sv was assigned to the northward gyre flow in the thermocline layer from the surface to 27.1σ_θ. Neither of the next two layers below this, which encompass the rest of the upper 2000 m, can accommodate 10 Sv of northward transport (Fig. 10b). The deep water transport could accommodate the ITF volume transport, and in some older global scenarios it has been assumed that the ITF waters originate as upwelled Pacific deep waters (e.g. Gordon, 1986; Broecker, 1991). However, since the thermocline layer does have an excess of 10 Sv of northward transport (Fig. 10b), assignment of this ITF transport to the deepest waters would require that the surface 10 Sv be eliminated somewhere north of the section through downwelling (and that this be replaced by upwelling from the deep layers to the surface layer to feed the ITF). This is unphysical, since the only dense water formation is in the northern North Pacific, and the rate does not exceed 2 Sv. Therefore, the ITF throughput is most likely in the upper ocean, as suggested by Schmitz (1995).

Probing uncertainties as for the Indian 32°S above, first assign the 10 Sv to the entire 28°S section, which has a freshwater transport component of 0.13 FSv, hence 0.12 FSv for the 10 Sv (Table 2), instead of the −0.05 FSv for the interior ocean's surface layer (Table 5); the total ITF loop in the Pacific would be 0.01 MSv instead of

−0.16 MSv. Assigning all 10 Sv to the deep water $36.80\sigma_2 - 45.80\sigma_4$ layer (Fig. 10b and c), the freshwater transport component is 0.06 FSv, and the net ITF loop for the Pacific is 0.06 − 0.11 = −0.05 MSv. Both of these choices are argued above to be physically implausible.

If all of the 10 Sv is assigned to the surface layer but just in the eastern South Pacific, where the salinity is lower than on the rest of the section (Fig. 10d), it would be assigned from 120°W to South America in order to accommodate the full 10 Sv (Fig. 10b). This is a quite plausible scenario for the influx from the Southern Ocean that would feed the ITF loop. The freshwater transport component would be 0.01 FSv, yielding a net for the Pacific ITF loop of −0.10 MSv.

To summarize, physically implausible assignments of the location of the ITF transport through the Indian and Pacific zonal sections can lead to quite large uncertainties in the ITF loop's contribution to the freshwater divergence. Restricting ourselves to more plausible choices leads to an uncertainty of about ±0.05 MSv for both the Indian and Pacific Oceans.

Moreover, the exercise of examining possible locations for the ITF throughput on the Indian and Pacific zonal sections suggests that the loop is almost entirely within the upper ocean layers, involving little exchange with deeper layers north of these sections, especially if the ITF transport is in the range 10–12 Sv. In particular, an upwelled deep water source for the ITF within the Pacific Ocean, which is a feature of the popularized "conveyor belt" schematic (Gordon, 1986; Broecker, 1991), is unnecessary and inconsistent with the intermediate and deep layer mass transports.

6. Bering Strait freshwater transport and impact on Pacific and Atlantic salinity

6.1. Freshwater transport divergences

Flow through Bering Strait (BS) is a much-discussed component of the global freshwater transport (e.g. Hall and Bryden, 1982; Wijffels et al., 1992; Wijffels, 2001; Aagaard and Carmack, 1989; Woodgate and Aagaard, 2005) since it carries nearly 1 Sv of relatively fresh water (salinity ~ 32.5) from the Pacific to the Atlantic through the Arctic. Closing Bering Strait in climate models affects dense water production in the Labrador Sea and Nordic Seas (e.g. Wadley and Bigg, 2002). Here examination of bulk freshwater balances shows that Bering Strait is a minor part of the total freshwater input to the high latitude North Atlantic and Arctic in terms of its impact on overall salinity of North Atlantic Deep Water, but it is important for Pacific freshwater export and the NPIW salinity. Note though that this bulk consideration does not examine specifics of delivery of the Bering Strait freshwater to, for instance, the Labrador Sea, in terms of impact on local vertical stratification and hence overturn; that is, it is likely that location of freshwater delivery rather than total amount is the overriding factor for NADW production.

Wijffels et al. (1992) and Wijffels (2001) chose Bering Strait salinity and freshwater transport as the (arbitrary) baseline for global freshwater transports because BS is a useful, nearly closed boundary at which to begin meridional integrations for Atlantic/Arctic and Pacific meridional transports. If this baseline had been adopted here, the arbitrary reference salinity chosen for all freshwater component calculations would have been the Bering Strait salinity of ~32.5. An arbitrary reference salinity of 34.9 is used instead throughout this present work, since it is close to the mean 34.83 of all sections in this analysis (Fig. 6a). As emphasized above, only the sums in each mass-balanced circuit are associated with air-sea fluxes of freshwater; these freshwater transport divergences, reported here in units of MSv, are independent of reference salinity.

Two major issues are considered here, both with robust results. The first is the BS role in maintaining the lower average salinity of the Pacific compared with the Atlantic and Indian. Here it is seen that BS is one of three approximately equivalent freshwater export pathways for the Pacific, the other two being export through the Indonesian Throughflow and freshening of upwelling saline deep and bottom waters due to downward diffusion. (There is also import of freshwater from the Southern Ocean in the upper ocean's subtropical gyre that must be accounted for in the total Pacific balance.) Moreover, in the North Pacific north of 24°N, the freshwater loss through Bering Strait is comparable in magnitude to freshening in the shallow overturning gyre and in NPIW formation. In the Atlantic/Arctic north of 32°S, BS is also one of three freshwater inputs, the other two being a small input due to NADW export across 32°S and the much larger input of freshwater across 32°S due to the subtropical gyre circulation.

The second issue is the BS role in freshening North Atlantic Deep Water (NADW) relative to saline North Atlantic surface waters. Much has been made of this role, but as shown in this section, the actual impact of BS freshwater on NADW is minor in comparison with that of air-sea fluxes of freshwater, including runoff, into the Arctic and subpolar North Atlantic.

Leading in to these two issues, it is first shown that the passage of 1 Sv of water through all zonal sections in the Atlantic and Pacific has almost no effect on local freshwater divergences between the sections, except between the strait itself and the adjoining sections. Thus, BS is primarily a bookkeeping nuisance for most of the zonal sections.

The ~1 Sv that enters the Arctic through Bering Strait requires that 1 Sv runs through each Pacific and Atlantic section. Since salinity varies only a little from one section to the next, the freshwater convergence between sections due to the 1 Sv is mostly unimportant. Freshwater transport components for 1 Sv passing through each section at the mean, minimum and maximum salinity are shown in Table 7. The minimum and maximum salinities provide error bounds on this calculation at an assumed mass transport of 1 Sv. The BS freshwater transport component through each section in the Pacific at the mean salinity is less than 0.01 FSv with a mean square uncertainty of 0.03 FSv based on the minimum and maximum salinities on each section. Changes in freshwater transport from section to section are in the third decimal place because of the small change in salinity from section to section, confirming that the local freshwater divergence between adjacent sections due to BS throughput is small.

Non-trivial freshwater divergence is found in the regions that border Bering Strait since the salinity of ~32.5 at BS is considerably lower than the mean salinity on any of the sections. Net precipitation and runoff of 0.06 MSv in the North Pacific north of 47°N is associated with the BS throughput, computed as the difference of components 0.07 FSv through Bering Strait and 0.01 FSv associated with 1 Sv crossing 47°N (Table 7). This 0.06 MSv is about half of the total 0.10 MSv of precipitation/runoff between 47°N and Bering Strait (Fig. 5a). The other half must be carried southward across 47°N, and presumably mostly contributes to NPIW (next paragraph). If BS were closed, then all of the North Pacific's excess freshwater would be exported southward; this could both reduce the salinity and density of NPIW and possibly also reduce its already small production rate in the Okhotsk Sea (e.g. Talley et al., 2003; Shcherbina et al., 2004).

If a larger North Pacific region is examined, from 24°N to Bering Strait, the total precipitation/runoff is 0.19 MSv (Fig. 5a), which must be exported either northward through Bering Strait or southward across 24°N (Fig. 5a). The Bering Strait component remains 0.06 MSv since the associated freshwater transport component

across 24°N is almost identical to that at 47°N. The shallow overturning circulation at 24°N moves −0.08 MSv southward (Fig. 7b; Section 4.3). The remaining southward freshwater transport of −0.05 MSv across 24°N is due to NPIW formation, since deeper overturns do not contribute to freshwater transport across this section, as shown in Section 7.3. Therefore, in the freshwater budget for the North Pacific's 24°N section, Bering Strait is equivalent in impact to the shallow overturning gyre and NPIW formation.

Extending our view to the complete Pacific north of either 28°S or 43°S, transport through Bering Strait must be accounted for in the total set of freshwater exchanges, but it is only one of several freshwater exchange mechanisms. The net Bering Strait influence is 0.08 MSv, since the freshwater transport component crossing the South Pacific sections is −0.01 FSv due to 1 Sv flowing northward at a salinity slightly higher than 34.9, which is added to the 0.07 FSv exiting northward through BS (Table 5). The total precipitation/runoff required north of 28°S is 0.05 MSv, based on top-to-bottom transports at 28°S and at BS (Fig. 5b). Therefore, at first glance, it might seem that the Bering Strait net impact of 0.08 MSv yields all and more of the 0.05 MSv freshwater export that is needed to maintain the mean, fresher salinity of the Pacific, within any plausible assumption of uncertainty (±0.02 FSv for the BS component itself, Section 6.3). However, BS is just one part of the Pacific export, which also includes: (1) freshwater export through the Indonesian Passages, associated with net precipitation in the Pacific of 0.16 ± 0.05 MSv (Sections 4.4 and 5), (2) freshwater export of −0.03 ± 0.03 MSv in the deep Pacific overturn due to northward flow of saline deep water that upwells and returns southward at lower salinity (Section 7.3), and (3) freshwater import from the Southern Ocean of 0.23 ± 0.05 MSv in the shallow overturning gyre (Section 4.3, Fig. 7b; Section 5). Ignoring any one of these components would result in an incorrect salinity balance for the Pacific.

In the North Atlantic, the new NADW that flows southward across 24°N is approximately 1 salinity unit fresher than the northward-flowing surface waters that are its primary volume source (Section 7.1 below). All of the freshwater acquired in the Arctic/subpolar North Atlantic and from Bering Strait is mixed into the new NADW/LSW and exported southward in the NADW layer (Section 7.1 below), rather than by the shallow overturning gyre (Section 4.1) (e.g. McCartney and Talley, 1984; Rahmstorf, 1996).

In the North Atlantic, the Bering Strait's 0.07 FSv, when combined with freshwater transport across the 59°N North Atlantic section, yields a total freshwater divergence for the Arctic/subpolar North Atlantic of 0.52 ± 0.24 MSv (Fig. 5a, Table 3). This is larger than the 0.31 MSv from NCEP air-sea fluxes and DT02 runoff for this area; it also requires unphysical evaporation between 59°N and 53°N. The relatively large uncertainty in the value arises from spatial variability in salinity along the section. If the 45°N or 53°N transports are used instead, the net freshwater divergence for the Arctic/subpolar North Atlantic is 0.31 ± 0.12 MSv (Fig. 5b), which is somewhat smaller than the regional NCEP/DT02 flux (0.38–0.46 MSv). These ranges are consistent with a net air-sea flux for the Arctic/subpolar North Atlantic of 0.3–0.5 MSv.

The net freshwater convergence due to Bering Strait for the whole Atlantic north of 32°S requires 0.07 ± 0.02 MSv of evaporation, summing the freshwater components at Bering Strait (0.07 FSv) and at 32°S (−0.003 FSv). This is a small part of the net evaporation of 0.27 ± 0.04 MSv in the Atlantic Ocean north of 32°S (Fig. 5b), which means that other freshwater sources to the Atlantic Ocean must greatly exceed that of Bering Strait. These sources are air-sea fluxes/runoff in the Arctic/subpolar North

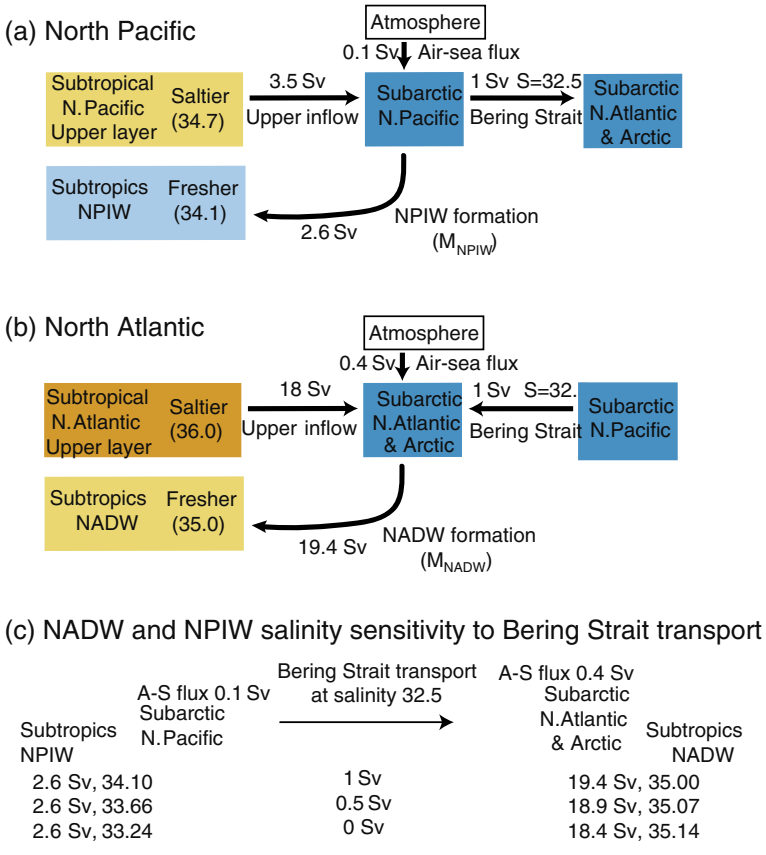

Fig. 11. Illustrative freshwater balances for basic calculations involving Bering Strait, air-sea fluxes and (a) North Pacific Intermediate Water formation and (b) North Atlantic Deep Water formation. Transports and salinities are from base calculations in Table 8. See text (Eqs. (5) and (6)) for symbol definitions.

Atlantic and in the Southern Ocean south of 30°S (which includes for instance all of the SAMW and AAIW formation regions).

6.2. Sensitivity of NADW and NPIW salinity and production estimates to Bering Strait transport

Consider first the sensitivity of NADW salinity and production rate estimate to the Bering Strait throughput (Fig. 11 and Table 8), using these heuristic bulk freshwater and salt balances for a simplified two-layer (surface and deep water) representation of the North Atlantic:

$$M_{NADW} = M_{upper} + M_{BS} + M_{ASF}$$
$$M_{NADW}S_{NADW} = M_{upper}S_{upper} + M_{BS}S_{BS} \quad (6a, b)$$

M is volume transport, S is salinity, "NADW" is the NADW/LSW outflow, "upper" is the saline Atlantic surface water inflow, "BS" is Bering Strait water, and "ASF" is freshwater input through precipitation, evaporation and runoff into the Arctic/subpolar North Atlantic.

As a base state for considering NADW sensitivities (Fig. 11a and Table 8), Bering Strait transport and salinity are 1 Sv and salinity 32.5, the transport and salinity of the northward-flowing surface Atlantic waters are 18 Sv and salinity 36 (Fig. 12a below), and the NADW/LSW salinity is 35. These salinities are based on layer mean salinities (Section 7.1; Table 9) and the potential temperature/salinity relation for the North Atlantic (Fig. 8). From these, an air-sea–runoff flux of M_{ASF} = 0.44 Sv from (6) and NADW transport of 19.44 Sv are diagnosed. (For 15 and 20 Sv overturn, M_{ASF} = 0.36 and 0.50 Sv, not listed in the table.) This air-sea flux is consistent with that shown above for the Arctic and subpolar North Atlantic north of 45°N (Fig. 5a and Table 3).

If there were no Bering Strait transport (M_{BS} = 0), then M_{NADW} = 18.51 Sv and M_{ASF} = 0.51 Sv. This air-sea/runoff freshwater flux appears to be a little large, but is not outside the range of possibility.

If Bering Strait were the only source of freshening for the NADW, with no air-sea fluxes/runoff, then M_{BS} = 7.2 Sv (also, 6 or 8 Sv for a 15 or 20 Sv overturn). This BS transport is far outside the range of observed transports.

If the Arctic/subpolar North Atlantic air-sea flux is set at 0.44 Sv ("base" solution), and Bering Strait is turned off, the resulting salinity of the NADW would be 35.14 rather than 35. (At 15 Sv instead of 18 Sv, and at the 0.36 Sv air-sea flux of the 15 Sv overturn, the NADW salinity would be 35.15.) This salinity sensitivity is several times larger than observed salinity anomalies of order 0.05 in northern North Atlantic water masses documented between 1963 and 2002. However, these anomalies have been ascribed to Arctic and subpolar North Atlantic variability, which have a proportionally stronger effect than Bering Strait variations (Dickson et al., 2003).

If the NADW salinity is set to 35 compared with an inflow salinity of 36, air-sea flux is set at 0.44 Sv, and Bering Strait is turned off, the NADW overturn is decreased to about 15.5 Sv, which is within the range of quoted NADW production rates.

Thus, the freshening of NADW relative to its saline low latitude Atlantic source water results is largely (~85%) due to the accumulated precipitation and runoff into the subpolar North Atlantic and into the Arctic (0.4 Sv at 0 salinity units), with Bering Strait a minor component (1 Sv at 32.5 salinity units).

Water from Bering Strait clearly flows through the Arctic and the Canadian archipelago and into the Labrador Sea (e.g. Wadley and Bigg, 2002). However, the simple balances here show that the effect of changes in Bering Strait transport or salinity on NADW salinity and hence North Atlantic freshwater transport cannot be any more important than variability in the many other aspects of the high northern latitude freshwater balance, including air-sea fluxes, runoff and changes in sea or land ice.

In contrast, the salinity and production rate of NPIW in the North Pacific are much more sensitive to Bering Strait. Use the same bulk balances:

$$M_{NPIW} = M_{upper} - M_{BS} + M_{ASF}$$
$$M_{NPIW}S_{NPIW} = M_{upper}S_{upper} - M_{BS}S_{BS} \quad (7a, b)$$

where "NPIW" is the NPIW outflow, "upper" is the saline North Pacific surface water inflow, and "ASF" is freshwater input through precipitation, evaporation and runoff into the subpolar North Pacific south of Bering Strait (Fig. 11). The "base" state, representing layer means (Section 7.3; Table 11) and the potential temperature/salinity relation in Fig. 8a, is 1 Sv at salinity 32.5 for Bering Strait, 3.5 Sv at salinity 34.7 for surface inflow, and NPIW salinity of 34.1. Using these values, an air-sea flux/runoff of 0.11 and 2.6 Sv NPIW production rate are diagnosed, which are close to the values shown in Fig. 5a and Table 11.

If Bering Strait is turned off, and it is assumed that all freshwater flux is incorporated in NPIW, keeping the inflow transport at 2.5 Sv (3.5 Sv minus 1 Sv for BS) and the air-sea flux at 0.11 Sv, then the NPIW salinity is greatly reduced to 33.2. That is, the salinity change for NPIW would be 2.5 times larger than with Bering Strait exporting freshwater. This is far more sensitive than the equivalent calculation for NADW salinity sensitivity.

If Bering Strait is turned off and the salinity difference between inflow and outflow for NPIW is set at 0.6, keeping an air-sea flux of 0.11 Sv, then the production rate of NPIW would have to be more than 6 Sv, or more than double any observed rate. Again, this is far more sensitive than for NADW, whose diagnosed overturn rate for the same calculation is within the range of observed rates.

Of course, deletion of the Bering Strait outflow might have a much greater impact on the northern North Pacific than these simple calculations suggest, by freshening it too much to permit NPIW production. The salinity of 33.2 diagnosed for NPIW, holding production rate and air-sea fluxes constant, would reduce its density from about 26.8 to 26.2σ_θ, if potential temperature were held constant. This suggests that, even though the mechanism for producing NPIW would remain because of the cyclonic subpolar gyre with buoyancy loss culminating in maximum density within the Okhotsk Sea (e. g. Talley, 1993), the process would shift to a lower salinity and density, with the North Pacific even more extreme than now in terms of freshness and limited dense water production compared with comparable sites in other oceans.

6.3. Uncertainties

Observed Bering Strait annual mean transport and salinity are 0.8 ± 0.1 Sv at 32.5 ± 0.3, plus an annual mean component of 0.08 ± 0.02 Sv at 30.3 ± 0.5 in the Alaska Coastal Current, based on the most recent comprehensive treatment (Woodgate and Aagaard, 2005). Together these suggest a best estimate of 0.9 ± 0.1 Sv at 32.3 ± 0.3.

The best estimate of the BS freshwater transport component is therefore 0.067 ± 0.015 FSv relative to the arbitrary reference salinity of 34.9, using 0.9 Sv and 32.3 salinity. The value used herein is 0.069 Fv, using 1.0 Sv and 32.5, with the errors in transport and salinity (coincidentally) compensated. For all calculations reported herein, only two decimal places are used, hence a freshwater transport component for BS of 0.07 ± 0.02 FSv.

A similar uncertainty of about ±0.02 FSv is obtained for freshwater transport divergence between each pair of zonal sections due to the throughput of 1 Sv of BS water, in this case assigned to the maximum and minimum salinities on the sections (Table

7). (The net impact of BS freshwater transport on each zonal section's freshwater transport is of order 0.01 FSv, also in Table 7.)

7. Intermediate and deep overturning transports

Water mass transformations between different isopycnal layers, such as creation of the global deep and intermediate waters, have associated freshwater transports. These are estimated here from the zonally integrated transports in isopycnal layers. For the main subtropical sections (24°N and ~30°S), the mass-balanced shallow overturn (Section 4) is first removed from the upper layer. Then the throughput (Bering Strait or ITF) is assigned to one of the layers, which accounts for all mass imbalances. The freshwater transport associated with each layer-to-layer transformation is calculated from a mass balance between northward and southward-flowing waters in different isopycnal layers, following Talley (2003).

In this section, the freshwater transports are described in terms of water mass transformations occurring *north* of each of the sections. For the Atlantic, this is formation of the components of NADW. For the Pacific, this is formation of NPIW and PDW, and for the Indian the formation of IDW. In the Pacific and Indian Oceans, upwelling of LCDW into the intermediate water and surface layers is also found.

All of these transports should also be interpreted in terms of transformations to the south of each section. In Section 8, transports are described in terms of water mass transformations occurring south of the 30°S sections, hence in terms of formation of Circumpolar Deep Water.

A table and figure are provided for each zonal section, listing the component mass, freshwater and heat (temperature) transports for each layer and illustrating the salinity and water mass distribution on each section (Figs. 12–14 and Tables 9–13). The deep potential temperature–salinity relations (Figs. 8 and 9b) show the isopycnals bounds for each section's layers. Transports for the composite 30°S Southern Ocean section are discussed in Section 8. The net balances for the shallow and deep overturns are listed in the left data column of the tables. The center data column lists the components of the overturning transports for each layer (FSv and PWT). The rightmost column shows the transports associated with transformation to another layer (MSv and PW). Because these latter are mass-balanced, the freshwater and heat transports are absolute, and associated with freshwater and heat divergences.

The mean salinity for each layer is also listed in Tables 9–13 as a general guide to relative freshness or saltiness, but can be a misleading indicator of the potential contribution of a given layer to freshwater transport (Section 2.2).

All of the deep overturning freshwater transports are summarized in Fig. 15b.

Freshwater transports are listed in thousandths throughout this section and in the figures because values are small and the uncer-

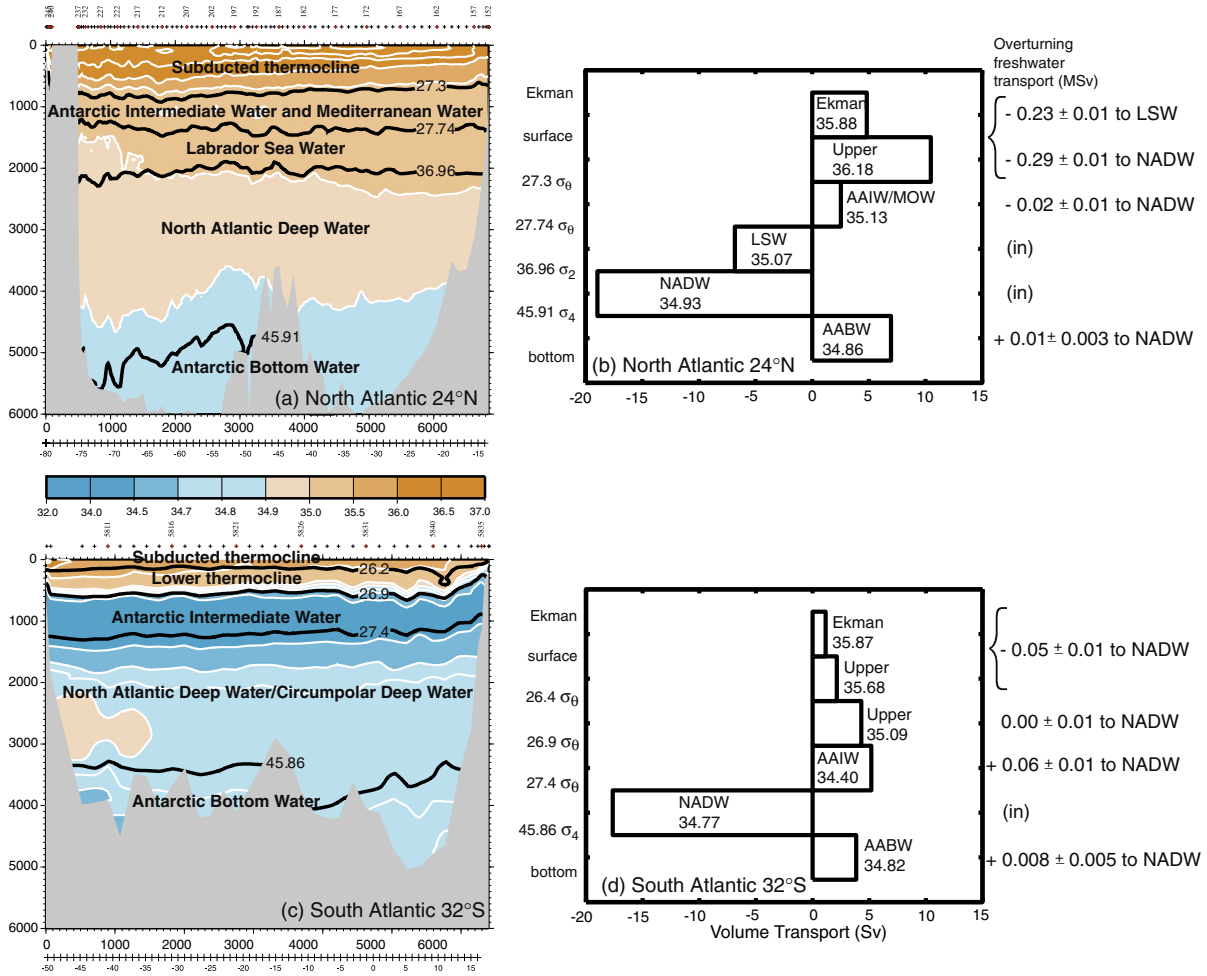

Fig. 12. North Atlantic at 24°N and South Atlantic at 32°S. (a, b) Salinity sections, with isopycnals used for layer analysis. The shallowest isopycnal is the base of subtropical subduction, at 27.3σ_θ in the North Atlantic and 26.4σ_θ in the South Atlantic. White contours: salinity, corresponding to color bar. Black contours: potential densities used in right-hand panels. (c, d) Meridional overturning volume (Sv) and freshwater transports (MSv). Isopycnal layers used for the zonal averages were chosen to maximize overturning volume transport. The mean salinity of each layer is listed. (See Tables 9 and 10.) (For interpretation of the references to color in this figure legend, the reader is referred to the web version of this article.)

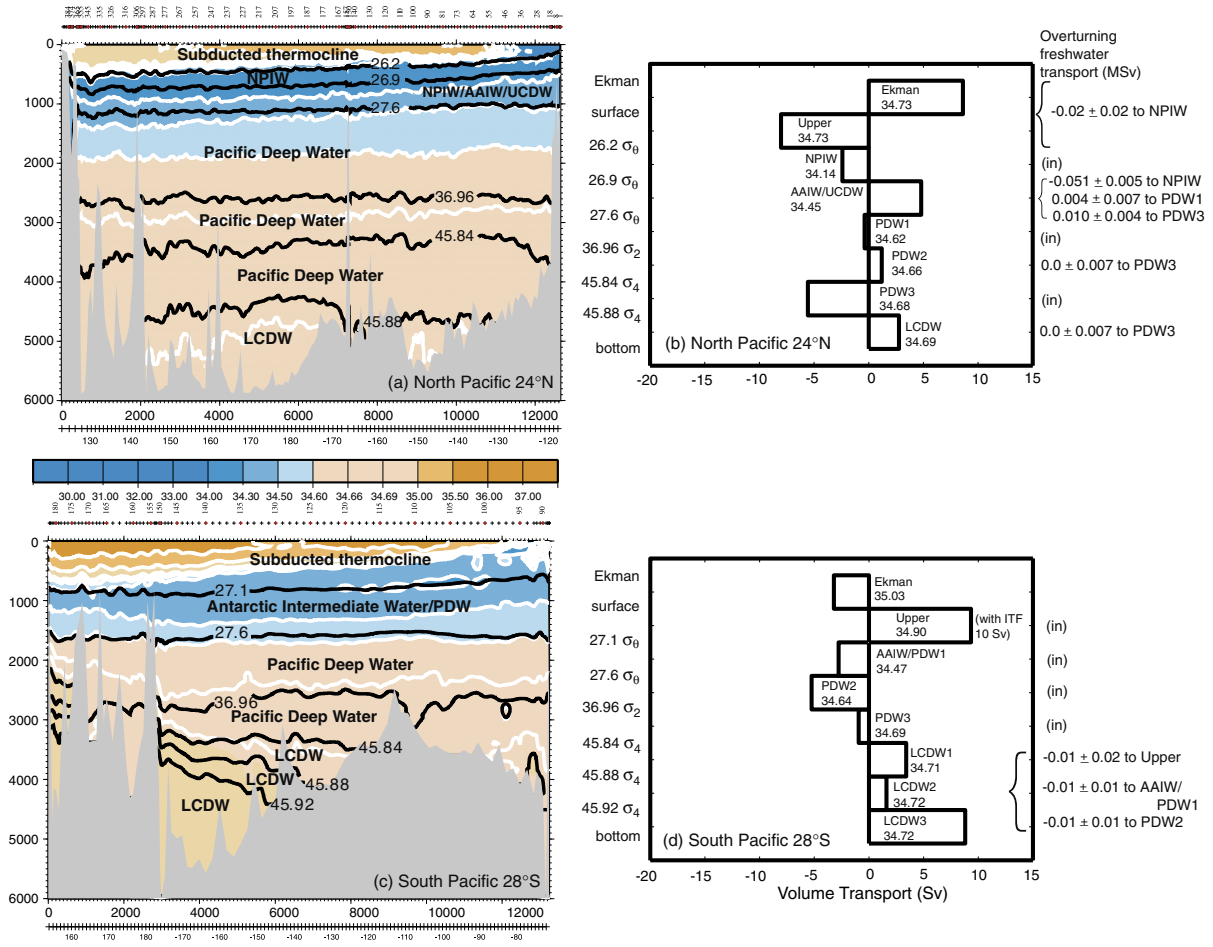

Fig. 13. North Pacific at 24°N and South Pacific at 28°S. (a, b) Salinity sections, with isopycnals used for layer analysis. The shallowest isopycnal is the base of subtropical subduction, at 26.2σ_θ in the North Pacific and 27.1σ_θ in the South Pacific. White contours: salinity, corresponding to color bar. Black contours: potential densities used in right-hand panels. (c, d) Meridional overturning volume (Sv) and freshwater transports (MSv). Isopycnal layers used for the zonal averages were chosen to maximize overturning volume transport. The mean salinity of each layer is listed. (See Tables 11 and 12.) (For interpretation of the references to color in this figure legend, the reader is referred to the web version of this article.)

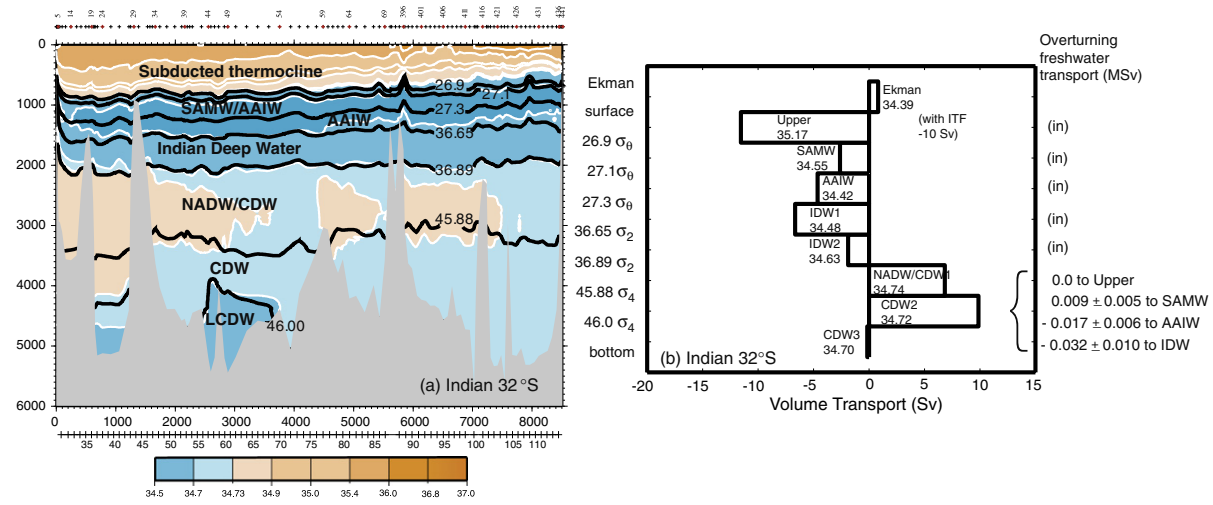

Fig. 14. Indian Ocean at 32°S. (a) Salinity section, with isopycnals used for layer analysis. The shallowest isopycnal is the base of subtropical subduction, at 26.9σ_θ. White contours: salinity, corresponding to color bar. Black contours: potential densities used in right-hand panel. (b) Meridional overturning volume (Sv) and freshwater transports (MSv). Isopycnal layers used for the zonal averages were chosen to maximize overturning volume transport. The mean salinity of each layer is listed. (See Table 13.) (For interpretation of the references to color in this figure legend, the reader is referred to the web version of this article.)

tainties are proportional to these small values. Rounding to tenths or hundredths, which is appropriate for the large, shallow freshwater transports, does not reflect the actual information content for deep transports and the signs of salinity differences.

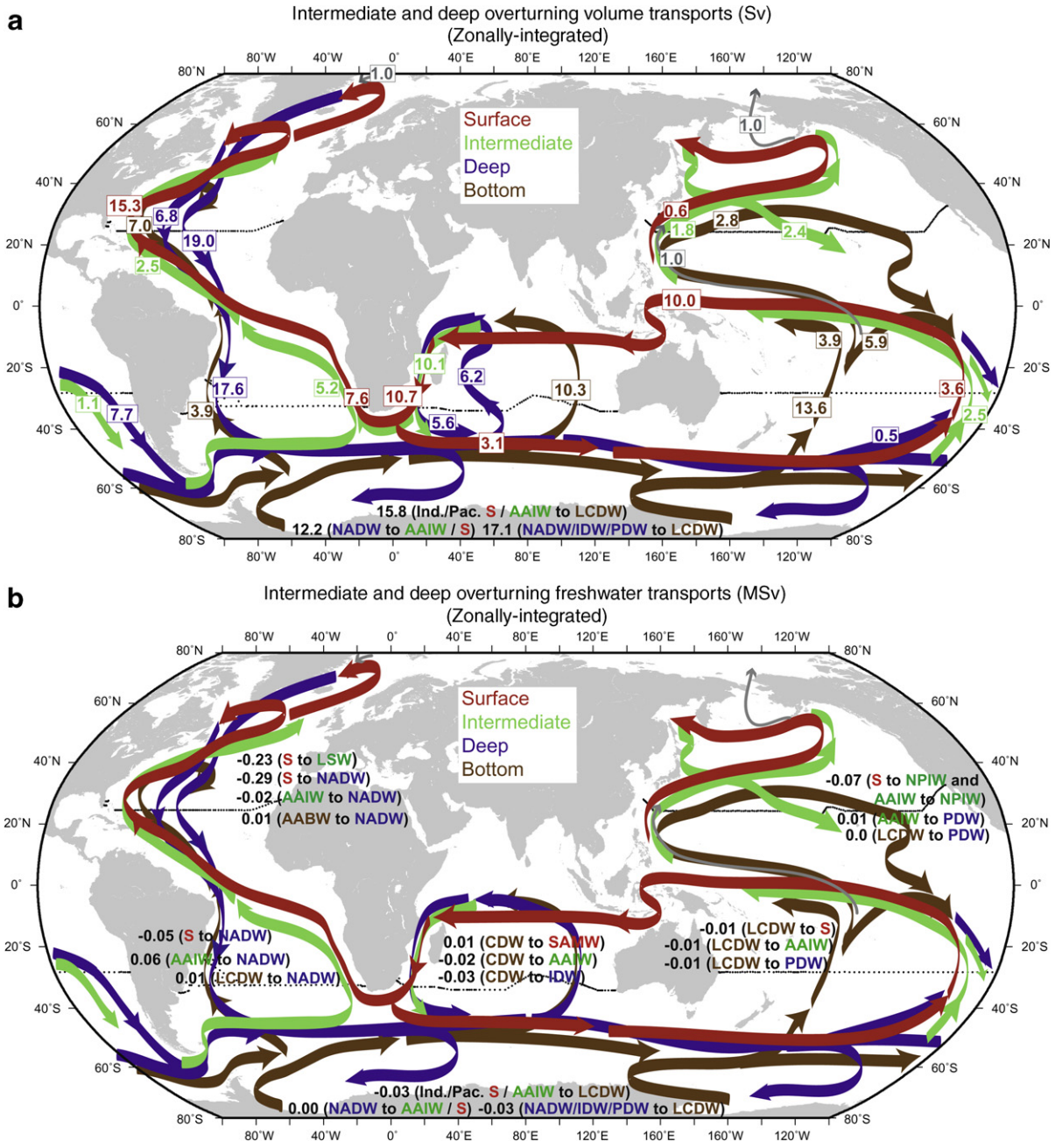

Fig. 15. Zonally integrated overturning transports for intermediate, deep and bottom waters: (a) mass transports (Sv) and (b) overturning freshwater transports (MSv), based on Tables 9–15 and Figs. 12–14. Southern Ocean freshwater transports are from Table 16. Water masses as in Figs. 7, 8 and 12–14 and Table 1.

7.1. North Atlantic at 24°N

The Labrador Sea Water (LSW) and Nordic Seas Overflow Water (NSOW) components of North Atlantic Deep Water (NADW) are formed north of this North Atlantic section from the near-surface water and Antarctic Bottom Water (AABW) that flow northward across this section plus the Arctic input (Section 6) (Fig. 12 and Table 9). (The water mass transformations south of this section are therefore upwelling from the NADW to the surface layers and transformation of some NADW to the higher density AABW.) The northward-flowing upper layers are the very saline thermocline layer and the layer dominated by the saline Mediterranean Overflow Water (MOW), with a small amount of fresher Antarctic Intermediate Water (AAIW) in the Gulf Stream (e.g. Schmitz and Richardson, 1991; Tsuchiya, 1989).

The total freshwater transport associated with the water mass transformations into LSW and NSOW is consequently *equatorward*, despite the net saline influence of NADW in the other ocean basins. This southward freshwater transport had been clearly demonstrated (e.g. Rahmstorf, 1996; Weijer et al., 1999) but bears repeating to highlight the importance of NADW overturn in distributing the "Arctic" freshwater to the rest of the ocean. The upper layer source waters include 15.3 Sv in the surface layer and 2.5 Sv in the MOW/AAIW. Both are more saline than the outflowing NSOW and LSW, and are also much saltier than the equivalent subtropical waters in any of the other oceans. The freshening results mainly from the Arctic/subpolar North Atlantic input (McCartney and Talley, 1984), including a minor component from Bering Strait, discussed extensively in Section 6.

The freshwater transport across 24°N associated with transformation of surface waters into LSW and NSOW is −0.23 ± 0.01 MSv

and −0.29 ± 0.01 MSv, respectively; adding the AAIW and AABW components, there is a net southward freshwater transport of −0.52 ± 0.01 MSv for NADW. These LSW and NSOW components are the same order of magnitude as the subducting gyre freshwater transport (Section 4.1). This reflects the direct role of air-sea fluxes in the adjacent northern North Atlantic and Nordic Seas in transforming these water masses. The net freshwater transport associated with NADW formation is comparable to the net precipitation in the Arctic and subpolar North Atlantic, and indeed carries most of this freshwater southward out of the North Atlantic (Section 9.3).

The freshwater transports across 24°N associated with the southern source waters, AAIW and AABW, are much smaller: −0.03 ± 0.01 MSv and 0.01 ± 0.003 MSv, respectively, which are comparable to deep overturning freshwater transports in the other basins, discussed below.

The uncertainties in layer freshwater transports listed in Table 9 are an order of magnitude smaller than the uncertainty in total and shallow gyre freshwater transports.

7.2. South Atlantic at 32°S

The intermediate and deep portion of the freshwater transport across this section is associated with transformation of surface and bottom layers into NADW north of the section (Fig. 12 bottom row, and Table 10). The net freshwater transport is small, with a near balance between transformation of fresh AAIW (northward freshwater transport) and transformation of salty Benguela waters (southward freshwater transport) into NADW, which is intermediate in salinity.

In detail, the principal water mass transformation north of this section is overturn of 17.6 Sv into the NADW layer from above and below, mirrored south of this section as NADW upwelling into the upper layers and transforming downward into denser AABW. Within the NADW layer, the most saline water is at the western boundary (Fig. 12b), which is also the location of the southward transport. The remainder of the layer is Circumpolar Deep Water and is significantly fresher than the NADW. The CDW flows northward between the deep western boundary current and the mid-Atlantic Ridge, with a nearly balancing southward transport at the eastern boundary (Fig. 18b in Section 8 below; Reid, 1994; SR2001).

The uppermost layer includes the Benguela Current, assumed to contribute to NADW formation. Even though the South Atlantic on the whole is fresher than the North Atlantic (section mean salinities in Fig. 6a and Table 2), the surface layer is saltier than NADW (Fig. 12b and Table 10). This leads to a net southward freshwater transport of −0.047 ± 0.011 MSv for overturn from the Benguela Current to NADW.

Lower thermocline circulation (26.4–26.9σ_θ) mirrors the upper layer, with a saline southward Brazil Current, relatively saline northward interior flow, and intensified fresher northward flow in the Benguela Current. The saline freshwater transport components cancel each other, yielding a negligible freshwater transport (−0.004 ± 0.007 MSv) for conversion from this layer to NADW.

The AAIW layer is fresher than the NADW layer at all longitudes, and has a net northward mass transport, from the interior and Benguela Current. The freshwater transport due to AAIW transformation to NADW is thus northward, estimated at 0.057 ± 0.009 MSv.

The AABW (LCDW) layer upwells into the NADW north of this latitude, with a small net northward freshwater transport of 0.007 ± 0.005 MSv. This occurs even though the "NADW" layer salinity is lower than the AABW layer salinity, since the "NADW" layer includes a recirculating fresher CDW.

The total freshwater transport associated with overturn into NADW is 0.014 ± 0.017 MSv northward, indistinguishable from zero. This "zero" is the nearly canceling sum of about 0.05 MSv northward due to fresh AAIW conversion and −0.05 MSv due to salty Benguela Current conversion, both to intermediate-salinity NADW. Thus, even though the salty, southward-flowing NADW dominates the appearance of the salinity sections in contrast with the fresher, northward-flowing AAIW and AABW, these fresh components are significantly offset (reduced) by the northward flow of the saline Benguela Current surface waters. If AAIW were the sole upper ocean source for NADW, the freshwater transport would be more strongly northward.

This negligible freshwater transport across 32°S for NADW differs from Weijer et al. (1999), who found small southward freshwater transport due to NADW overturn, using the 30°S velocity analysis of Holfort and Siedler (2001), based on a more recent occupation of the section than herein. But these freshwater transports are in any case small; as shown in deRuijter et al. (1999) and here, the sign of the freshwater transport depends on the relative amounts of more saline surface Benguela waters and fresher AAIW in the northward mass transport, since the NADW salinity is intermediate to them.

The Benguela Current waters are fresher than the western and central surface waters on the section (Figs. 12b and 18a below), but only slightly fresher than the Agulhas surface waters (Sections 7.5 and 8.2), which argues for near-continuity of flow around Africa and minimal freshwater transport into the Atlantic via this pathway. Identification of the northward Benguela flow with the Indonesian Throughflow waters that round Africa from the Agulhas is a central part of the Gordon (1986) global NADW "conveyor belt". On the other hand, the main mechanism for "Agulhas leakage" into the South Atlantic includes about six large rings of Agulhas water per year; capturing their impact using single hydrographic sections is not possible. There were no Agulhas rings on the 32°S section used here. The existence of this Indian–Atlantic connection could tip the freshwater balance towards net southward freshwater transport for the NADW overturn measured at 30°S (Weijer et al., 2001), but depends on the proportion of Agulhas ring water in the NADW overturn compared with the portion that participates in the extended Atlantic–Indian subtropical gyre.

7.3. North Pacific at 24°N

North Pacific Intermediate Water (NPIW) formation north of this subtropical North Pacific section is the principal water mass transformation below the shallow overturning gyre that contributes to freshwater transport through this section (Fig. 13a and c and Table 11). Summarizing results from above, the total freshwater budget north of this section was 0.19 ± 0.05 MSv of net precipitation/runoff (Fig. 5a and Table 3; Section 3). Of this, 0.05 ± 0.02 MSv is exported northward through Bering Strait, including the component 0.01 FSv passing through 24°N itself (Section 6), leaving −0.13 ± 0.05 MSv to be exported southward across 24°N. The shallow overturning freshwater transport across 24°N is −0.09 ± 0.03 MSv southward (Fig. 7b; Section 4.3). Intermediate and deep overturns, including NPIW formation, therefore contribute −0.05 MSv of freshwater transport southward across 24°N.

Looking at the intermediate and deep overturns, 2.4 Sv of fresh NPIW are formed north of this section, with associated southward freshwater transport of −0.07 ± 0.02 MSv (using NCEP winds) or −0.08 MSv (using Hellerman and Rosenstein (1983) winds). The first value of −0.06 FSv comes from Table 11, and is the sum of −0.02 ± 0.02 FSv and −0.05 ± 0.005 FSv from downwelling of 0.59 Sv from above and upwelling of 1.82 Sv from below into the NPIW. Using the weaker NCEP winds, there is not enough northward transport in the surface layer to balance the NPIW outflow transport. With stronger northward Ekman transport at 24°N using the stronger Hellerman and Rosenstein winds (Table 5), as in Talley

(2003), all of the NPIW can come from excess northward transport in the Kuroshio's upper layer, hence all from downwelling from the surface layer; the corresponding freshwater transport of −0.08 MSv is larger since the surface waters are more saline than those in the layer below the NPIW. The NCEP reanalysis winds have recently been determined to be too weak (Large, personal communication, 2007), so in fact the NPIW might indeed all result from downwelling, as per the Hellerman and Rosenstein results.

The deeper overturns across this section yield a small northward freshwater transport of 0.01 to 0.02 ± 0.008 MSv, due to a small downwelling of 2.0 Sv from the NPIW/AAIW layer to the Pacific Deep Water. The deep 4.0 Sv upwelling and downwellings from LCDW and portions of the PDW into the densest PDW have no impact on the freshwater balance.

Bering Strait requires that ~1 Sv passes northward through the 24°N section. With the weak NCEP Ekman transports used here, this 1 Sv is assigned to the NPIW/AAIW layer. The net freshwater transport associated with this throughflow is associated with net precipitation of −0.05 ± 0.03 MSv between 24°N and Bering Strait, as noted in Section 6, and a net heat loss of 0.02 PW.

7.4. South Pacific at 28°S

The deep water mass transformation north of this South Pacific section (Fig. 13b and d and Table 12) is due to the northward flow of 13.8 Sv of saline bottom waters (Lower Circumpolar Deep Water or LCDW), that upwell and return southward as fresher Pacific Deep Water (6.2 Sv) and also in the AAIW (2.8 Sv) and surface layers (4.9 Sv). Before reporting the freshwater transports, it is useful to pause and remark on the similarity of this overturning structure to the well-known overturn of the subtropical Indian Ocean, in which densest deep waters upwell into the local deep water, the intermediate water, and the thermocline (Toole and Warren, 1993; Robbins and Toole, 1997; Talley et al., 2003). This South Pacific upwelling, into all layers including the thermocline, is masked by the net northward transport of 10 Sv in the upper ocean to feed the ITF. When the ITF transport is removed, then the overturning structure is similar to that of the Indian (Section 7.5).

The deep transformation from more saline deepest to mostly fresher overlying waters has very weakly southward freshwater transport of −0.03 ± 0.03 MSv. This is composed of −0.02 ± 0.02 MSv due to upwelling of LCDW into PDW and AAIW, and −0.01 ± 0.02 MSv due to upwelling of LCDW to the thermocline, with southward net flow across 28°S in all layers above the LCDW. To arrive at this part of the transport, the freshwater transports of 0.23 ± 0.04 MSv, −0.16 ± 0.05 MSv and −0.07 ± 0.02 MSv due to the shallow gyre overturn, the ITF and the Bering Strait, respectively, were first removed from the total loss of −0.04 ± 0.09 MSv of freshwater from the complete Pacific box including 28°S, the ITF and Bering Strait (Sections 3–5 and 6). The uncertainties in each of these deep quantities are of the same order as the freshwater transports, so the significance of the exact values is small; note that quantities are reported to thousandths in the tables to arrive at these values and uncertainties on the order of hundredths. The order of magnitude of these transports is accurate, and the signs are sensible based on the salinity difference and direction of flow in the circulation components.

The source of freshwater for the deep water that upwells north of 28°S is downward diffusion from the overlying fresher intermediate layers, including both NPIW and AAIW. The overturning mass transport of 13.8 Sv is the same order of magnitude as the shallow overturning gyre's transport (22.3 Sv), whereas its freshwater transport is an order of magnitude smaller. This reflects how weak diapycnal diffusion is in comparison with direct surface forcing in creating salinity differences that are associated with freshwater transport. On the other hand, this −0.03 MSv is the right size to balance the entire Pacific freshwater gain, and of the same order of magnitude as the Bering Strait impact. Thus, a full accounting of mechanisms for maintaining the Pacific Ocean's freshness relative to the Atlantic and Indian should include this deep overturn.

7.5. Indian at 32°S

The Indian Ocean overturning north of 32°S (Fig. 14 and Table 13) consists of upwelling from saline deep Lower Circumpolar Deep Water into Indian Deep Water and lower Antarctic Intermediate Water, with some upwelling penetrating to the upper ocean (e.g. Toole and Warren, 1993; Robbins and Toole, 1997; Talley et al., 2003). The deep upwelling cell transports a significant amount of heat (Talley, 2003). IDW and AAIW salinities are lower than LCDW salinity, but thermocline salinity is much higher. The overturning mass balance though is dominated by transformation of LCDW to IDW and lower AAIW, so the net freshwater transport is southward, totaling −0.04 ± 0.03 MSv. This is equivalent to that for the South Pacific (Section 7.4), and, like the South Pacific, is very small compared with freshwater transport in the shallow subducting gyre and ITF loop (Fig. 7b). The deep freshening is due to downward diapycnal diffusion from the overlying fresher AAIW and the intermediate-depth part of the fresher ITF that forms the Indonesian Intermediate Water in the tropical Indian Ocean (e.g. Talley and Sprintall, 2005). This is despite the input of high salinity intermediate water from the Red Sea (Bryden and Beal, 2001).

The smallness of the Indian's deep overturning freshwater transport may reflect the inefficiency of diapycnal processes compared with direct air-sea fluxes, the long distance from the North Atlantic and hence reduction in salinity contrast between NADW and the other deep waters, and the small salinity change accompanying LCDW formation in the Antarctic (Section 8).

7.6. Summary

Freshwater transports associated with deep and intermediate water overturning are summarized in Fig. 15b. A large contrast is immediately apparent between the values in the North Atlantic (>0.2 MSv per component) and elsewhere (0.01–0.06 MSv). The North Atlantic overturns creating NADW (composed of LSW and NSOW) involve transformation through convection and entrainment of a large volume of surface water nearly directly to intermediate and deep waters. This transformation incorporates almost all of the excess freshwater accumulated in the Arctic and subpolar North Atlantic. This direct surface influence creates freshwater transports that are the same order of magnitude as those of the shallow overturning gyres and the Indonesian Throughflow loops (Sections 4 and 5), which are also directly affected by air-sea fluxes. Formation of NPIW also involves direct air-sea fluxes, but the total overturning mass transport is small so the net freshwater transport (0.04 MSv) is much smaller than that associated with LSW and NSOW. Bottom water formation in the Antarctic also occurs near the sea surface, but the difference in salinity between the inflowing deep waters and the bottom waters is small (discussed further in Section 8).

Associated with the deep overturns in the Atlantic is a large deep convergence of 0.55 ± 0.14 MSv between 24°N and 32°S due to southward freshwater transport across 24°N and northward freshwater transport across 32°S. This is accomplished by the large net surface evaporation (calculated at 0.56 MSv) in the low latitude Atlantic (e.g. Fig. 5b with a slightly different choice of bounding latitudes). Thus, the freshwater transport associated with the meridional overturning in the North Atlantic and Arctic north of 32°S is almost a closed loop, with a balance between freshwater input at the highest latitudes and evaporation at lower latitudes. This loop

requires diapycnal diffusion of salinity (Talley et al., 2003). As noted in Section 6, the Bering Strait throughput of freshwater from the Pacific is dwarfed by this much larger cycle.

The remaining deep and intermediate transformations, from LCDW/AABW to deep water in all three basins, and from LCDW to intermediate water in the Indian and Pacific, have very small freshwater transports. They are governed by diapycnal diffusion viewed from north of 30°S. Viewed from south of 30°S, the salinity difference between the new bottom waters and their source waters is limited (Section 8). However, the sign of each of these weak transports is well determined by the difference in salinity and direction of mass transport in the opposing layers, even though the calculated Monte Carlo uncertainties are nearly as large as the freshwater transports. For instance, in the South Pacific and Indian Oceans, the southward freshwater transport associated with LCDW conversion to overlying "AAIW" and PDW/IDW is due to higher salinity of the northward-flowing LCDW compared with the southward-flowing overlying layers, even though most of the low salinity signal in the AAIW comes itself from the south (Figs. 12 and 13 and Tables 12 and 13). In the Indian Ocean, the low salinity Indonesian Intermediate Water might also contribute to the reduced salinity of the southward flow (Talley and Sprintall, 2005).

We next view these overturns from a Southern Ocean perspective.

8. Southern Ocean perspective on freshwater transports

The Southern Ocean is a region of large net freshwater input due to net precipitation. This freshwater must be transported northward (0.61 MSv across "30°S", Fig. 5b). Despite the major deep water mass transformations that occur in the Southern Ocean, this freshwater is carried almost entirely by the shallow overturning circulations of the three ocean basins, as partially revealed in Sections 4 and 7, and described in detail in this section and in Section 9. This shallow export process is completely different from the northern hemisphere, in which the Arctic/subarctic freshwater export southward is achieved almost entirely through deep and intermediate water formation. The dichotomy between the southern and northern hemisphere freshwater export mechanisms is congruent with the "Drake Passage effect" in which northward Ekman transport at Drake Passage can be returned southward geostrophically only by deep water below Drake Passage sill depth, hence requiring deep northern sinking which can only be due to NADW formation (e.g. Toggweiler and Samuels, 1995a; Warren et al., 1996; Gnanadesikan, 1999; Keeling, 2002).

The other apparent dichotomy in this Southern Ocean freshwater export result is that the zonally integrated deep overturning cell in the Southern Ocean, which has a very small meridional freshwater transport, is volumetrically much stronger than the zonally integrated shallow overturning cell, as shown in Talley et al. (2003), and further explored here. Nevertheless, the small amount of freshwater transport in the deep overturn is important to examine, since salinity changes, though small, are utterly significant for the deep overturn itself.

Results from the three southern hemisphere "30°S" sections are combined here to emphasize the zonally averaged southern hemisphere overturning cells (Section 8.1). Zonal averaging does obscure the shallow gyre mechanisms in each ocean, but is important to explore since overturns and transports are very often studied through zonal integrals. After looking at the zonally averaged results, the discussion returns to the horizontal structures of Section 4 to show how the upper ocean overturning circulation is related to the upper ocean gyres and the ITF (Section 8.2.1), and to understand the individual ocean contributions to the deep overturn (Section 8.2.2).

In the deep overturn, northern-source deep waters (NADW, IDW, PDW) are transformed into denser LCDW/AABW. Here and in Section 9, it is emphasized that the return pathway for NADW most likely goes through *both* the Southern Ocean and the low latitude Indian and Pacific Oceans, since most of the NADW is transformed first to LCDW and must then upwell to IDW, PDW, intermediate water and surface water, which is accomplished in both the Indian and Pacific Oceans and in the Southern Ocean. Speer et al. (2000) and SR2001 described this important intermediate role of LCDW and the low latitude Indian and Pacific Oceans, which differs from the simpler hypotheses of some of the above-

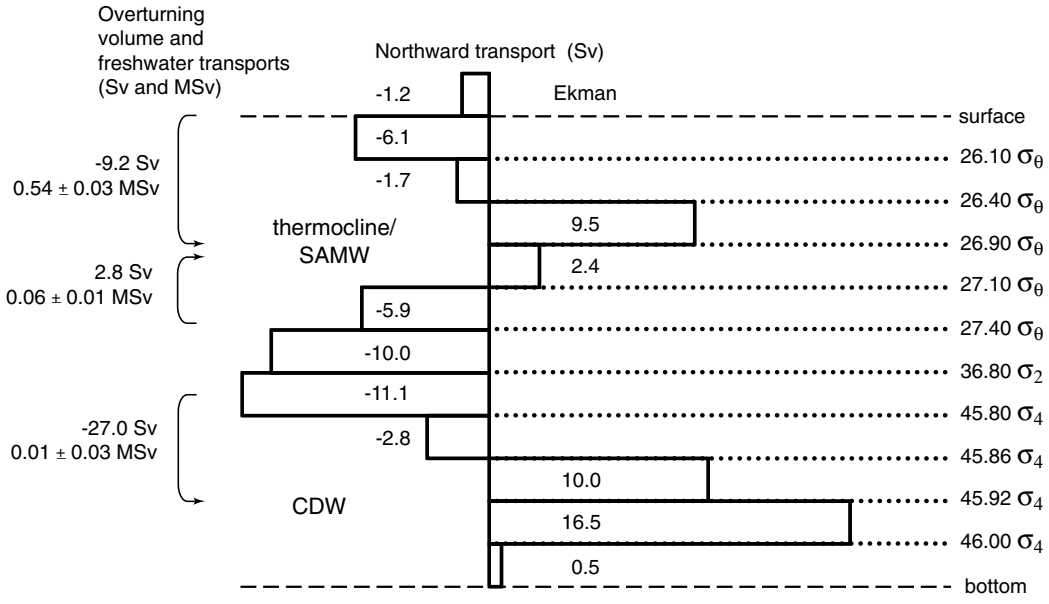

Fig. 16. Meridional overturning volume (Sv) and freshwater transports (MSv) for the Southern Ocean across 30°S (sum of South Atlantic, South Pacific and Indian sections). Isopycnal layers are chosen to maximize net volume transport in each layer in the total circumpolar zonal integral. (See Table 14.)

listed references that focus on a direct cycle between the Southern Ocean and NADW.

8.1. Zonally integrated overturning circulation and freshwater transport at 30°S

First consider the zonally integrated volume transports in the Southern Ocean. The zonally integrated overturning circulation across the composite 30°S section has two nearly independent overturning cells in the vertical (Fig. 16 and Table 14), as previously reported for this geostrophic velocity analysis by Talley et al. (2003). The upper cell consists of southward volume transport of −9.0 Sv in the surface layers, sinking into the lower thermocline and returning northward as Subantarctic Mode Water (SAMW) and AAIW. This cell occurs in the Indian/Pacific (Section 8.2; Table 14 columns for individual oceans). The Atlantic transports are fundamentally different, but not large enough to cancel the overall Indian/Pacific cell.

The deeper overturning cell consists of southward volume transport of −29.8 Sv of intermediate and deep waters into the Southern Ocean between 27.1σ_θ and 45.86σ_4, nearly balanced by 27.0 Sv of bottom waters flowing northward out of the Southern Ocean below 45.86σ_4. Thus, this deep cell is mainly associated with conversion of southward-flowing deep waters (NADW, IDW, PDW) into northward-flowing bottom waters (AABW and LCDW) south of 30°S. The layer 45.92–46.0σ_4 carries the largest northward mass transport.

Weak upwelling in the Southern Ocean and northward flow in the SAMW/AAIW layer balance the small volume transport imbalance of −2.8 Sv southward in the deep water layer. This is an order of magnitude weaker than the 34 Sv of upwelling estimated by SR2001, which can be partially but not wholly explained by the zonal integration here that obscures the larger magnitude upwelling of particular components (see Section 8.2).

Second, consider the zonally integrated freshwater transports. The freshwater transports associated with the shallow and deep overturning cells differ significantly. The shallow 9.2 Sv overturn carries almost all of the freshwater northward out of the Southern Ocean, at a rate of 0.54 ± 0.03 MSv. This is due to precipitation in the Southern Ocean that reduces the salinity of SAMW and AAIW and other deep thermocline waters compared with the saline subtropical surface waters that flow southward. Adding the 0.06 ± 0.01 MSv associated with upwelling of 2.8 Sv from deep waters to the SAMW/AAIW layer in the Southern Ocean, which likely passes through the directly forced surface layer (Section 8.2), the total freshwater transport between the sea surface and the thermocline is 0.60 ± 0.03 MSv, which approximately accounts for the total freshwater transport out of the Southern Ocean without including the deep overturn.

The much larger deep volume overturn of 27.0 Sv carries a small freshwater transport of 0.009 ± 0.030 MSv. If the sign is accurate despite the uncertainty, the northward-flowing bottom water is very slightly fresher than the southward-flowing deep waters, which obtain their higher salinity from the Atlantic with an opposing freshening from the Pacific (Figs. 12, 13b and 18a below). On the other hand, when the deep and bottom layers are subdivided differently, as in Section 8.2, the net freshwater transport is small and southward (−0.033 ± 0.025 MSv) (Table 16 below). The salient point is that the deep overturning freshwater transport is small, especially given the large volume transport involved.

This freshwater transport for deep Antarctic overturn is an order of magnitude smaller than for the Arctic/subpolar North Atlantic, even though the net surface fluxes are about the

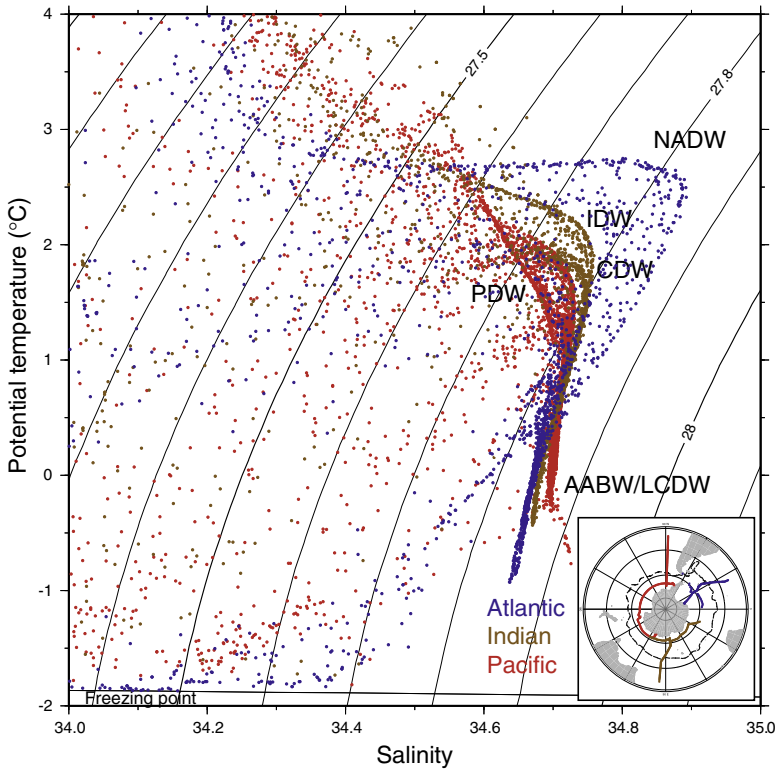

Fig. 17. Potential temperature (°C) vs. salinity in the Southern Ocean. Potential density (σ_θ) is contoured. The freezing point is shown. Bottle salinities from WOCE cruises A23, A16, S4, S4P and S4I (stations in inset). Dashed curve in inset is the Subantarctic Front from Orsi et al. (1995).

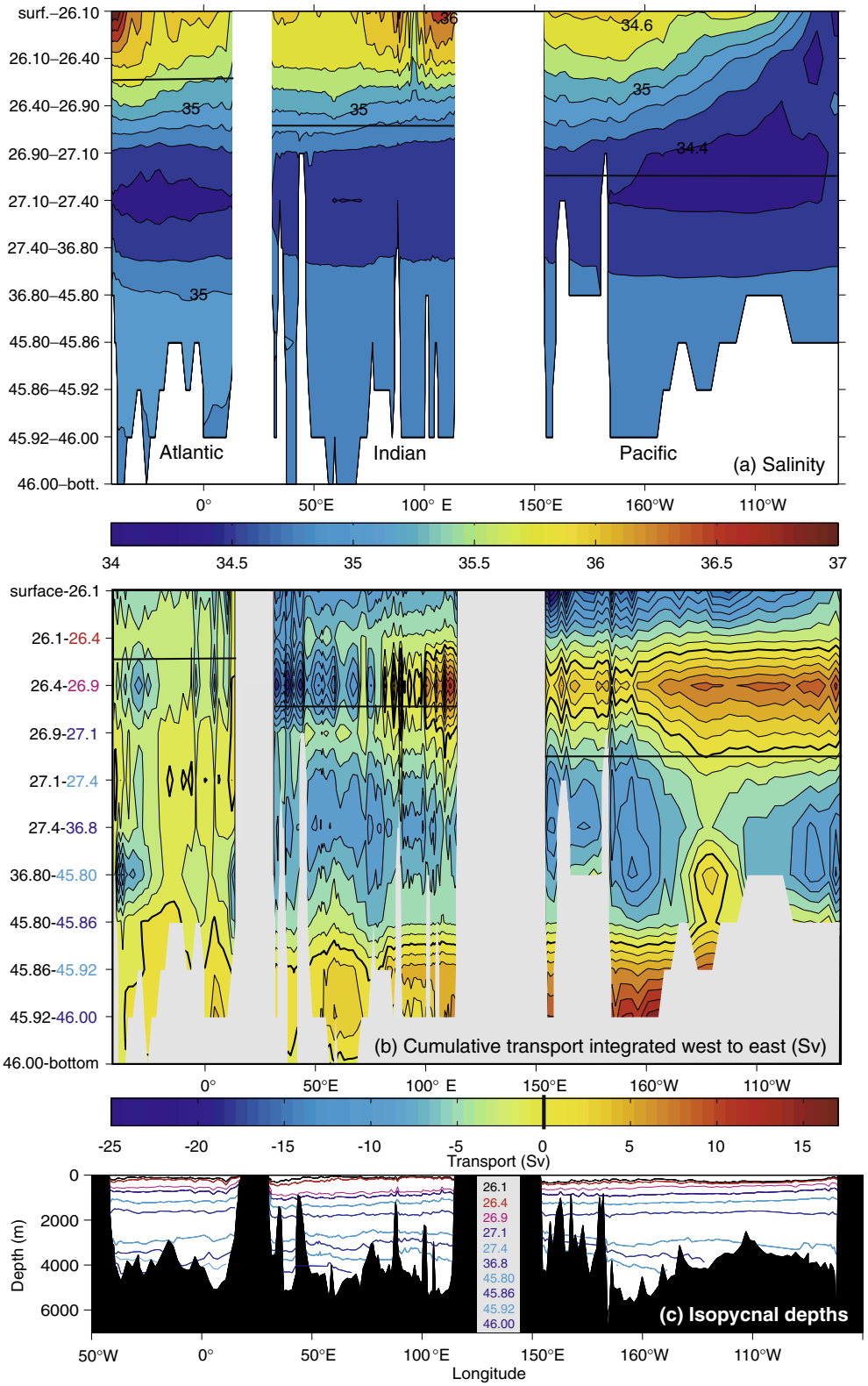

Fig. 18. Composite 30°S section-based on the isopycnal layers of Fig. 16. (a) Salinity (vertically averaged in each layer); contour interval is 0.2. (b) Cumulative transport (Sv) in the isopycnal layers of the bottom panel, integrated from west to east along 30°S; contour interval is 2 Sv. Positive cumulative transport is northward; heavy black is the 0 contour. (c) Isopycnal depths; colors for contours are in axis labels in (b). (For interpretation of the references to color in this figure legend, the reader is referred to the web version of this article.)

same size, and even though formation of the densest waters in both regions involves air-sea fluxes. A potential temperature–salinity diagram for the Southern Ocean is useful for understanding this difference (Fig. 17), as are salinity sections for individual oceans (Figs. 12–14) and in isopycnal layers in a circumpolar section at 30°S (Fig. 18a). Several factors contribute to the smallness of the deep overturning freshwater transport:

1. Saline subtropical surface waters are not the source of Antarctic deep waters, unlike the situation in the North Atlantic (and North Pacific). This greatly reduces the potential for freshwater transport due to dense water formation for the next two reasons.
2. The new bottom waters must be denser than their source waters, which are PDW, IDW and NADW (Fig. 17). NADW is the densest of these. These source waters are already cold, and can only be cooled to at most the freezing point. The maximum possible salinity decrease for waters that become bottom waters is limited by this temperature change to about 0.2 salinity units; using (5) this yields a maximum freshwater transport of 0.006 MSv per Sv of volume overturn (hence 0.06 MSv for 10 Sv of formation).
3. Bottom and dense water formation in the Antarctic occur through brine rejection, which releases salt into the water column. Thus, even though the surface layer is freshened relative to the inflowing, upwelling deep waters, the added salt partially counterbalances the freshening, hence reducing the net northward freshwater transport due to the overturn. A pronounced example of the result of brine rejection in the Ross Sea is apparent in the potential temperature/salinity diagram (Fig. 17, red dots at lower right) (Whitworth et al., 1998). The large group of points at salinity >34.6 and potential temperature <1 °C is the new dense water (CDW and LCDW).

To summarize, the required northward freshwater transport out of the Antarctic is carried almost exclusively by the shallow overturns above the base of the subtropical gyre thermoclines. Antarctic dense water formation carries very little freshwater, likely due to the combined effect on the upwelled source waters of brine rejection and limited maximum cooling with concomitant limited freshening.

Toggweiler and Samuels (1995b) demonstrate the smallness of the salt enrichment in LCDW relative to the inflowing deep waters; this is also clear in observations of new bottom water (Gill, 1973; Whitworth et al., 1998). The small salinity change in LCDW compared with its source waters has a parallel in the low anthropogenic CO_2 burden in LCDW compared with, say, NADW (e.g. Poisson and Chen, 1987; Sabine et al., 2004). CO_2 of course is subject to other factors, including direct air-sea exchange which is limited by sea ice cover, and stronger buffering for CO_2 uptake by the ocean.

Note that the dominant shallow overturn includes the important upper ocean water masses SAMW (all three oceans) and AAIW (Pacific), which are thus important vehicles for northward freshwater export. In the South Atlantic's deeper overturn (Section 7.2), significant northward freshwater transport due to AAIW conversion to NADW is nearly canceled by significant southward freshwater transport due to northward volume transport of more saline surface Benguela Current water, also converted to NADW.

8.2. Ocean basin contributions to total Southern Ocean layer freshwater transports

8.2.1. Upper ocean overturn

Most of the northward freshwater transport out of the Southern Ocean across 30°S is carried by the upper ocean's zonally integrated overturning cell, above 27.1σ_θ (Fig. 16 and "Layer overturn" column in Table 14). It was previously concluded in Section 4 that most of this northward freshwater transport is carried by the shallow overturning gyres of the southern hemisphere oceans. In this subsection, these two apparently-conflicting views of the upper ocean overturn are reconciled by looking at the individual ocean basin and gyre components of the complete zonally integrated overturn. Therefore, each ocean's contribution is reexamined using the same set of isopycnal layers for all oceans (Table 14 and layers as in Fig. 16). Layer transports integrated from west to east across the whole 30°S section, from the Atlantic to the Pacific, show the regional distributions of the volume transports relative to the layer salinity distribution (Fig. 18).

First it is noted that the upper ocean's integrated downwelling cell of 9.0 Sv, with a northward freshwater transport of 0.54 ± 0.03 MSv, is nearly completely mass-balanced for layers above 26.9σ_θ ("Total" column in Table 14, layers 1–4). Secondly, the southward transport is dominated by the Indian Ocean (−14.2 Sv in layers 2–3), with the only other southward contribution coming from the Pacific's Ekman transport (−3.2 Sv in layer 1). All of these layers have northward net transport in the Atlantic (7.6 Sv in layers 1–4), as do the non-Ekman layers in the Pacific (6.8 Sv in layers 2–4), and the densest of these layers in the Indian (3.5 Sv in layer 4). The net transport of these parts is −17.4 Sv southward and 17.9 Sv northward, with the extra 0.5 Sv balanced by some of the southward flow in the next layer down in the Indian (layer 5).

Thus, one sees already that the putative upper ocean meridional overturn of 9.0 Sv is composed of larger lateral elements, at a minimum in excess of 17 Sv, composed of the zonally integrated layer transports in each of the three oceans. The net southward Indian volume transport is due to the Indonesian Throughflow. The net northward Atlantic transport is due to the Benguela Current (Fig. 12b; Section 4.2). The net northward Pacific transport is part of the ITF and BS throughput. The subsurface northward transport in the Indian Ocean (layer 4) is the only one of these that can be easily seen to be part of the shallow gyre overturn (Section 4.5), since otherwise the shallow gyre overturns are subsumed within all of these zonally integrated upper ocean layers.

The total freshwater transport associated with just these basin-integrated components, carefully balanced in mass, is 0.49 MSv, which is a large portion of the required 0.53 MSv in the complete zonal integral (Fig. 16 and Table 14). This 0.49 MSv comes from (1) 0.33 MSv for the Indian–Atlantic connection (northward upper Atlantic transport of 7.6 Sv/0.17 FSv and balancing southward Indian transport of −7.6 Sv/0.16 FSv); (2) 0.07 FSv for the Indian thermocline connection (3.5 Sv/−0.005 FSv in the 26.4–26.9σ_θ layer and balancing −3.5 Sv/0.07 FSv in the surface to 26.4σ_θ layer); and (3) 0.09 FSv for the Indian–Pacific connection (remaining −3.1 Sv/0.07 FSv Indian transport balanced with 3.1 Sv/0.02 FSv in the upper Pacific layers that eventually join the ITF flow exiting the Pacific).

The large (0.33 MSv) Indian–Atlantic upper ocean contribution to the northward freshwater transport might lead the erroneous impression that the ITF dominates freshwater transport in this part of the system, via throughput of excess saline Agulhas water into the fresher Benguela Current. The ITF is of course important, but for Pacific–Indian redistribution of freshwater and not for Indian–Atlantic redistribution (Sections 4 and 5). It is straightforward to see that the Agulhas–Benguela connection in itself can transport little freshwater because their salinity contrast is small. The Benguela Current is the excess northward flow east of 11°E in the South Atlantic (cumulative transport shown in Fig. 18b), marked by lower salinity (Figs. 12b and 18a). Assuming that the Benguela Current is fed by part of the excess southward Agulhas transport (7.6 Sv from the surface to 26.9σ_θ), the net freshwater transport is small and northward: 0.04 MSv (sum of −0.04 FSv in the Benguela and 0.08 FSv from −7.6 Sv in the slightly saltier Agulhas). Even if the intermediate water layer 26.9–27.1σ_θ is included (since there is a clear continuity of mass transport from the Indian to the Atlantic in this layer), adding 2.5 Sv to the connection, the total Agulhas–Benguela freshwater transport is only 0.06 MSv (Table 14).

The large freshwater transport for the combined shallow Indian–Atlantic is due to the separate, large subtropical gyre freshwater transports in each of the two oceans. If the Indian Ocean's thermocline overturning freshwater transport, 0.07 MSv, from the Indian layer averages described above, is added to the 0.33 MSv for the Indian–Atlantic connection, the total Indian/Atlantic freshwater transport is 0.40 MSv, which is close to the 0.38 MSv diagnosed strictly from the subtropical gyres in Section 4 (Fig. 7b). (The 0.02 MSv might well be due to choice of $26.4\sigma_\theta$ as the base of South Atlantic overturn rather than a slightly higher density.)

Thus, the nearly horizontal shallow gyres carry most of the freshwater northward out of the Southern Ocean, and the three gyres contribute almost equally to this freshwater transport.

8.2.2. Deep ocean overturn

The zonally integrated view of Southern Ocean overturn (Fig. 16; Section 8.1; Table 14) suggests a simple deep cell of 27.0 Sv of deep water moving southward and being converted to bottom waters returning northward. However, as soon as the individual oceans are considered, this simple cell becomes more complicated (Fig. 18b and Table 14), including aspects of the global NADW overturning cell defined by Gordon (1986), and aspects of the much more complete schematic circulations by Schmitz (1995) and SR2001 that include IDW and PDW and the Antarctic deep waters (UCDW, LCDW). The continuity of layer transports from ocean to ocean can be visualized using the overturning schematic in Fig. 15a. This schematic is based quantitatively only on the layer transports across "24°N" and "30°S" and assigned ITF and BS transports, and is therefore not as complete as the Schmitz or SR2001 analyses.

Focusing on transports across 30°S and implications for overturn in the Southern Ocean, the total freshwater transport for intermediate and deep overturning at this latitude is -0.06 ± 0.04 MSv (Tables 15 and 16). This is balanced almost entirely and coincidentally by freshwater transports due to the ITF and Bering Strait volume transports across 30°S. (This result differs from the 0.01 ± 0.03 MSv for the deep 27 Sv cell in the circumpolar-integrated view of Section 8.1. Here the layers in each ocean are chosen for maximum overturn, hence are not the same from ocean to ocean [Table 16]; this optimizes the interpretation of the freshwater transport associated with each component of deep water transformation in the Southern Ocean.)

The Atlantic sends 17.6 Sv southward in the NADW layer. Of this, 1 Sv continues to the Pacific to balance the BS. The remaining transport returns northward from the Southern Ocean in the upper ocean, in the intermediate water layer (AAIW), and in the bottom layer (LCDW). This requires upwelling somewhere beyond 30°S into the upper two layers, and sinking into the bottom layer. The net freshwater transport for these diapycnal cells is northward and small, dominated by conversion of NADW to fresher AAIW, but is nearly offset by conversion of NADW to more saline surface water that ultimately re-enters the Atlantic in the Benguela Current (Section 7.2).

The layer transports in the Indian and Pacific require sinking in the Southern Ocean and (North) Atlantic since the Indian and Pacific have net outflow in the mid to upper water column and inflow near the bottom. The associated freshwater transports for the Indian and Pacific are equivalent in size, -0.04 ± 0.03 MSv and -0.03 ± 0.03 MSv, which is a small net export of freshwater to the Southern Ocean even though the Southern Ocean is a region of major net precipitation. The required net southern salinity increase is partially associated with dense and bottom water formation that increase the salinity of LCDW relative to IDW/PDW, and also with input from saline NADW as it also cycles through LCDW (Fig. 15).

9. Global overturning circulation: freshwater and heat transports

Pulling all of the above elements into a global discussion of freshwater transports, the discussion begins in Section 9.1 with a description of the global overturning circulation from the Reid (1994, 1997, 2003) velocity analyses (adjusted to include Ekman transports and more realistic ITF transport in the mass balances). The freshwater transports associated with each of the overturning elements in the global circulation were described in Section 7.6 (Fig. 15b).

Freshwater and heat transports are brought together in Section 9.2. Heat transports (Talley, 2003) were recalculated throughout this work and listed in many tables. Large freshwater and/or heat transports are, for obvious reasons, associated with water mass transformations that include surface waters and direct air-sea fluxes rather than diapycnal diffusion. Small combined freshwater and heat transports are associated with regions that are distant from major water mass transformation, with the important exception of the densest water formation in the Southern Ocean, for which freshwater and heat transports are also small, due to limitations on maximum salinity and temperature changes that can be achieved with air-sea fluxes (Section 9.3).

9.1. Global overturning circulation

The global overturning circulation (Fig. 15a; Sections 5–8) has elements of the global NADW circulation described by Gordon (1986), with important low latitude upwelling for the return of deep waters to the surface, but it also includes Southern Ocean transformations (Speer et al., 2000; SR2001) that are best explained by Drake Passage control on deep water passage to the Antarctic (e.g. Toggweiler and Samuels, 1995a; McDermott, 1996; Speer et al., 2000). The circulation is not as complex as Schmitz's (1995) because only zonal subtropical sections are used here, but it shares most of the basic elements.

When NADW exits the South Atlantic, a portion (6.2 Sv) flows directly into the Indian Ocean and the rest (6.6 Sv) into the ACC. The NADW in the Indian Ocean joins LCDW (which itself is formed partially from NADW in the Southern Ocean, next paragraph), which upwells into the local IDW, and also into the intermediate and surface layers. LCDW also upwells in the Pacific into the PDW, intermediate and surface layers. Some NADW and LCDW also upwells in the Indian and Pacific to the intermediate and surface layers that eventually feed NADW formation in the northern North Atlantic. This highlights the need to evaluate diapycnal processes in low latitude regions, which might be intensified in the equatorial band (e.g. Talley et al., 2003).

In contrast with Gordon (1986), there is an important excursion of all of the deep waters through the Southern Ocean, as described by Speer et al. (2000) and SR2001. It is reassuring to find a similar overturning pattern supported by the Reid (1994, 1997, 2003) velocity analyses, although there are major differences in magnitude of deep overturn and smaller differences in the shallow overturning cell. The NADW portion that crosses the ACC is modified and upwells *isopycnally* to a few hundred meters below the sea surface, where it is significantly modified by brine rejection and diapycnal mixing as well as by mixing with PDW and IDW that also flow into the ACC. The modified shelf waters then sink; the deep water that emerges and flows northward into all three ocean basins is LCDW. (Note that the preponderance of LCDW volume must come from IDW and PDW: at least 16.8 Sv versus 6.6 Sv for NADW.) LCDW, plus the direct input of NADW to the Indian Ocean, then upwells *diapycnally*, mostly within the Indian and Pacific, forming the bulk of PDW and IDW. These flow back southward

to the ACC, mix, modify and upwell *isopycnally* to near the sea surface as UCDW.

The vertical separation of the UCDW (low oxygen core) and NADW (high salinity core) south of the ACC is clear in all of the meridional WOCE sections in the Southern Ocean (Orsi and Whitworth, 2005), supporting the hypothesis of two separate loops of deep waters through the Southern Ocean. Thus, as pointed out by Speer et al. (2000) and SR2001, UCDW, rather than NADW, is the source water for the northward Ekman transport that figures heavily in Southern Ocean control scenarios for NADW formation, in which geostrophic southward return flow to the Antarctic Zone can only occur in the deep waters that are below the Drake Passage sill depth (Toggweiler and Samuels, 1995a; Warren et al., 1996, 1997; Gnanadesikan and Hallberg, 2000). This northward transport of UCDW could partially enter the SAMW and AAIW layers in all three ocean basins and thus be part of the upper ocean's northward transport of freshwater out of the Southern Ocean. These surface waters make their way back to the North Atlantic through various routes, including directly northward in the South Atlantic, around the subtropical gyre in the Indian Ocean, and from the Pacific through the Indonesian Passages and Drake Passage.

Speer et al. (2000) and SR2001 show an upper ocean overturning cell in the Southern Ocean that requires upwelling from UCDW to the surface layer, rather than the downwelling zonally integrated upper ocean cell at 30°S of this present analysis (Fig. 16). These views are not actually contradictory, as they depend strongly on which layers in the upper ocean are summed together to view possible overturns, coupled with small but important differences in given layer transports in given oceans. For comparison, the layer mass transports from SR2001 are listed in the rightmost column of Table 14. If the top four layers are summed in both this analysis and SR2001, both show northward upper ocean flow that must be balanced by upwelling from the deep water layer just below (2.85 Sv here, 9.1 Sv in SR2001). SR2001 is larger because of a large northward Pacific transport in the upper ocean that does not appear here. This single detail made it natural for SR2001 to show upwelling into the surface layer, whereas the dominant layer sums here (layers 1–3) suggest southward flow in the topmost layer returned by northward flow just below. The much bigger difference between SR2001 and this analysis is the magnitude of the deep overturning cell, which is 27 Sv here but 49 Sv in SR2001, possibly because imposed, but poorly observed, air-sea fluxes in their inverse model resulted in large Southern Ocean upwelling, as discussed in Talley et al. (2003).

9.2. Components of the circulation that transport freshwater and heat

The meridional volume, freshwater and heat transports at "24°N" and "30°S" are summarized in Fig. 19, using components from Tables 9–15. Freshwater transports on the order of tenths of Sverdrups are "large" compared with those of order hundredths of Sverdrups.

All of the shallow overturns have large freshwater (order 0.1–0.3 MSv) or heat transports, or both. The freshwater magnitudes are sensitive to the section location relative to the evaporation maximum. The northward freshwater transport out of the Southern Ocean is primarily carried by the shallow overturning circulations that transport saline, warm, light water southward in the western boundary current and return slightly fresher, cooler and denser water northward in the interior. In the South Pacific, the

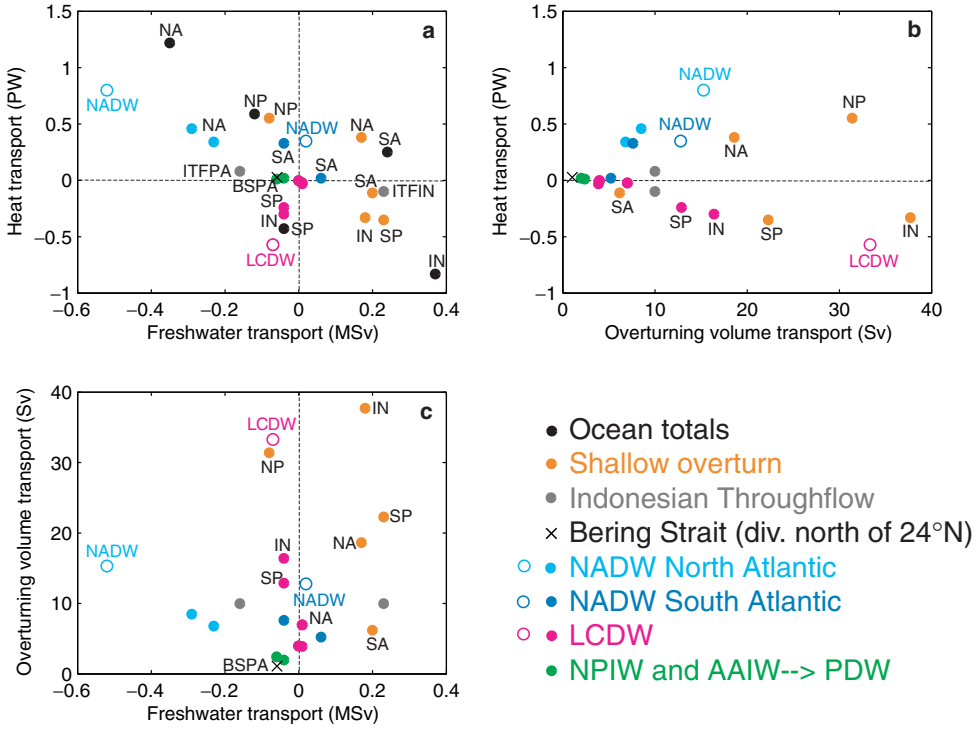

Fig. 19. Overturning volume (Sv), freshwater (MSv) and heat (PW) transports based on Tables 9–13. Blue: total (shown only for heat and freshwater graph). Red: shallow subtropical gyres. Black: ITF loops in Pacific and Indian. Black ×: divergence of heat and freshwater transports between 24°N and Bering Strait in the Pacific (negative MSv is net precipitation; positive PW is net cooling). Cyan: North Atlantic NADW, from thermocline to LSW and Nordic Seas Overflow Water (solid dots), and their sum (open dot). Gray blue: South Atlantic NADW, from Benguela Current thermocline and AAIW to NADW (solid dots), and their sum (open dot). Magenta: LCDW for each ocean (solid dots), and total for the southern hemisphere at 30°S (open dot). Green: NPIW and AAIW/PDW conversion in North Pacific. Abbreviations: NA (North Atlantic), SA (South Atlantic), IN (Indian), NP (North Pacific), SP (South Pacific), ITFIN (ITF in Indian), ITFPA (ITF in Pacific). (For interpretation of the references to color in this figure legend, the reader is referred to the web version of this article.)

northward component includes AAIW. In the Indian Ocean, this fresher gyre component is dominated by the Southeast Indian SAMW. In the South Atlantic Ocean, this fresher northward component includes part of the Benguela Current, which is fresher than the southward Brazil Current (Figs. 12b and 18a). (This may seem paradoxical because the excess northward transport of the Benguela Current is associated with southward freshwater transport since it is saltier than the NADW that is returned southward at depth; see below.)

The Indonesian Throughflow (black dots) is more important for freshwater than heat transport. The heat transports are small because the average temperature within the Indonesian passages (10 °C) is similar to the average upper layer temperature at 30°S in both oceans. Freshwater transports are large because the ITF salinity (about 34.5) is lower than the upper layer salinity on both the South Pacific and Indian sections (e.g. Figs. 7, 9, 10, 13, 14 and 18). The Pacific is fresher than the Indian at 30°S; thus the net precipitation in the Pacific that reduces the ITF salinity is smaller than the net evaporation in the Indian Ocean that increases it. The loop is closed in the Southern Ocean, requiring a net −0.07 MSv freshening of the waters that leave the Indian and enter the Pacific.

NADW formation is a major factor in global freshwater and heat transports (open cyan circle in Fig. 19). In the North Atlantic, freshwater transport is large and southwards (Rahmstorf, 1996), carrying all of the Arctic and Bering Strait inputs of freshwater, balanced by northwards transport of very saline surface water. Even the individual components in the North Atlantic (transformation to LSW and to NSOW, solid cyan dots) are each comparable to all of the shallow overturns and the ITF. In the South Atlantic, NADW overturning freshwater transport is northwards but very small, due to the near balance in the inflow between the saline Benguela surface water and fresher AAIW (open gray blue circle). This accounts for the marginal differences between various model outcomes, some showing northward and some southward freshwater transports at the South Atlantic boundary (Marsh et al., 2007; Weijer et al., 2001). The progression from very small to large freshwater transport from the South Atlantic to the North Atlantic is almost entirely due to evaporation that increases the upper ocean salinity along the northward pathway. (NADW also freshens slightly towards the south due to mixing with fresher AAIW, UCDW and LCDW.)

LCDW formation has large volume and heat overturning transports when considered globally across the three 30°S sections, with an impact that rivals NADW formation's impact at 24°N (27 Sv, −0.6 PW compared with NADW's 25 Sv, 0.8 PW). However, the LCDW impact on freshwater transport is extremely small in comparison (−0.05 MSv compared with NADW's −0.52 MSv) (Section 8.2).

The individual oceans' roles in LCDW upwelling north of 30°S can also be compared from Fig. 19. The South Pacific and Indian participation in the LCDW cycle are major and about equivalent; both have volume transports between 10 and 20 Sv, and make up almost all of the total LCDW overturning freshwater and heat transports. Upwelling of LCDW (AABW) into NADW in the South Atlantic, at least in this analysis with the old 32°S section and a small northward AABW transport, has little impact on heat or freshwater budgets.

Even though the North Pacific is the fresh end member of the global ocean (Figs. 1, 6 and 8), freshwater transports below the shallow (Kuroshio) overturn are small. That is, although NPIW formation in the Okhotsk Sea (Talley, 1991; Yasuda, 1997; Shcherbina et al., 2003) and injection into the North Pacific in the Oyashio–Kuroshio confluence region (Talley, 1993) creates a salinity minimum layer, and does carry freshwater equatorward, the overturning volume transport of about 2 Sv results in a much smaller freshwater transport than that associated with LSW in the North Atlantic. Also, NPIW formation does not carry all of the freshwater out of the subpolar North Pacific; Bering Strait moves a comparable (small) amount of freshwater northward to the Arctic (Section 6). Low salinities in the deep North Pacific are acquired through diapycnal diffusion with negligible overturning volume transport, and have very small associated meridional freshwater transport.

9.3. North–south asymmetry in freshwater transport mechanisms

Nearly equal amounts of freshwater are transported southward from the Arctic/subpolar North Atlantic and northward from the Antarctic, but by very different processes: transformation of surface waters to NADW and shallow gyre circulation in all three southern hemisphere basins, respectively. This is despite the similar large volume of deep water formed in both regions, and the existence of surface gyres in both regions. This asymmetry has several origins. The most important is arguably the "Drake Passage effect" (Toggweiler and Samuels, 1995a). In both the northern and southern subpolar regions there are equatorward Ekman transport and equatorward transport of locally formed deep water (NSOW/LSW and LCDW, respectively). However, the poleward transports that feed the deep waters are very different: they are within the upper ocean in the North Atlantic but below Drake Passage sill depth in the Southern Ocean. Therefore, the fresh surface layer in the northern North Atlantic is partially caught up in the northward near-surface flow that feeds NADW/LSW. Therefore, equatorward freshwater transport in the North Atlantic can be divided between NADW/LSW and the surface gyre. The freshwater transport for the NADW as measured at 24°N is large because of the large salinity difference between the inflowing, salty, subtropical surface waters and the outflowing, fresher, new NADW, due to the incorporation of the 0.5 MSv of freshwater from the Arctic, Bering Strait, and surface layer of the northern North Atlantic.

In the Southern Ocean on the other hand, only deep waters can cross southward across the Drake Passage gap if the southward transport is geostrophic (Warren, 1990; Toggweiler and Samuels, 1995a). These deep waters must be the source for UCDW and LCDW and cannot incorporate fresh Antarctic surface waters until they upwell isopycnally south of the ACC. Part of the UCDW upwells to the bottom of the fresh surface layer, and is incorporated in it as it is pushed northward by the winds, and then mixes into the surface layers north of the ACC (SR2001). This upwelled water and the rest of the Antarctic Surface Water that is forced northward by Ekman transport joins the upper ocean gyres in the SAMW and AAIW layers. This mostly moves northward as part of the surface gyres. On the other hand, the large volume of new LCDW that should be equivalent to NADW is formed mostly from deep waters, and not from salty and fresh surface waters. LCDW is only slightly fresher than its sources, which are NADW, IDW and PDW (see Section 8.2 for details). Therefore, LCDW transformation has only a very small freshwater transport.

10. Summary

1. Total freshwater transports maintain the mean salinity differences between the three oceans, between high and low latitudes, and between the subtropical high salinity regions and bordering lower salinity regions. These freshwater transports were diagnosed here from hydrographic sections. Integrated over large regions, these direct estimates are similar to previous direct estimates, particularly of GW03, and to the net precipitation, runoff and evaporation.

   Freshwater is transferred from the Pacific to the more saline Atlantic and Indian Oceans through the Indonesian Throughflow and Bering Strait, plus a much smaller export in the deep

water overturn. Taken together, these freshwater exports from the Pacific are larger than the net air-sea/runoff fluxes; the total freshwater balance includes a large input of freshwater from the Southern Ocean that nearly balances the exports.

Freshwater is transferred from the Arctic and subpolar North Atlantic to the mid-latitude North Atlantic, including a minor component from Bering Strait. The estimate of net precipitation of about 0.5 MSv for the entire region north of 45°N is similar to GW03 and to the NCEP/DT02 air-sea–runoff fluxes for the region.The total freshwater transferred northward from the Southern Ocean to all three oceans is 0.6–0.7 MSv depending on whether 28°S or 43°S is used for the South Pacific's southern boundary. This also compares favorably with the other two analyses. The mid-latitudes and tropics, taken together, are a region of net evaporation.

2. Separation of the circulation into shallow subtropical gyres, inter-ocean transports (ITF and Bering Strait) and zonally integrated isopycnal layers reveals major differences in mechanisms for moving freshwater. The upper ocean gyres, subject to direct air-sea fluxes and advection of large volumes of water, have large freshwater transports towards the subtropical evaporation centers.

   High northern latitude freshwater input is transported equatorward through deep and intermediate water formation, that is, mostly through NADW formation, with a small component due to NPIW. Both of these northern mechanisms involve transformation of saline, subtropical surface water to fresher, denser intermediate/deep water. In contrast, high southern latitude freshwater surface input is transported equatorward by the upper ocean subtropical gyres within the thermocline, hence resulting from subduction. There is only a very small component of northward freshwater transport due to LCDW/AABW formation. The asymmetry between the northern and southern exports of excess freshwater from high to low latitudes can be related to the "Drake Passage" effect (Toggweiler and Samuels, 1995a), and the consequently very small salinity difference between new bottom water (LCDW/AABW) and its deep water sources in the Southern Ocean, compared with the large salinity difference between the new deep water (NADW) and its surface water sources in the North Atlantic/Arctic.

   Bering Strait contributes only a minor amount to the freshening of NADW, with most of the NADW freshening due to net precipitation/runoff in the Arctic and subpolar North Atlantic. Bering Strait's contribution to removing freshwater from the Pacific is about half the contribution of the ITF and about double that of the Pacific's deep overturning circulation that removes freshwater southward. Bering Strait is, however, a major part of the freshwater balance for the subpolar North Pacific, equivalent to the southward freshwater transport carried by NPIW formation and the subtropical gyre.

   The ITF's freshwater role is much more important than its role in heat redistribution (Talley, 2003). The Indonesian Throughflow moves fresher water from the Pacific to the Indian Ocean, as one of the three ocean transport processes that maintain the Pacific's mean lower salinity value compared with the Indian and Atlantic, the other two being Bering Strait export and freshwater export associated with deep overturn in the Pacific. There is more net evaporation in the Indian than net freshening in the Pacific. Thus, the ITF mass transport loop exports freshwater from the Southern Ocean into the combined Pacific/Indian Oceans. The rate of export, about 0.1 MSv, is equivalent in magnitude to the 0.2 MSv exported northward by each of the southern hemisphere subtropical gyres.

3. As a caveat for interpretation of this work, and as possible focus for future work, while these zonally integrated transports provide one view of freshwater and heat transport pathways, within every isopycnal layer there may be major circulation components in the opposite direction from the total (Reid, 1994, 1997, 2003) (Fig. 18b). In this presentation, these more complete circulations have been considered only in the upper layer. But in order to most carefully answer questions about how, for instance, AAIW or CDW act to move freshwater and heat, some of the layer transports could be split into northward and southward components, as in Schmitz (1995) and Sloyan and Rintoul (2001a,b). Because of these more complex circulations, zonally integrated transports do not yield precise overturning rates of water masses. At best they provide a lower bound, since in a given layer there can be opposing water masses whose volume transports partially cancel.

4. Absent in this description of global freshwater transports was specific focus on the intermediate waters that are primarily identified by their salinity extrema, including the low salinity water masses LSW, AAIW and NPIW, and the high salinity Mediterranean Overflow Water and Red Sea Water (Fig. 2). Some scenarios of climate change effects consider the impact on global stratification of radical changes in production of such water masses (e.g. Keeling, 2002). This absence is directly related to the focus here on the ocean's freshwater transports and how they balance air-sea fluxes rather than on vertical stratification. LSW and NPIW were specifically assessed here simply because they are subthermocline water masses for which zonally integrated budgets identified by isopycnal layers are useful. LSW formation has a large freshwater transport, but is in fact no more important than NSOW formation, which does not have a salinity extremum. Both LSW and NSOW incorporate the fresh Arctic and subpolar North Atlantic waters and combine to make NADW a dominant factor in southward freshwater transport in the Atlantic Ocean. NPIW, while having a large-scale, obvious salinity signature, has relatively low impact on freshwater transport since its volume transport is so small.

   The impact of newly formed AAIW on global freshwater transport is not easily separated in this method from freshwater transports by the southern hemisphere's subtropical gyres, or from the zonally integrated transports below these gyres. This is because: (1) the upper part of AAIW is within the shallow, subducting gyre in the South Pacific where it contributes to the large equatorward freshwater transport in that gyre but is not sensibly separated from the rest of the thermocline waters, and (2) zonally integrated volume transport in the AAIW layers in the Indian and AAIW below the South Pacific's subducting gyre is small and even southwards because deeper waters upwell into this layer. In the South Atlantic, freshwater transport associated with northwards surface to southwards NADW conversion was composed of nearly canceling components from the AAIW and from the saltier surface flow in the Benguela Current. Sloyan and Rintoul (2001b) consider the pathways, formation and modification of AAIW and SAMW in great detail in each basin, separating northwards and southwards transports within the isopycnal layers; extension to freshwater transport might in principle be possible.

   The role of high salinity intermediate waters was not assessed because these transport constructs did not easily isolate their sources. It is worth repeating from earlier work (Gordon and Piola, 1983; Talley, 1996) that the high salinity of the Mediterranean Outflow Water, while important for the mid-depth presence of high salinity in the North Atlantic, accounts for only about 30% of the North Atlantic's excess high salinity compared with the Pacific; high evaporation over the open subtropical Atlantic is responsible for the remainder. So even without a Mediterranean Sea, the North Atlantic would be a highly saline ocean, thus retaining its capacity for deep water formation, and hence would likely remain the only major deep vehicle for glo-

bal freshwater transport, equivalent in impact to the upper ocean circulation elements.

Acknowledgements

Input from Joe Reid, and the contribution of his analyzed geostrophic velocity fields, was invaluable. Conversations with Paul Robbins were very helpful. The anonymous reviewers suggested the Monte Carlo uncertainty analysis. Support was obtained from National Science Foundation Grant OCE- 0327544, and NSF funding for the World Ocean Circulation Experiment, through Grants OCE-0118046, OCE-9712209 and OCE-9529584.

References

Aagaard, K., Carmack, E.C., 1989. The role of sea ice and other fresh water in the Arctic circulation. Journal of Geophysical Research 94, 14485–14498.
Baumgartner, A., Reichel, E., 1975. The World Water Balance. Elsevier. 179 pp.
Beal, L.M., Chereskin, T.K., 2003. The volume transport of the Somali Current during the 1995 southwest monsoon. Deep-Sea Research II 50, 2077–2089.
Beal, L.M., Chereskin, T.K., Lenn, Y.D., Elipot, S., 2006. The sources and mixing characteristics of the Agulhas Current. Journal of Physical Oceanography 36, 2060–2074.
Boyer, T.P., Antonov, J.I., Levitus, S., Locarnini, R., 2005. Linear trends of salinity for the world ocean: 1955–1998. Geophysical Research Letters 32 (L01604). doi:10.1029/2004GL021791.
Broecker, W.S., 1991. The great ocean conveyor. Oceanography 4, 79–89.
Broecker, W.S., Andree, M., Wolfli, W., Oeschger, H., Bonani, G., Kennett, J., Peteet, D., 1988. The chronology of the last deglaciation: Implications to the cause of the Younger Dryas event. Paleoceanography 3, 1–19.
Broecker, W.S., Peng, T.-H., Jouzel, J., Russell, G.L., 1990. The magnitude of global fresh-water transports of importance to ocean circulation. Climate Dynamics 4, 73–79.
Bryden, H.L., Beal, L.M., 2001. Role of the Agulhas Current in Indian Ocean circulation and associated heat and freshwater fluxes. Deep-Sea Research I 48, 1821–1845.
Curry, R., Dickson, B., Yashayaev, I., 2003. A change in the freshwater balance of the Atlantic Ocean over the past four decades. Nature 426 (6968), 826–829.
Curry, R., Mauritzen, C., 2005. Dilution of the northern North Atlantic Ocean in recent decades. Science 308, 1772–1774.
Dai, A., Trenberth, K.E., 2002. Estimates of freshwater discharge from continents: latitudinal and seasonal variations. Journal of Hydrometeorology 3, 660–687.
deRuijter, W.P.M., Biastoch, A., Drijfhout, S.S., Lutjeharms, J.R.E., Matano, R.P., Pichevin, T., van Leeuwen, P.J., Weijer, W., 1999. Indian–Atlantic interocean exchange: Dynamics, estimation and impact. Journal of Geophysical Research 104, 20885–20910.
Dickson, R.R., Lazier, J., Meincke, J., Rhines, P., Swift, J., 1996. Long-term coordinated changes in the convective activity of the North Atlantic. Progress in Oceanography 38, 241–295.
Dickson, R.R., Curry, R., Yashayaev, I., 2003. Recent changes in the North Atlantic. Philosophical Transactions of the Royal Society A 361, 1917–1934.
Domingues, C.A., Maltrud, M.E., Wijffles, S.E., Church, J.A., Tomczak, M., 2007. Simulated Lagrangian pathways between the Leeuwin Current System and the upper-ocean circulation of the southeast Indian Ocean. Deep-Sea Research II 54, 797–817.
Ganachaud, A., Wunsch, C., 2000. Improved estimates of global ocean circulation, heat transport and mixing from hydrographic data. Nature 408, 453–456.
Ganachaud, A., Wunsch, C., 2003. Large-scale ocean heat and freshwater transports during the World Ocean Circulation Experiment. Journal of Climate 16, 696–705.
Gill, A.E., 1973. Circulation and bottom water production in the Weddell Sea. Deep-Sea Research 20, 111–140.
Gnanadesikan, A., 1999. A simple predictive model for the structure of the oceanic pycnocline. Science 283, 2077–2079.
Gnanadesikan, A., Hallberg, R.W., 2000. On the relationship of the Circumpolar Current to southern hemisphere winds in coarse-resolution ocean models. Journal of Physical Oceanography 30, 2013–2034.
Gordon, A.L., 1986. Interocean exchange of thermocline water. Journal of Geophysical Research 91, 5037–5046.
Gordon, A.L., Piola, A.R., 1983. Atlantic Ocean upper layer salinity budget. Journal of Physical Oceanography 13, 1293–1300.
Gordon, A.L., Susanto, R.D., Ffield, A.L., 1999. Throughflow within Makassar Strait. Geophysical Research Letters 26, 3325–3328.
Hall, M.M., Bryden, H.L., 1982. Direct estimates and mechanisms of ocean heat transport. Deep-Sea Research 29, 339–359.
Hanawa, K., Talley, L.D., 2001. Mode Waters. In: Siedler, G., Church, J. (Eds.), Ocean Circulation and Climate, International Geophysics Series. Academic Press, pp. 373–386.
Hátún, H., SadØ, A.B., Drange, H., Hanse, B., Valdimarsson, H., 2005. Influence of the Atlantic subpolar gyre on the thermohaline circulation. Science 309, 1841–1844.
Hellerman, S., Rosenstein, M., 1983. Normal monthly wind stress over the world ocean with error estimates. Journal of Physical Oceanography 13, 1093–1104.
Holfort, J., Siedler, G., 2001. The meridional oceanic transports of heat and nutrients in the South Atlantic. Journal of Physical Oceanography 31, 5–29.
ICES, 2006. ICES report on ocean climate 2005. In: Hughes, S.L., Holliday, N.P. (Eds.), ICES Cooperative Research Report, vol. 280, 53 pp.
Intergovernmental Panel on Climate Change Fourth Assessment Report, 2007. Climate Change 2007: The physical science basis. In: Solomon, S., Qin, D., Manning, M., Chen, Z., Marquis, M., Avery, K.B., Tignor, M., Miller, H.L. (Eds.), Contribution of Working Group I to the Fourth Assessment Report of the Intergovernmental Panel on Climate Change. Cambridge University Press, Cambridge, United Kingdom/New York, NY, USA.
Kalnay, E., Kanamitsu, M., Kistler, R., Collins, W., Deaven, D., Gandin, L., Iredell, M., Saha, S., White, G., Woollen, J., Zhu, Y., Leetmaa, A., Reynolds, B., Chelliah, M., Ebisuzaki, W., Higgins, W., Janowiak, J., Mo, K.C., Ropelewski, C., Wang, J., Jenne, R., Joseph, D., 1996. The NCEP–NCAR 40-year reanalysis project. Bulletin of the American Meteorological Society 77 (3), 437–471.
Keeling, R.F., 2002. On the freshwater forcing of the thermohaline circulation in the limit of low diapycnal mixing. Journal of Geophysical Research, 107. doi:10.1029/2000JC000685.
Keeling, R.F., Stephens, B.B., 2001. Antarctic sea ice and the control of Pleistocene climate instability. Paleoceanography 16, 112–131.
Levitus, S., Boyer, T.P., 1994. World Ocean Atlas 1994, vol. 4: Temperature. NOAA Atlas NESDIS 4, US Department of Commerce, Washington, DC, 117 pp.
Levitus, S., Burgett, R., Boyer, T.P., 1994. World Ocean Atlas 1994, vol. 3: Salinity. NOAA Atlas NESDIS 3, US Department of Commerce, Washington, DC, 99 pp.
Macdonald, A.M., 1998. The global ocean circulation: a hydrographic estimate and regional analysis. Progress in Oceanography 41, 281–382.
Macdonald, A.M., Wunsch, C., 1996. An estimate of global ocean circulation and heat fluxes. Nature 382, 436–439.
Marsh, R., Hazeleger, W., Yool, A., Rohling, E.J., 2007. Stability of the thermohaline circulation under millennial CO_2 forcing and two alternative controls on Atlantic salinity. Geophysical Research Letters 34, L03605. doi:10.1029/2006GL027815.
Marshall, J., Schott, F., 1999. Open-ocean convection: observations, theory, and models. Reviews of Geophysics 37, 1–64.
McCartney, M.S., Talley, L.D., 1984. Warm water to cold water conversion in the northern North Atlantic Ocean. Journal of Physical Oceanography 14, 922–935.
McDermott, D., 1996. The regulation of northern overturning by southern hemisphere winds. Journal of Physical Oceanography 26, 1234–1254.
Meijers, A.J., Bindoff, N.L., Roberts, J.L., 2007. On the total, mean and eddy heat and freshwater transports in the southern hemisphere of a 1/8° by 1/8° global ocean model. Journal of Physical Oceanography 37, 277–295.
Ochoa, J., Bray, N.A., 1991. Water mass exchange in the Gulf of Cadiz. Deep-Sea Research 38, S465–S503.
O'Connor, B.M., Fine, R.A., Olson, D.B., 2005. A global comparison of subtropical underwater formation rates. Deep-Sea Research I 52, 1569–1590.
Orsi, A.H., Whitworth, T., 2005. In: Sparrow, M., Chapman, P., Gould, J. (Eds.), Hydrographic Atlas of the World Ocean Circulation Experiment (WOCE), vol. 1: Southern Ocean. International WOCE Project Office, Southampton, UK, 223 pp.
Orsi, A.H., Whitworth, T., Nowlin, W.D., 1995. On the meridional extent and fronts of the Antarctic Circumpolar Current. Deep-Sea Research I 42, 641–673.
Peterson, B.J., McClelland, J., Curry, R., Holmes, R.M., Walsh, J.E., Aagaard, K., 2006. Trajectory shifts in the Arctic and subarctic freshwater cycle. Science 25, 1061–1066.
Piola, A.R., Gordon, A.L., 1984. Pacific and Indian Ocean upper layer salinity budget. Journal of Physical Oceanography 14, 747–753.
Poisson, A., Chen, C.-T. A., 1987. Why is there little anthropogenic CO_2 in the Antarctic bottom water? Deep-Sea Research Part A 45 (7), 1255–1275.
Rahmstorf, S., 1996. On the freshwater forcing and transport of the Atlantic thermohaline circulation. Climate Dynamics 12, 799–811.
Reid, J.L., 1994. On the total geostrophic circulation of the North Atlantic Ocean; Flow patterns, tracers and transports. Progress in Oceanography 33, 1–92.
Reid, J.L., 1997. On the total geostrophic circulation of the Pacific Ocean; Flow patterns, tracers and transports. Progress in Oceanography 39, 263–352.
Reid, J.L., 2003. On the total geostrophic circulation of the Indian Ocean; Flow patterns, tracers and transports. Progress in Oceanography 56, 137–186.
Ridgway, K.R., Dunn, J.R., 2007. Observational evidence for a Southern Hemisphere oceanic supergyre. Geophysical Research Letters, 34. doi:10.1029/2007GL030392.
Rintoul, S., 1991. South Atlantic interbasin exchange. Journal of Geophysical Research 96, 2675–2692.
Roach, A.T., Aagaard, K., Pease, C.H., Salo, S.A., Weingartner, T., Pavlov, V., Kulakov, M., 1995. Direct measurements of transport and water properties through the Bering Strait. Journal of Geophysical Research 100, 18443–18457.
Robbins, P.E., Toole, J.M., 1997. The dissolved silica budget as a constraint on the meridional overturning circulation of the Indian Ocean. Deep-Sea Research 44, 879–906.
Roemmich, D., Gilson, J., 2001. Eddy transport of heat and thermocline waters in the North Pacific: a key to interannual/decadal climate variability? Journal of Physical Oceanography 31, 675–687.
Sabine, C.L., Feely, R.A., Gruber, N., Key, R.M., Lee, K., Bullister, J.L., Wanninkhof, R., Wong, C.S., Wallace, D.W.R., Tilbrook, B., Millero, F.J., Peng, T.-H., Kozyr, A., Ono, T., Rios, A.F., 2004. The oceanic sink for anthropogenic CO_2. Science 305, 367–371.

Saenko, O.A., Weaver, A.J., Robitaille, D.Y., Flato, G.M., 2007. Warming of the subpolar Atlantic triggered by freshwater discharge at the continental boundary. Geophysical Research Letters, 34. doi:10.1029/2007GL030674.
Schmitz, W.J., 1995. On the interbasin-scale thermohaline circulation. Reviews of Geophysics 33, 151–173.
Schmitz, W.J., Richardson, P.L., 1991. On the sources of the Florida Current. Deep-Sea Research 38 (Suppl.), S389–S409.
Schott, F.A., McCreary, J.P., 2001. The monsoon circulation of the Indian Ocean. Progress in Oceanography 51, 1–123.
Schott, F.A., Dengler, A.M., Schoenefeldt, R., 2002. The shallow overturning circulation of the Indian Ocean. Progress in Oceanography 55, 373–384.
Seidov, D., Haupt, B.J., 2003. Freshwater teleconnections and ocean thermohaline circulation. Geophysical Research Letters 30, 1329. doi:10.1029/2002GL016564.
Shcherbina, A., Talley, L.D., Rudnick, D.L., 2003. Direct observations of brine rejection at the source of North Pacific Intermediate Water in the Okhotsk Sea. Science 302, 1952–1955.
Shcherbina, A., Talley, L.D., Rudnick, D.L., 2004. Dense water formation on the northwestern shelf of the Okhotsk Sea. Part II: Quantifying the transports. Journal of Geophysical Research Oceans, 109. doi:10.1029/2003JC002197.
Sloyan, B.M., Rintoul, S.R., 2001a. The Southern Ocean limb of the global deep overturning circulation. Journal of Physical Oceanography 31, 143–173.
Sloyan, B.M., Rintoul, S.R., 2001b. Circulation, renewal, and modification of Antarctic mode and intermediate water. Journal of Physical Oceanography 31, 1005–1030.
Speer, K., Rintoul, S.R., Sloyan, B., 2000. The diabatic Deacon cell. Journal of Physical Oceanography 30, 3212–3222.
Speich, S., Blanke, B., de Vries, P., Drijfhout, S., Doos, K., Ganachaud, A., Marsh, R., 2002. Tasman leakage: A new route in the global ocean conveyor belt. Geophysical Research Letters, 29. doi:10.1029/2001GL014586.
Stammer, D., Wunsch, C., Giergin, R., Eckert, C., Heimbach, P., Marotzke, J., Adcroft, A., Hill, C.N., Marshall, J., 2003. Volume, heat, and freshwater transports of the global ocean circulation 1993–2000, estimated from a general circulation model constrained by World Ocean Circulation Experiment (WOCE) data. Journal of Geophysical Research 108 (C1), 3007. doi:10.1029/2001JC001115.
Stommel, H., 1961. Thermohaline convection with two stable regimes of flow. Tellus 13, 224–230.
Stommel, H., Csanady, G.T., 1980. A relation between the T–S curve and global heat and atmospheric water transports. Journal of Geophysical Research 85 (C1), 495–501.
Talley, L.D., 1991. An Okhotsk Sea water anomaly: implications for sub-thermocline ventilation in the North Pacific. Deep-Sea Research 38, S171–S190.
Talley, L.D., 1993. Distribution and formation of North Pacific Intermediate Water. Journal of Physical Oceanography 23, 517–537.
Talley, L.D., 1996. North Atlantic circulation and variability reviewed for the CNLS conference. Physica D 98, 625–646.
Talley, L.D., 1999. Some aspects of ocean heat transport by the shallow, intermediate and deep overturning circulations. In: Clark, Webb, Keigwin (Eds.), Mechanisms of Global Climate Change at Millenial Time Scales, Geophysical Monograph Series, vol. 112. American Geophysical Union, pp. 1–22.
Talley, L.D., 2003. Shallow, intermediate and deep overturning components of the global heat budget. Journal of Physical Oceanography 33, 530–560.
Talley, L.D., Sprintall, J., 2005. Deep expression of the Indonesian Throughflow: Indonesian Intermediate Water in the South Equatorial Current. Journal of Geophysical Research, 110. doi:10.1029/2004JC002826.
Talley, L.D., Reid, J.L., Robbins, P.E., 2003. Data-based meridional overturning streamfunctions for the global ocean. Journal of Climate 16, 3213–3226.
Toggweiler, J.R., Samuels, B., 1995a. Effect of Drake Passage on the global thermohaline circulation. Deep-Sea Research I 42 (4), 477–500.
Toggweiler, J.R., Samuels, B., 1995b. Effect of sea ice on the salinity of Antarctic Bottom Waters. Journal of Physical Oceanography 25, 1980–1997.
Toole, J.M., Warren, B.A., 1993. A hydrographic section across the subtropical South Indian Ocean. Deep-Sea Research 40, 1973–2019.
Tsuchiya, M., 1989. Circulation of the Antarctic Intermediate Water in the North Atlantic Ocean. Journal of Marine Research 47, 747–755.
Van Bennekom, Kastoro, A.J., Patzert, W.C., 1988. Recirculation in the Banda Throughflow, traced with dissolved silica. Netherlands Journal of Sea Research 22, 355–359.
Vellinga, M., Wood, R.A., 2002. Climatic impacts of a collapse of the Atlantic thermohaline circulation. Climate Dynamics 54, 251–267.
Vranes, K., Gordon, A.L., Ffield, A., 2002. The heat transport of the Indonesian Throughflow and implications for the Indian Ocean heat budget. Deep-Sea Research II 49 (7–8), 1391–1410.
Wadley, M.R., Bigg, G.R., 2002. Impact of flow through the Canadian Archipelago and Bering Strait on North Atlantic and Arctic circulation: an ocean modelling study. Quarterly Journal of the Royal Meteorological Society 128, 2187–2203.
Warren, B.A., 1990. Suppression of deep oxygen concentrations by Drake Passage. Deep-Sea Research A 37, 1899–1907.
Warren, B.A., LaCasce, J.H., Robbins, P.E., 1996. On the obscurantist physics of "form drag" in theorizing about the Circumpolar Current. Journal of Physical Oceanography 26, 2297–2301.
Warren, B.A., LaCasce, J.H., Robbins, P.E., 1997. Reply (to Hughes). Journal of Physical Oceanography 27, 211–212.
Weaver, A.J., Bitz, C.M., Fanning, A.F., Holland, M.M., 1999. Thermohaline circulation: high-latitude phenomena and the difference between the Pacific and Atlantic. Annual Reviews of Earth and Planetary Science 27, 231–285.
Weijer, W., de Ruijter, W.P.M., Dijkstra, H.A., van Leeuwen, P.J., 1999. Impact of interbasin exchange on Atlantic overturning circulation. Journal of Physical Oceanography 29, 2266–2284.
Weijer, W., de Ruijter, W.P.M., Dijkstra, H.A., 2001. Stability of the Atlantic overturning circulation: competition between Bering Strait freshwater flux and Agulhas heat and salt sources. Journal of Physical Oceanography 31, 2385–2402.
Whitworth, T., Orsi, A.H., Kim, S.-J., Nowlin, W.D., 1998. Water masses and mixing near the Antarctic slope front. In: Jacobs, S.S., Weiss, R.F. (Eds.), Interactions at the Antarctic Continental Margins, Antarctic Research Series, vol. 75. American Geophysical Union, Washington, DC, pp. 1–27.
Wijffels, S.E., 2001. Ocean transport of fresh water. In: Siedler, G., Church, J., Gould, J. (Eds.), Ocean Circulation & Climate. Academic Press, pp. 475–488.
Wijffels, S.E., Schmitt, R.W., Bryden, H.L., Stigebrandt, A., 1992. Transport of freshwater by the oceans. Journal of Physical Oceanography 22, 155–162.
Wijffels, S.E., Toole, J.M., Davis, R., 2001. Revisiting the South Pacific subtropical circulation: a synthesis of World Ocean Circulation Experiment observations along 32°S. Journal of Geophysical Research 106, 19481–19514.
Wong, A.P.S., Bindoff, N.L., Church, J.A., 1999. Large-scale freshening of intermediate waters in the Pacific and Indian oceans. Nature 400 (6743), 440–443.
Wong, A.P.S., Bindoff, N.L., Church, J.A., 2001. Freshwater and heat changes in the North and South Pacific Oceans between the 1960s and 1985–1994. Journal of Climate 14 (7), 1613–1633.
Woodgate, R.A., Aagaard, K., 2005. Revising the Bering Strait freshwater flux into the Arctic Ocean. Geophysical Research Letters, 32. doi:10.1029/2004GL021747.
Worthington, L.V., 1976. On the North Atlantic circulation. In: Johns Hopkins Oceanographic Studies, vol. 6, 110 pp.
Yasuda, I., 1997. The origin of the North Pacific Intermediate Water. Journal of Geophysical Research 102 (C1), 893–909.
Zaucker, F., Broecker, W.S., 1992. The influence of atmospheric moisture transport on the fresh water balance of the Atlantic drainage basin: General circulation model simulations and observations. Journal of Geophysical Research 97, 2765–2773.